JAERI-Review
2000-018

JAERI TANDEM ANNUAL REPORT 1999
APRIL 1, 1999-MARCH 31, 2000

November 2000

Department of Materials Science

日本原子力研究所
Japan Atomic Energy Research Institute

本レポートは、日本原子力研究所が不定期に公刊している研究報告書です。
入手の問合わせは、日本原子力研究所研究情報部研究情報課（〒319-1195　茨城県那珂郡東海村）あて、お申し越し下さい。なお、このほかに財団法人原子力弘済会資料センター（〒319-1195　茨城県那珂郡東海村日本原子力研究所内）で複写による実費頒布を行っております。

This report is issued irregularly.
Inquiries about availability of the reports should be addressed to Research Information Division, Department of Intellectual Resources, Japan Atomic Energy Research Institute, Tokai-mura, Naka-gun, Ibaraki-ken 〒319-1195, Japan.

編集兼発行　日本原子力研究所

JAERI－Review 2000－018

JAERI TANDEM
Annual Report
1999
April 1, 1999 – March 31,2000

Department of Materials Science※

Tokai Research Establishment
Japan Atomic Energy Research Institute
Tokai-mura, Naka-gun, Ibaraki-ken

(Received September 20, 2000)

This annual report describes research activities which have been performed with the JAERI tandem accelerator and the Van de Graaff accelerator from April 1, 1999 to March 31, 2000. Summary reports of 49 papers, and lists of publication, personnel and cooperative research with universities are contained.

Keywords: JAERI Tandem, Nuclear Structure, Nuclear Reactions, Nuclear Theory, Atomic Physics, Solid State Physics, Radiation Effects in Materials, Progress Report.

※ Editors: Suehiro TAKEUCHI, Hiroshi IKEZOE, Satoshi CHIBA, Yuichiro NAGAME, Masao SATAKA and Akira IWAMOTO

JAERI－Review 2000－018

原研タンデム加速器
１９９９年度年次報告

日本原子力研究所東海研究所
物質科学研究部※

（２０００年９月２０日受理）

本年次報告書は、東海研究所の原研タンデム及びバンデグラフ加速器で、１９９９年４月１日から２０００年３月３１日までの間に行われた研究活動をとりまとめたものである。

(1) 加速器の運転と開発研究　(2)核構造　(3)核反応　(4)核理論　(5)原子分子物理・固体物理及び材料の放射効果の５部門にまたがる４９編の研究報告、公表された文献、関与した職員及び大学等との協力研究のリストを収録している。

東海研究所：〒319-1195　茨城県那珂郡東海村白方白根２－４
※（編集者）竹内末広・池添　博・千葉　敏・永目諭一郎・左高正雄
岩本　昭

PREFACE

This report covers research and development activities using the tandem accelerator and its superconducting booster at JAERI, Tokai, for the period of April 1, 1999 to March 31, 2000. During this period, the tandem accelerator was operated over 5200 hours and delivered light- and heavy-ion beams to the experiments in the fields of nuclear structure, nuclear reactions, atomic physics, solid state physics and radiation effects in materials. The superconducting booster was utilized for 13 experimental subjects. Twenty-three research programs have been carried out in collaboration with about a hundred researchers from universities and research institutes.

The fruits of studies in FY1999 are the following: A technique of complete spectroscopy based on multiple Coulomb excitation was developed and applied to the investigation of electromagnetic properties of ^{74,76}Ge nuclei. Fusion evaporation residues at sub-barrier energy in the reactions ^{76}Ge+^{150}Nd and ^{64}Ni+^{182}W were measured with the recoil mass separator (JAERI-RMS). A new neutron deficient actinide isotope ^{237}Cm, which was produced via the ^{237}Np (^{6}Li, 6n) reaction, was identified with the gas-jet coupled JAERI-ISOL. From in-situ measurements of low temperature electrical resistivity of ion-irradiated $EuBa_2Cu_3O_y$ superconductors, the size of the induced columnar defects and the resistivity inside the defects were found to have close correlation to the density of primary ionization along ion paths.

A study on the accelerator complex adding a linear accelerator as an injector of radioactive beams and high intensity stable beams to the tandem booster started in collaboration with KEK. In the plan, the KEK linear accelerator for radioactive beams is to be moved into a target room. The radioactive beams of fission fragments will be produced by bombarding an actinide target with proton beams from the tandem accelerator.

The tandem accelerator laboratory has a plan of replacing the accelerator tubes with compressed-geometry-type ones. With this replacement, the terminal voltage will be increased toward 20 MeV in a few years.

Akira Iwamoto
Director
Department of Materials Science

This is a blank page.

Contents

目 次

1. Accelerator Operation and Development

This is a blank page.

1.1 TANDEM ACCELERATOR AND BOOSTER OPERATION

TANDEM ACCELERATOR GROUP

Tandem Accelerator and Booster: There were three scheduled machine times in this fiscal year and the operations of the tandem accelerator and booster for experiments were performed as scheduled. The operation time of the tandem accelerator was 5279 hours in 229 days. The super-conducting booster was operated steadily for 41 days for 13 experimental subjects. During these times, the helium refrigeration systems for the tandem booster were operated 3 periods during 3 scheduled machine time periods including a during stop the year end holidays. The helium refrigeration systems were in operation for 178 days from May 23, 58 days from October 25 in 1999 and 51 days from January 11 to May 2 in 2000. The summary of the operation from April 1, 1999 to March 31, 2000 is as follows.

1) Time distribution in terms of terminal voltages (Tandem accelerator)

>16 MV	39 days	17.0 %
15-16	89	38.9
14-15	27	11.8
13-14	9	3.9
12-13	16	7.0
11-12	6	2.6
10-11	20	8.7
9-10	12	5.2
8-9	2	0.9
<8	9	3.9

Booster operation

^{35}Cl	345 MeV	3 days
^{58}Ni	~310	9
^{70}Zn	565	4
^{76}Ge	635	8
^{82}Se	~680	13
^{90}Zr	390	1
^{127}I	~600	2
^{136}Xe	500	1

The tandem accelerator had 3 scheduled maintenance times. The first and the second machine time and a maintenance time were arranged to be shorter than usual term for maintaining the time to inspection works with the gas handling systems. The governmental inspection is scheduled almost at the same time of the year and we have to do self inspection as a duty before governor's inspection for the gas handling system. We performed it on early September for the tandem gas handling system. From the middle of September, the helium refrigerator systems also had similar maintenance jobs prescribed in the law, and the inspection by governor also passed in the end of 1999.

1.2 UTILIZATION OF TANDEM ACCELERATOR AND BOOSTER

T. YOSHIDA and S. KANDA

The utilization of the tandem accelerator facility was carried out for 229 days for various experiments in three scheduled machine times in the FY 1999. Collaboration research proposals for the FY 1999 were examined at late November in 1998, and 23 subjects were accepted by the program committee. These programs accounted for approximately 66% of the whole machine time. Eighteen ion species were utilized in the 3 experimental periods as follows. The RF power amplifier in the in terminal failed at middle of the year. We had to cancel the inert gas ion operation. About the ECR ion source report are described in the section of Operation and Accelerator Development of this annual report.

1) Time distribution in terms of projectiles

^{1}H	19 days	^{58,60}Ni	28 days
^{6,7}Li	25	^{64}Zn	10
^{12,13}C	25	^{74}Ge	24
^{16,18}O	9	^{82}Se	15
^{20}Ne	1	^{90}Zr	6
^{31}P	4	^{107}Ag	1
^{28}Si	6	^{127}I	15
^{32,33}S	12	^{136}Xe	6
^{35,37}Cl	9	^{197}Au	14

The experimental terms allotted in the three periods were 81 days in May 11 to August 9, 85 days in September 24 to January 21 in 1999 and 21 days in March 11 to end of March. The last term continued to the 1st machine time period in FY 2000. The summary of allotted days to various experimental subjects are as follows.

Research field	allotted days	total number of subjects
Nuclear physics	111	34
Atomic and Solid-state physics	54	45
Nuclear chemistry	48	14
Material research	14	11
Accelerator development	5	3

1.3 ECR PLASMA PROCESSING OF SUPERCONDUCTING RESONATOR SURFACES

S. TAKEUCHI

Electron cycrotron resonance(ECR) plasma precessing has been investigated for a future surface re-treatment of the superconducting quarter wave resonators used in the tandem-booster.

Niobium cavity walls of the resonators have been electro-chemically polished. Some of them were polluted with hydrogen so heavily that the on-line resonator performances were significantly lowered[1]. This is called as "Q-disease" that happens due to precipitation of hydrides at around 120K during precooling process. An ideal cure of the Q-disease requires hydrogen outgassing from the niobium walls. The resonators, however, contains outer-conductor walls made of niobium-copper composite plates which do not allow heat treatment. Heat treatment can be partly applied to the center conductor part purely made of niobium. With these reasons, ECR plasma processing which is a dry cleaning method and brings no hydrogen pollution has been investigated in preparation for a resonator-surface treatment in the future. It is also hoped that the Q-disease is relieved to some extent by surface cleaning with ECR plasma.

An ECR plasma processing apparatus was set up and experiments were carried out with a spare resonator or a full-scale stainless steel model, as illustrated in Fig. 1. A resonator was placed in a solenoid, pumped by a turbo-molecular pump and fed with 2.45 GHz rf wave. The magnetic field at the ECR condition is in the vicinity of 0.088 T. ECR discharge was formed at a pressure of $1 - 6 \times 10^{-3}$ Pa .

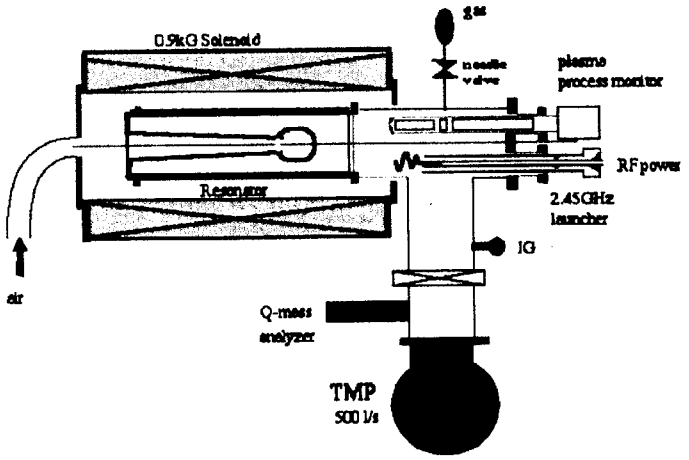

Fig. 1. Set-up for ECR plasma surface processing

There was an improvement of resonator Q in the experiments done in FY 1998 with helium gas. After each ECR processing, Q-values were measured at 4.2K for the two cases of fast(40-60K/h) and slow(10-12K/h) precoolings from 130K to 90 K. After a helium processing with 100W RF input for 60 hours, we had 30% and 50 % increases in Q for the fast and slow precoolings, respectively[2].

In FY 1999, we measured characteristics of plasma in a stainless steel cavity with different gases and rf input powers, investigated effect of hydrogen outgassing from niobium samples, and examined ECR discharges of sulfuric hexa-floraide and argon with a spare resonator.

In the plasma diagnostics, electron temperatures and densities were measured by using a Langmuir probe for helium, oxigen, argon and other gases. The following are a part of the measured data;

gas,	pressure(Pa),	rf power(W),	electron temperature(eV),	electron density(/cm3)
helium	3×10^{-3}	100	16.9	1.0×10^{9}
		200	16.9	1.7×10^{9}
		400	23.9	1.8×10^{9}
	6×10^{-3}	200	4.3	6.3×10^{9}
oxigen	3×10^{-3}	200	16.5	1.5×10^{9}
argon	2.4×10^{-3}	200	29.5	1.1×10^{9}

Information about ions, on the other hand, was obtained from a plasma process monitor which allows to measure mass and energy spectra of charged and neutral atoms from the plasma. Energy spectra of helium and argon 1+ ions obtained for different pressures and an rf input of 200W are shown in Fig.2, for example.

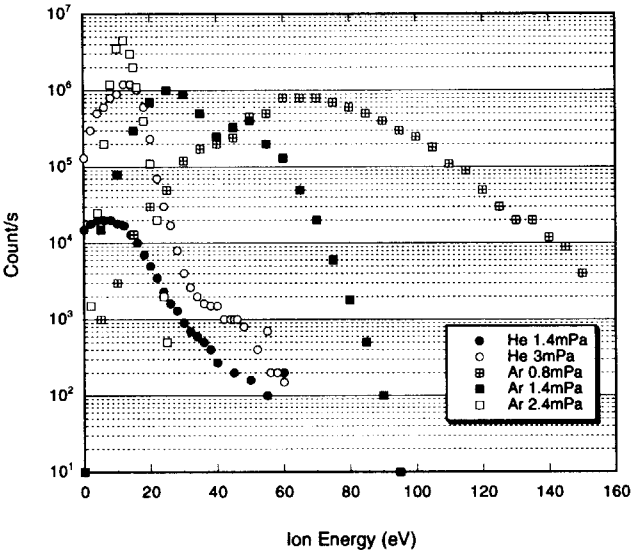

Fig.2. Energy distributions of He and Ar 1+ ions from ECR discharges

More energetic ions are included in the Ar plasma than in the He plasma and with decreasing pressure. From this result, the ECR Ar plasma seems to be useful in case of expecting a physical sputtering effect on the cavity surface.

In the sample experiments, the hydrogen content in any niobium sample was not appreciably changed by the ECR plasma processing, or it indicated that outgassing from the bulk niobium did not occur.
With respect to experiments with a real resonator, Ar and SF_6 gases were examined in FY 1999, expecting physical and chemical sputtering effects, respectively. However, depositions of dirt or decomposed sulfuric compound were found in several areas on the surface during the discharges. Another strong Ar discharge degraded the Q values at 4.2K. These results were probably attributed to an un-uniform plasma distribution. We have to find a good condition for making uniform plasma distributions in order to continue the study of ECR plasma surface cleaning.

References

[1] S. Takeuchi and M. Matsuda, Proc. of the Eighth Workshop on RF Superconductivity, Abano Terme(1997)pp237-247.
[2] S. Takeuchi, Proc. of the 2nd Superconducting Linear Accelerator Meeting in Japan, Tsukuba (1999) pp122-125.

1.4 PROGRAMS OF ACCELERATOR DEVELOPMENTS

S. TAKEUCHI and T. YOSHIDA

The tandem accelerator has been constantly operating more than 200 days a year for experiments since 1982 and its energy performance was raised by the addition of a superconducting booster in 1994. The tandem accelerator itself is already older than 20 years. It would be hoped that there exist new revolutionary developments in the facility. Presently, beam current increase is increasing its importance in experiments and we are making an effort of increasing beam current from the tandem and booster. The program started with installing an ECR ion source into the high voltage terminal. The second program is increasing the terminal voltage of the tandem accelerator. It improves energy performances of the beams from the tandem and beam current performances of very heavy ions from the booster. On the other hand, acceleration of radioactive nuclear beams(RNB) is attractive to nuclear physists. JAERI and KEK is planning to move a RNB linac system built at KEK-Tanashi to this tandem accelerator lab. Not only RNB, but also very intense normal heavy-ion beams(NB) will become available, if the plan is carried out.

In-terminal ECRIS: A 10 GHz ECRIS, NANOGAN, is presently in the terminal. Ions of H, N, O, Ne, Ar, Kr and Xe can be extracted from it. The gases of Kr and Xe which could not be pumped out for a long time by ion pumps became allowable by implementing a turbo-molecular pump to the in-terminal ion injector at the end of the FY 1999. The ECR in-terminal injector expanded range of ion spieces and energies as well as their beam intensities. The performances will be improved more by replacing the small source to a high-performance ECRIS, SuperNANOGAN, in a few years.

Replacement of accelerator tubes and voltage dividers: The present accelerator tubes have been used for 21 years since their installation in1979. After 18 MV was achieved in 1982, the operating voltages gradually decreased to a level of 16.5 MV in twenty years. This level down was partly due to our safety operation stance of protecting electronics in the accelerator against sparks with break-down of high stored energy at ultimately high voltages. The superconducting booster was designed for a terminal voltage of higher than 18 MV in early 1980s. The present terminal voltages are too low to inject very heavy ions and need a second stripper foil which is situated at the1/3 point from the top in the high energy tube and reduces the beam current by approximately one-tenth. If the terminal voltage is raised up to 20 MV, very heavy ions can be accepted to the booster without using second strippers, and beam current performances can be improved a lot. The energy performance increase, of course, benefits users of the beams from the tandem accelerator as well.
New "compressed geometry" tubes are available from NEC. Old 1 MV modules are composed of 17.3 cm-long three tubes with 11 layers of ceramic and three heater plates. The heater plates are removed in the compressed geometry. New 1 MV modules comprise two 30 cm long new tubes with 21 ceramic layers for each. The ceramic layers will be increased from 33 to 42 by replacing the tubes. The old corona needle voltage dividers are also to be replaced by resister systems. Resisters of 1.2G ohm and 4 G ohm have been prepared in FY1999, which are for tube and column dividers. A wider stable range of the terminal voltage can be expected with the resister system. Procurement of the tubes was partly done in the FY1999. The replacement will be carried out in

FY2000. The replacement work will be carefully carried out including cleaning, baking and setting clean installation environment.

Use of KEK-Tanashi linac for RNB and NB: For producing RNB, proton beams of 3 μA from the tandem accelerator are to be bombarded on a target which fits to obtain suitable nuclear reaction products. A prospective target is UC which emits a number of fission products. An existing ISOL system will be utilized for isotope separation. A charge breeder needs to be developed for heavy RNB. A high performance ECRIS is also planned to be implemented as an injector. The first accelaration unit is a Split-Coaxial RFQ linac of 26MHz with acceleration energy of 0.17 MeV/u and the second a IH(inter-digital) linac of 52 MHz with exit energy of 1 MeV/u. And, the third one is another IH linac of 104 MHz with exit energy of 2 MV, which needs to be built in future to inject the beams into the booster(of which freqency is 130 MHz). In FY1999, layout plans, building re-constructions, budget plan and related problems were investigated by an adhoc working group. The neutron target room in the tandem lab was also cleaned up in preparation for the installation site. The plan may start as early as in 2001. Low energy RNB may be available in 2 - 3 years and high energy RNB or NB in several years.

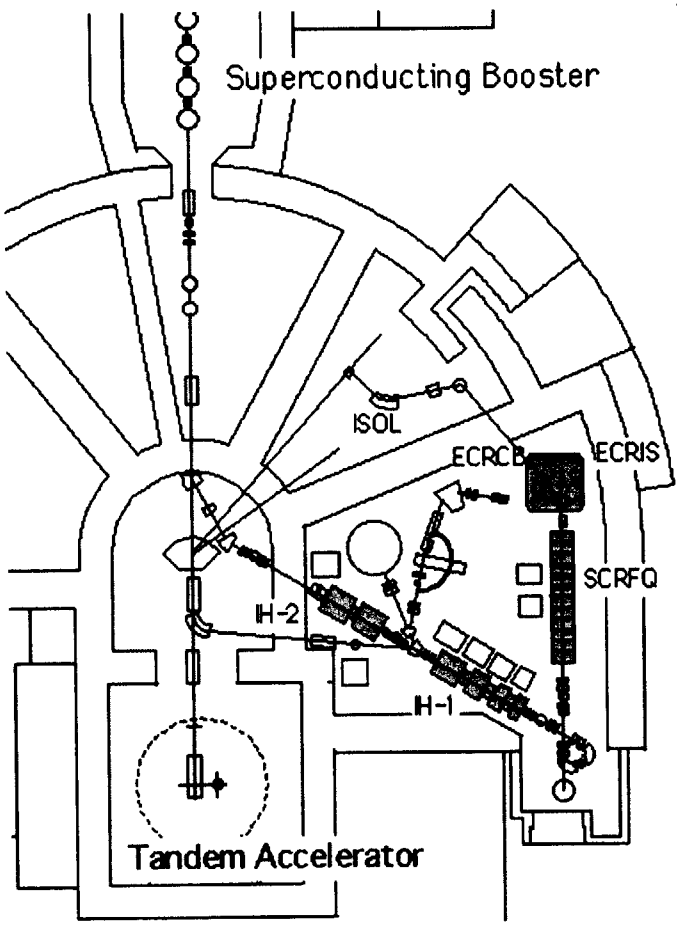

Fig. 1. A preliminary layout plan of the RNB & NB acceleration system at the JAERI Tandem-Booster

2. Nuclear Structure

This is a blank page.

2.1 DECAY OF ^{236g,m}Am

M. ASAI, M. SAKAMA[1], K. TSUKADA, S. ICHIKAWA, H. HABA,
I. NISHINAKA, Y. NAGAME, S. GOTO[2], Y. KOJIMA[3], Y. OURA[1],
H. NAKAHARA[1], M. SHIBATA[4], and K. KAWADE[4]

The decay of neutron-deficient americium nuclei with the mass number ≤ 236 has been scarcely studied because of experimental difficulties. These nuclei predominantly decay by electron capture, and their half-lives are shorter than 10 min. In order to observe γ rays following the EC decay of these nuclei, it is necessary to isolate the nuclei of interest from other reaction products. In the present work, the EC decay of ^{236}Am were studied using the JAERI on-line isotope separator (ISOL) [1] coupled to a gas-jet transport system.

The ^{236}Am nuclei were produced by the reaction of ^{235}U(^{6}Li, $5n$)^{236}Am. Reaction products recoiling out of the targets were transported into an ion source of the ISOL with gas-jet stream, and mass-separated. The separated ions were implanted into an aluminum-coated Mylar tape in a tape transport system, and periodically transported to a measuring position equipped with two Ge detectors. Gamma-ray singles and γ-γ coincidence measurements were performed.

Figure 1 shows a proposed decay scheme of ^{236}Am. Excited states in ^{236}Pu were established for the first time except for the known first 2^+, 4^+, and 6^+ states [2]. The 698, 758, and 866 keV levels were assigned to the 1^-, 3^-, and 5^- states in the $K^\pi = 0^-$ octupole band. Their level energies and γ-ray branching ratios were in reasonable agreement with systematic predictions. From an X- to γ-ray intensity ratio, the multipolarity of the 320 keV transition was determined to be $M1$, which led to the 5^- assignment for the 1186 keV state. This 1186 keV state was found to be the $K^\pi = 5^-$ isomer with a half-life of 1.2(3) μs which was deduced from an X-γ delayed coincidence analysis. The spin and parities of the 1312 and 1341 keV states were restricted to $0^\pm$, $1^\pm$, $2^\pm$, and 3^- due to γ feedings to a 1^- state.

According to systematics of Nilsson orbit assignments, the 95th proton and the 141st neutron of the ground state of ^{236}Am are expected to occupy the $\pi 5/2^-[523]$ and the $\nu 5/2^+[633]$ orbitals, respectively. Thus, the spin and parity of the ground state of ^{236}Am is expected to be 5^- by the Gallagher and Moszkowski coupling rule [3]. However, the EC decay of ^{236}Am strongly populates the 1312 and 1341 keV states as well as the 1186 keV 5^- state. This fact suggests that the ^{236}Am has another EC-decaying low-spin state. The half-life analyses revealed that the γ rays depopulating high-spin states had a longer half-life of 3.6(2) min, and those depopulating low-spin states showed a different half-life of 2.9(2) min, which are the direct evidence for the existence of an EC-decaying isomer.

The EC decays from the ^{236g,m}Am to the 1186, 1312, and 1341 keV states have log ft values of 4.9(1) and 5.4(1). Around this neutron-deficient actinide region, such fast EC or $\beta^\pm$

[1]Department of Chemistry, Tokyo Metropolitan University
[2]Department of Chemistry, Niigata University
[3]Faculty of Engineering, Hiroshima University
[4]Department of Energy Engineering and Science, Nagoya University

decays are scarce. Only the $\pi 5/2^+[642] \rightarrow \nu 5/2^+[633]$ transitions show small $\log ft$ values of ~5.3 [2]. Thus, the EC decays to the 1186, 1312, and 1341 keV states are considered as this transition. As a consequence, the configuration of these 1186, 1312, and 1341 keV states is assigned to the $\pi 5/2^+[633]\pi 5/2^+[642]$ two-quasiparticle one. Levels with the same configuration are also reported in ^{240}Pu [2]. Level energies, transition probabilities, and γ branching ratios of the 1186, 1312, and 1341 keV states in ^{236}Pu are similar to those of the 5^-, 0^-, and 2^- states in ^{240}Pu with the $\pi 5/2^+[633]\pi 5/2^+[642]$ configuration, respectively. Thus, we assigned the spins of the 1312 and 1341 keV states to 0^- and 2^-, respectively.

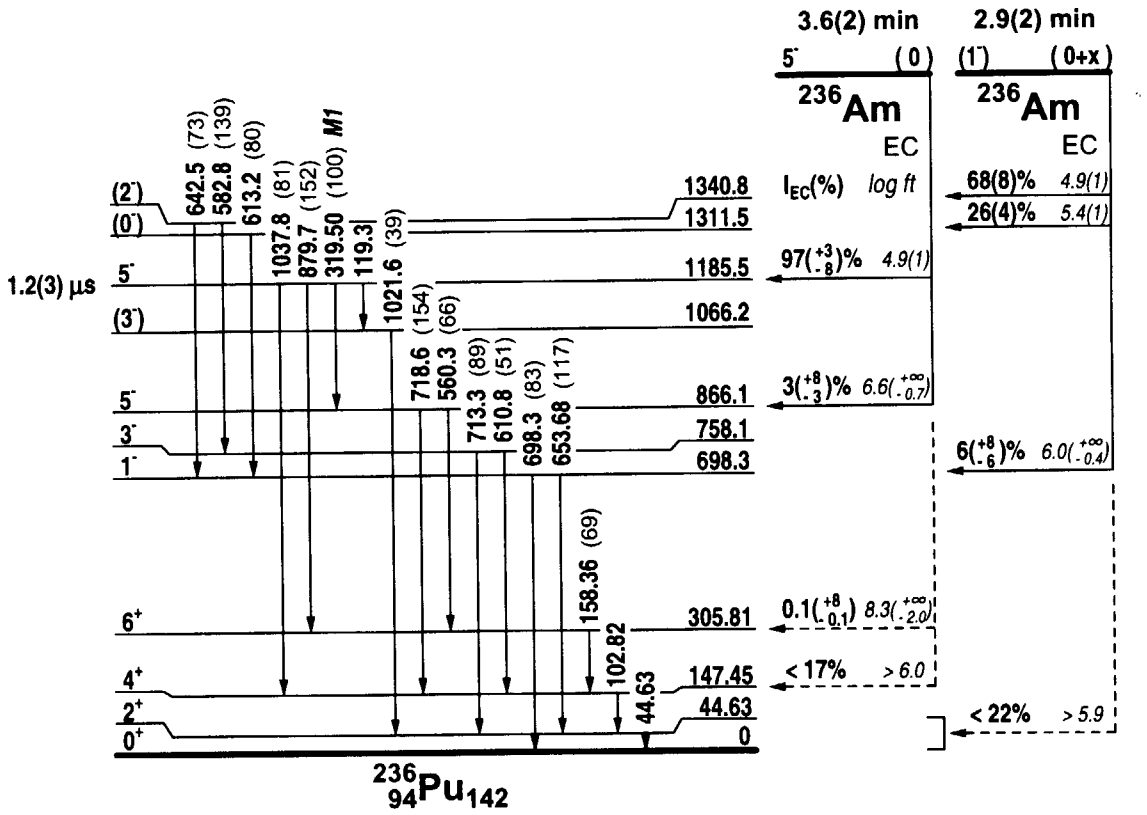

Fig. 1. A decay scheme of ^{236g,m}Am.

References

[1] K. Tsukada *et al.*, Phys. Rev. C **57** (1998) 2057.

[2] *Table of Isotopes*, 8th ed., edited by R. B. Firestone and V. S. Shirley (Wiley, New York, 1996).

[3] C. J. Gallagher, Jr. and S. A. Moszkowski, Phys. Rev. **111** (1958) 1282.

2.2 IDENTIFICATION OF NEW NEUTRON-DEFICIENT ACTINIDE NUCLIDES ^{233}Am AND ^{237}Cm

K. TSUKADA, M. SAKAMA[1], M. ASAI, S. ICHIKAWA, H. HABA, I. NISHINAKA, Y. NAGAME, S. GOTO, Y. KOJIMA[2], Y. OURA[1], H. NAKAHARA[1], M. SHIBATA[3] AND K. KAWADE[3]

There still remain many isotopes to be discovered in the region of neutron-deficient actinide nuclides which decay dominantly through electron capture. We have developed a composite system consisting of a gas-jet transport apparatus, a multiple-target chamber, and an on-line isotope separator (JAERI-ISOL) [1]. This system was successfully applied to identify the neutron-deficient americium isotope ^{236}Am [2]. In addition, a highly efficient detection system consists of a rotating wheel to measure α-particles was newly developed that system enables us to observe α-decays which occur with small branching ratios. In this report, we describe identification of new isotopes, ^{233}Am and ^{237}Cm.

Experiments were performed at the JAERI tandem accelerator facility. The reaction systems were ^{233}U(^{6}Li, 6n)^{233}Am and ^{237}Np(^{6}Li, 6n)^{237}Cm. A stack of twenty-one ^{233}U or ^{237}Np targets set in a multiple-target chamber was bombarded with $^{6}Li^{3+}$ beam with an intensity of ~300 pnA. Each target with a thickness of about 200 μg/cm^2 was prepared by electrodeposition on a 0.7 mg/cm^2 thick aluminum foil. The effective target thickness estimated from the recoil momentum of the compound nucleus is about 100 μg/cm^2 for each target. The reaction products recoiling out of the targets were stopped in He gas (640 mmHg) loaded with PbI_2 cluster. The products attached to the PbI_2 clusters were swept out from the target chamber with the He gas (1.3 l/min) into a capillary (1.5 mm i.d. and 8 m length). The transported nuclides were ionized in the thermal ion source of ISOL at 2450 K [1]. The overall efficiency including the gas-jet transport, the ionization of americium atoms, and the mass separation was estimated to be 0.3% using ^{237}Am produced in the ^{235}U(^{6}Li, 4n) reaction. The mass-separated products were implanted on a 10 μg/cm^2 thick PVC/PVA foil in the four-position rotating wheel system. The wheel was periodically rotated and the sources on the wheel were measured at each of the positions equipped with PIN-photodiode detectors in both sides of the sources. A short coaxial n-type HPGe (LOAX™; 51mm dia. x 20 mm thick, FWHM=0.57 keV at 122 keV) was settled behind the first measuring position for monitoring the x/γ rays. The event-by event data were recorded together with the time information.

α-decay of the new isotope ^{233}Am

The new isotope ^{233}Am was identified based on the correlation of the α decay chain. The expected decay chain of ^{233}Am [3,4] and an α- particle energy spectrum obtained at the mass-233 fraction produced in the ^{233}U+^{6}Li reaction are shown in Fig. 1. In the present spectrum the α peak of ^{233}Am together with those of all daughter nuclides were observed, and altogether

[1]Department of Chemistry, Tokyo Metropolitan University
[2]Faculty of Engineering, Hiroshima University
[3]Department of Energy Engineering and Science, Nagoya University

about 80 correlated chains were measured in the present experiments. The α particle energy and half-life of ^{233}Am were determined to be 6776±18 keV and 3.2±0.8 min, respectively.

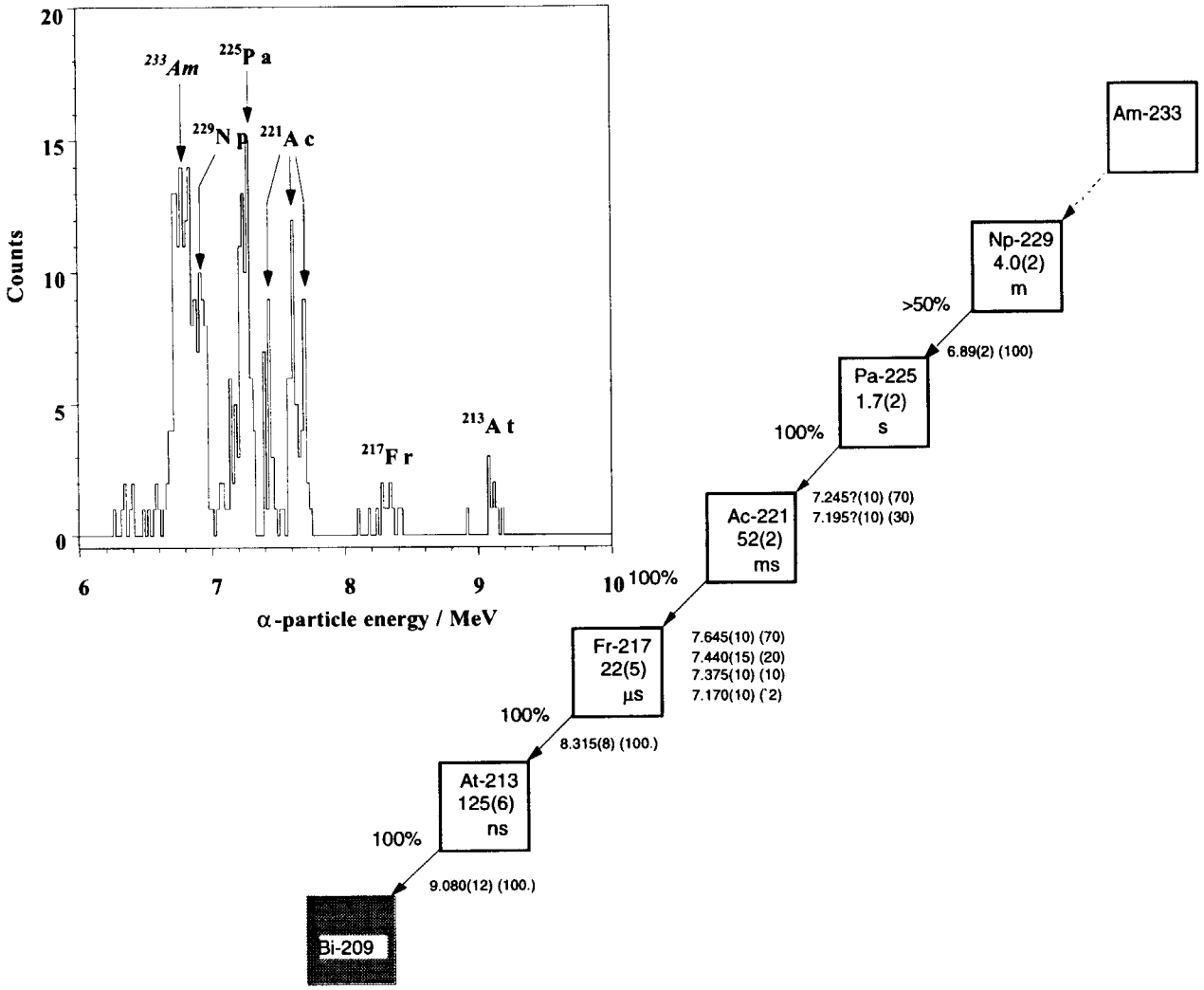

Fig. 1. α-particle energy spectrum of the mass-233 fraction produced in the ^{233}U+^{6}Li reaction and the expected α-decay chain [3,4] of ^{233}Am.

α-decay of the new isotope ^{237}Cm

The 6.66 MeV peak originating from the α-decay of ^{237}Cm was observed in an α-spectrum obtained at the mass-237 fraction produced in the ^{237}Np+^{6}Li reaction. The half-life measurement for ^{237}Cm is now being carried out.

References

[1] S. Ichikawa et al., Nucl. Instrum. Methods. Phys. Res. **A 374** (1996) 330.
[2] K. Tsukada et al., Phys. Rev. **C 57** (1998) 2057.
[3] R.L. Hahn et al., Nucl. Phys. **A113** (1968) 206.
[4] R.B. Firestone et al., *Table of Isotopes, 8th ed.*, John Wiley & Sons Inc., New York (1996).

2.3 ALPHA DECAY OF THE NEUTRON-DEFICIENT AMERICIUM ISOTOPE, ^{235}Am

M. SAKAMA[1], K. TSUKADA, M. ASAI, S. ICHIKAWA, Y. OURA[1], H. HABA, I. NISHINAKA, Y. NAGAME, S. GOTO, Y. KOJIMA[2], M. SHIBATA[3], K. KAWADE[3], M. EBIHARA[1], and H. NAKAHARA[1]

Experimental investigations of decay properties of neutron-deficient actinides are of importance. In particular, their α-decay contributes to our understanding of the systematics of α/EC-decay branching ratios and leads to precise values of nuclear masses in the region of neutron deficient actinides which decay dominantly through electron capture (EC). Previously we measured the half-life of the EC-decay of ^{235}Am with the gas-jet coupled JAERI-ISOL that was produced by the ^{235}U(^{6}Li,6n) reaction [1, 2]. In the present work, we have observed the α-decay of ^{235}Am for the first time using a new rotating-wheel α-detection system.

^{235}Am was produced by the ^{233}U(^{6}Li,4n) reaction. Twenty-one ^{233}U targets set in a multiple-target chamber were irradiated with a 45.5 MeV $^{6}Li^{3+}$ beam of about 1 eμA intensity. The effective thickness of each target was about 100 μg/cm^2. The α-detection system is schematically shown in Fig. 1. The mass-separated ^{235}Am atoms were implanted into ~8 μg/cm^2 polyvinylchloride-acetate copolymer foils placed on the periphery of a four-position rotating-wheel. The wheel periodically rotates 90° at 15 min intervals, which conveys implanted sources to three consecutive detector stations. In each of the detector stations, two Si PIN-photodiodes were placed on both sides of the wheel to measure α-particles with an approximately 80% efficiency. An HPGe (LOAX^{TM}) was also placed at the 1st detector station to measure Pu KX rays following the EC-decay of ^{235}Am simultaneously. The collecting station was also equipped with one Si PIN-photodiode. Energy calibrations for the Si detectors were made by using known α emitters, ^{221}Fr, ^{217}At and ^{213}Po, from an ^{225}Ac recoil source. The energy resolution of the Si detectors for the 7067 keV α-particles was about 45 keV.

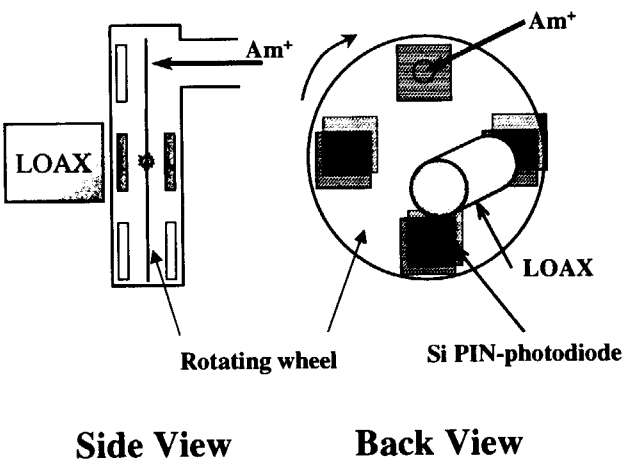

Fig. 1. Schematic drawing of the new rotating-wheel α-detection system.

The sum of α-particle spectra measured with seven Si detectors for the mass-235 fraction accumulated during the period of 900 s × 360 cycles is shown in Fig. 2. The α-line of ^{235}Am was unequivocally identified and its α-particle energy was determined to be 6457±14 keV.

[1]Department of Chemistry, Tokyo Metropolitan University
[2]Faculty of Engineering, Hiroshima University
[3]Department of Energy Engineering and Science, Nagoya University

The half-life of this α-line was in good agreement with that of Pu KX rays following the EC-decay of ^{235}Am observed in this experiment. The half-life of ^{235}Am was re-evaluated as 10.3±0.6 min. The branching ratio for the α-decay of ^{235}Am was determined to be 0.40±0.05% and the remaining 99.6% is for the EC-decay.

A relationship between partial α-decay half-lives and α-particle energies for odd-mass americium isotopes, from ^{243}Am to ^{237}Am, is shown in Fig. 3. It is found that the α-decay of ^{235}Am in the present work is consistent with this systematics and the present α-decay is a favored transition. Assuming that the α-transition is a ground-to-ground state transition, the Q_α-value of ^{235}Am is estimated to be 6569±14 keV.

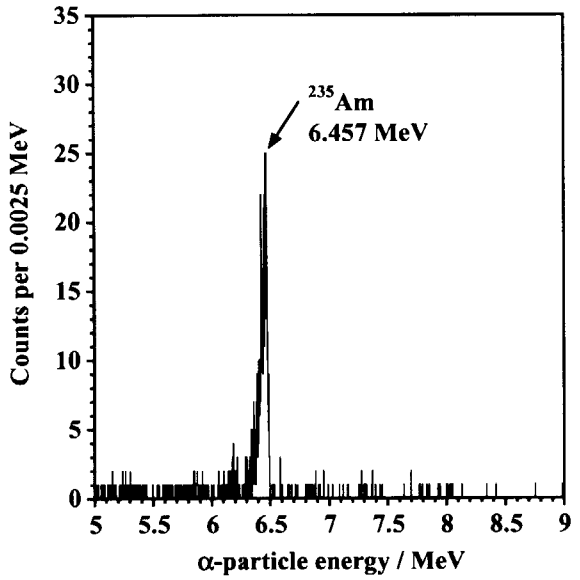

Fig. 2. Summed α-particle spectrum for the mass number A=235 measured with seven Si detectors.

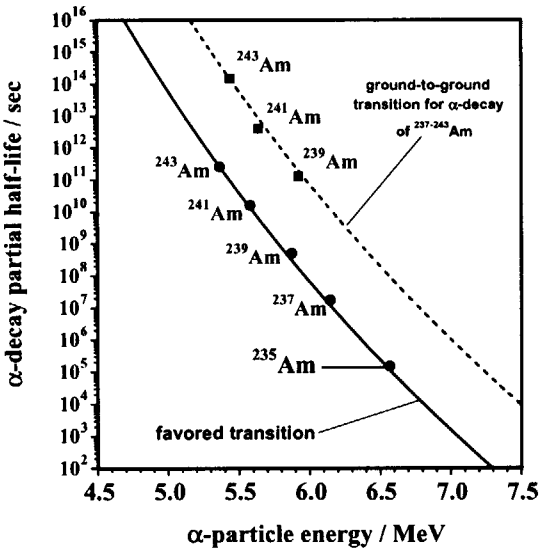

Fig. 3. Partial α-decay half-lives for odd-mass americium isotopes plotted as a function of the α-particle energy. The solid line represents a relationship for favored α transitions of $^{237-243}$Am and the dashed line is that for ground-to-ground transitions of $^{239-243}$Am by an empirical formula by Taagepera and Nurmia [3].

References

[1] M. Sakama *et al.*, JAERI 99-**028** (1999) 20.

[2] S. Ichikawa *et al.*, Nucl. Instrum. Methods B **126** (1997) 205.

[3] R. Taagepera and M. Nurmia., Ann. Acad. Sci. Fenn. Ser. A, No.78 (1961).

2.4 OBSERVATION OF ns-ISOMERS IN NEUTRON-RICH NUCLEI ^{64}Co AND ^{67}Cu

M. ASAI, T. ISHII, A. MAKISHIMA[1], I. HOSSAIN[2], M. OGAWA[2], and S. ICHIKAWA

Excited states in neutron-rich Co, Ni, Cu nuclei provide valuable information on nuclear structure around the Z=28 closed shell. Recent progress in experimental techniques has made it possible to study excited states in these nuclei, *e.g.*, β-decay spectroscopy using a laser ion-guide isotope separator [1], in-beam γ-ray spectroscopy using heavy-ion deep-inelastic collisions by aid of a large array of γ detectors [2,3], and isomer measurements through projectile fragmentations [4]. An isomer-scope we developed can also observe in-beam γ rays from neutron-rich nuclei produced in heavy-ion deep-inelastic collisions by measuring γ rays from only isomers with a lifetime $\geq$1 ns. Using the isomer-scope, we have identified many unknown isomers, and have been studying shell structure around the Z=28 and N=40, 50 closed shells [5–8]. In this report, we present new results for excited states in neutron-rich nuclei ^{64}Co and ^{67}Cu.

The nuclei ^{64}Co and ^{67}Cu were produced by heavy-ion deep-inelastic collisions of ^{198}Pt + ^{76}Ge (8 MeV/nucleon). An annular Si detector placed 55 mm downstream from the target catches projectile-like fragments (PLF's), and γ rays emitted from the stopped PLF's are measured with four Ge detectors by PLF-γ(-γ) coincidences. The atomic number of the PLF was identified using Si ΔE detectors. The mass number of the observed isomer was estimated from an empirical relation between the mass number and kinetic energy of the PLF. The lifetime of the isomer was deduced from PLF-γ time spectra. Multipolarities of γ transitions were assigned through an in-plane to out-of-plane γ-ray anisotropy analysis. Details of the experiments are described in Ref. [5].

Figure 1(a) shows a decay scheme of the 834 keV isomer in ^{64}Co. The half-life of this isomer was determined to be 6.4(3) ns, which indicates that the 64 keV $(5^+)\rightarrow(4^+)$ transition is a hindered $M1$ transition with $B(M1; 64\ \mathrm{keV}) = 0.011(1)$ W.u. This fact suggests that the main component of the (5^+) state is different from that of the (4^+) state. Considering the present experimental results and the nature of the proton-neutron residual interactions, we inferred that the main components of the 834 and 770 keV states were $(\pi f_{7/2}^{-1}\nu p_{3/2}^{-1})_{5^+}$ and $(\pi f_{7/2}^{-1}\nu f_{5/2}^{-1})_{4^+}$, respectively.

A decay scheme of the 3464 keV isomer in ^{67}Cu is shown in Fig. 1(b). Measured PLF-γ time distributions and the flight time of PLF's in the isomer-scope restricted the half-life of this isomer to $0.6 < T_{1/2} < 2.4$ ns. This isomeric transition is considered to be a hindered $M1$ transition from the $(\pi p_{3/2}\nu g_{9/2}\nu f_{5/2}^{-1})_{15/2^+}$ state to the $(\pi p_{3/2}\nu g_{9/2}\nu p_{1/2})_{13/2^+}$ state by analogy with the 3599 keV isomer in ^{66}Ni [2]. The 2503 keV $E3$ transition with $B(E3; 2503\ \mathrm{keV}) > 11$ W.u. was found between the $3/2^-$ ground state and the 2503 keV $9/2^+$ state which has predominantly the $\pi g_{9/2}$ configuration [9]. This fast $E3$ transition between the single-particle states would result from the strong particle-octupole vibration coupling as is also suggested in ^{63,65}Cu [10,11].

[1]Department of Liberal Arts and Sciences, National Defense Medical College
[2]Research Laboratory for Nuclear Reactors, Tokyo Institute of Technology

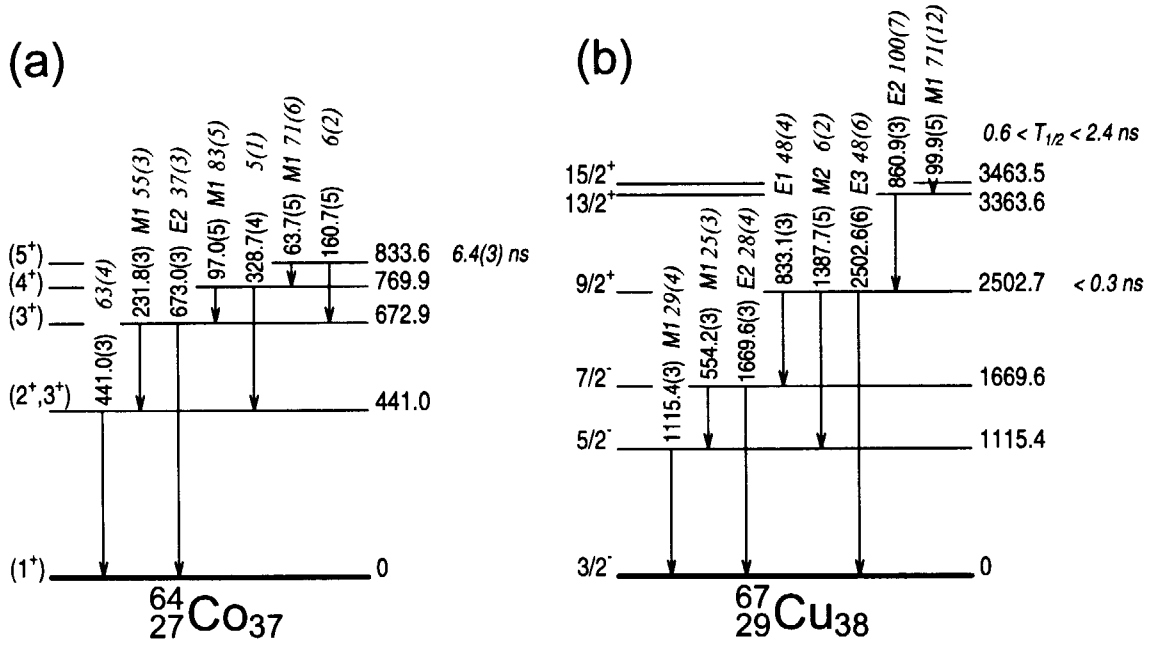

Fig. 1. Decay schemes of (a) the 834 keV isomer in ^{64}Co and (b) the 3464 keV isomer in ^{67}Cu.

References

[1] S. Franchoo *et al.*, Phys. Rev. Lett. **81** (1998) 3100.
[2] T. Pawłat *et al.*, Nucl. Phys. **A574** (1994) 623.
[3] R. Broda *et al.*, Phys. Rev. Lett. **74** (1995) 868.
[4] R. Grzywacz *et al.*, Phys. Rev. Lett. **81** (1998) 766.
[5] T. Ishii *et al.*, Phys. Rev. Lett. **84** (2000) 39.
[6] T. Ishii *et al.*, Phys. Rev. Lett. **81** (1998) 4100.
[7] A. Makishima *et al.*, Phys. Rev. C **59** (1999) R2331.
[8] I. Hossain *et al.*, Phys. Rev. C **58** (1998) 1318.
[9] D. Bucurescu *et al.*, Nucl. Phys. **A189** (1972) 577.
[10] A. L. McCarthy and G. M. Crawley, Phys. Rev. **150** (1966) 935.
[11] A. A. C. Klaasse and V. Paar, Nucl. Phys. **A297** (1978) 45.

2.5 YIELDS OF NEUTRON RICH ISOMERS PRODUCED VIA DEEP INELASTIC COLLISIONS

M. OGAWA[1], I. HOSSAIN[1], T. ISHII, M. ASAI, A. MAKISHIMA[2], S. ICHIKAWA, M. ITOH[1], P. KLEINHEINZ[1] and M. ISHII

Deep-inelastic collisions (DIC) are feasible for study of neutron-rich nuclei [1]. In particular, spectroscopic data on neutron rich nuclei including the doubly magic ^{68}Ni and ^{78}Ni are required to examine the nuclear shell structures for nuclei toward neutron drip line. Isomers contain fruitful information on nuclear shell structures. We have expected isomers of E2 type based on $(g_{9/2})^2$ configuration and of M2 type resulting from $g_{9/2}$-$f_{5/2}$ spin sequence in the mass region of A=60 to 90 [2].

We have performed three DIC experiments at the JAERI tandem-booster facility; (1)^{76}Ge (635 MeV), (2) ^{76}Ge (550 MeV) and (3) ^{74}Ge (625 MeV) projectiles with a ^{198}Pt target. An isomer scope [3] consisting of a γ-ray shield, an annular type of Si detector of 10 cm in diameter and four Ge detectors was employed to intensify the γ rays emitted from the isomers. Projectile-like fragments (PLF) ejected to the grazing angle were stopped with the Si detector where flight time of PLFs was about 1 ns. The PLF kinetic energy measured by the Si detector decreased roughly in proportion to the number of transferred mass, i.e., $\Delta|Z| + \Delta|N|$ [4]. Gamma rays in coincidence with the PLF signals were recorded event by event. Procedure of isomer identification, i.e., assignment of mass and atomic number is explained in our previous works [2-4].

About 40 isomers were observed and 26 of them were identified. Table 1 lists relative yield ratios of I(^{74}Ge)/I(^{76}Ge) where isomer yields of I(^{76}Ge) and I(^{74}Ge) were deduced from experiments 1 and 3, respectively. Less-neutron-rich isomers had the larger yields with the lighter projectile of ^{74}Ge for Ni and Cu isotopes. The similar trend was also observed for As isotopes. Figure 1 shows dependence of isomer yields on projectile energy resulting from experiments 1 and 2. Yield ratios of I(550 MeV)/I(635 MeV) are plotted as a function of isomer mass. Note that the ratios are separated into two groups taking an abrupt jump at the mass of projectile. The mechanism of this jump is not understood. However, the present data indicate that the lower beam energy leads to the higher yields of heavier isomers in the energy region of 7 to 8 MeV/u.

[1]Research Laboratory for Nuclear Reactors, Tokyo Institute of Technology
[2] Department of Liberal Arts and Sciences, National Defense Medical College

Table. 1 List of relative yield ratios of I(^{74}Ge)/I(^{76}Ge). Yield I(^{74}Ge) for ^{65}Ni was not obtained.

^{61}Cu	^{64}Co	^{63}Ni	^{65}Ni	^{66}Ni	^{67}Ni	^{64}Cu	^{66}Cu	^{67}Cu
90	150	317	NA	139	80	280	120	133
^{69}Cu	^{71}Cu	^{67}Zn	^{68}Ga	^{70}Ga	^{70}Ge	^{72}As	^{73}As	^{74}As
42	22	164	165	218	218	131	77	158
^{76}As	^{79}As	^{81}Br	^{83}Br	^{84}Kr	^{87}Rb	^{86}Sr	^{90}Zr	
89	17	74	37	32	119	47	119	

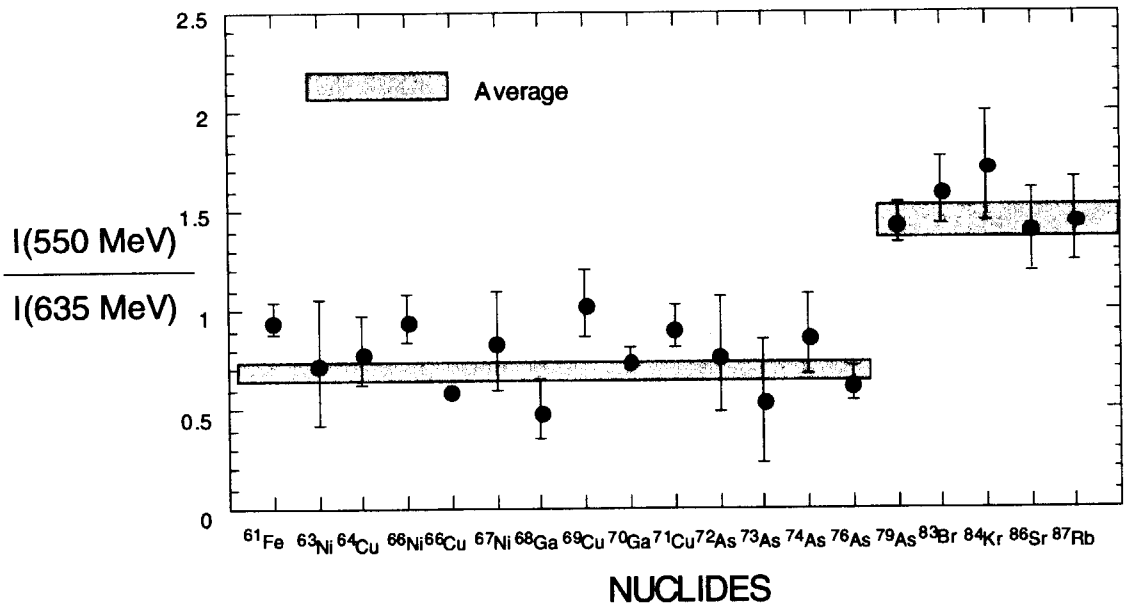

Fig.1. Ratios of isomer yields observed with ^{76}Ge projectile energies of 550 and 635 MeV for different isomers.

References

[1] R. Broda, B. Fornal, W. Królas, T. Pawlat, D. Bazzacco, S. Lunardi, C. Ross-Alvarez, R. Menegazzo, G. de Angelis, P. Bendnarczyk, J. Rico, D. De Acuna, P.J. Daly, R.H. Meyer, M. Sferrazza, H. Grawe, K.H. Maier and R. Schubartet, Phys. Rev. Lett. **74** (1995) 868.

[2] T. Ishii, M. Asai, I. Hossain, P. Kleinheinz, M. Ogawa, A. Makishima, S. Ichikawa, M. Itoh, M. Ishii and J. Blomqvis, Phys. Rev. Lett. **81** (1998) 4100.

[3] T. Ishii, M. Itoh, M. Ishii, A. Makishima, M. Ogawa, I. Hossain, T. Hayakawa and T. Kohno, Nucl. Instrm. Methods **A395** (1997) 210.

[4] I. Hossain, T. Ishii, A. Makishima, M. Asai, S. Ichikawa, M. Itoh, M. Ishii, P. Kleinheinz and M. Ogawa, Phys. Rev. **C58** (1998) 1318.

2.6 MULTIPLE COULOMB EXCITATION STUDIES OF ^{74}Ge BEAM

Y. TOH, T. CZOSNYKA[1], M. OSHIMA, T. HAYAKAWA,
Y. HATSUKAWA, J. KATAKURA, M. MATSUDA, N. SHINOHARA,
H. KUSAKARI[2], D. NISHIMIYA[2], M. SUGAWARA[3], Y.H. ZHANG[4]

The intriguing feature of the low-lying states in even-even germanium, selenium and krypton isotopes has been investigated by a number of experimental and theoretical methods. These isotopes being located around the N=40 semi-closed shell show common low-lying level structure. Previous experimental studies reported that the states of these nuclei have different types of deformation. The nucleus ^{72}Ge is one of a few even-even nuclei having a 0^+ first excited state. It had been proposed that the 0^+ first excited state in ^{72}Ge was a band-head of a strongly deformed band, coexisting with less deformed ground state[1-3]. Recently, however, Kotlinski *et al.* suggested that the 0^+ first excited state is an intruder state and has a spherical structure[4]. The ground and 2_1^+ excited states of ^{74}Ge having 2 more neutrons than ^{72}Ge have been investi-gated by some experimental and theoretical works[5-11]. Other low-lying states such as 2_2^+,0_2^+ and 4_1^+ remain ambiguious. In the present work, the E2 matrix elements related to the five low-lying states in ^{74}Ge were extracted from the primary beam multiple Coulomb excitation coupled with least squares analysis code GOSIA[12].

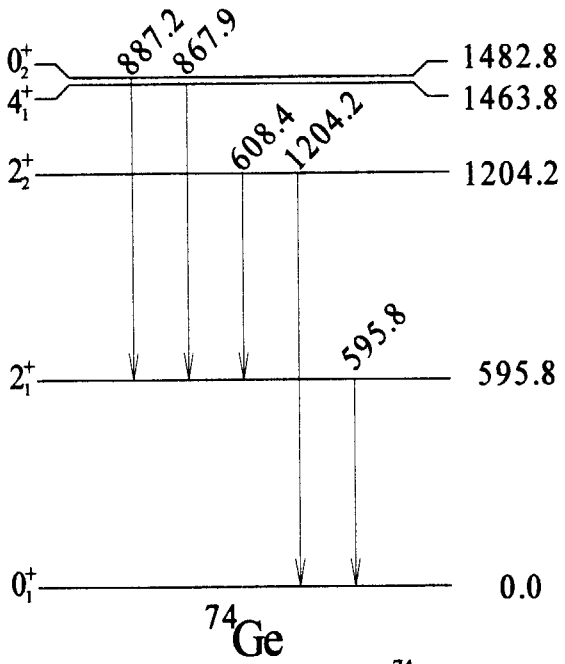

Fig.1. Partial level scheme for ^{74}Ge, related to the five gamma transitions observed in the present multiple Coulomb excitation experiments.

The ^{74}Ge beam of 300MeV and 2pnA from the tandem accelerator was bombarded on a self-supporting ^{nat}Pb target of 1.7mg/cm^2 thickness. The experimental setup, whose details are described suppressors, GEMINI[13], and a newly developed position-sensitive particle detector system with 4 photomultiplier elsewhere, consists of a gamma-ray detector

[1]SLCJ, University of Warsaw
[2]Faculty of Education, Chiba University
[3]Chiba Institute of Technology
[4]Institute of Modern Physics, Chinese Academy of Sciences

array of 12 Ge detectors with BGO anti-Compton tubes in combination with 2 plastic and 2 Yap Ce scintillators[14].

The partial level scheme of ^{74}Ge is shown in Fig.1. A closely spaced $0^+,2^+,4^+$ triplet appears at around twice the energy of the 2_1^+ state. It is viewed as having a structure with a vibrational character. The analysis based on GOSIA code determined the values of 10 E2 matrix elements, and could deduce $<Q^2>$ and $<\cos 3\delta>$ using the code SIGMA[12]. The rotational invariants were evaluated using the measured E2 properties of ^{74}Ge and the centroids are presented in Fig.2. The quadrupole asymmetry, as measured by $<\cos 3\delta>$, indicates triaxial shapes for the low-lying states except the 0_2^+ state which has large statistical error. The centroids $<Q^2>$ of the ground band imply a weakly deformed band while other states are more spherical, indicating shape coexistence in this nucleus.

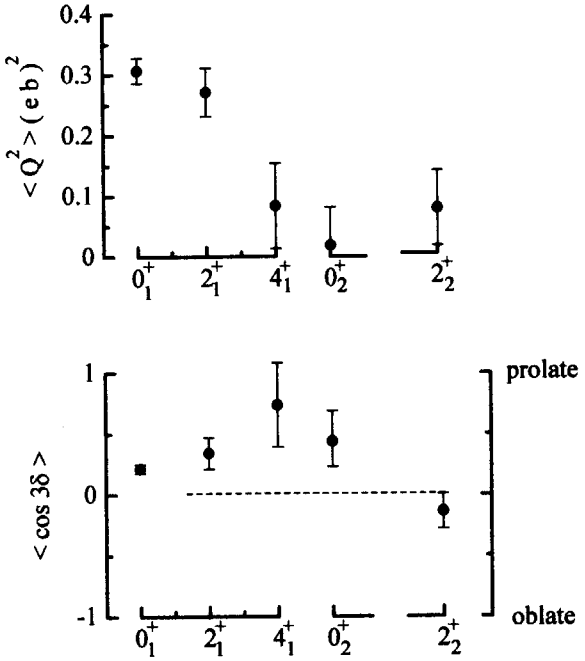

Fig.2. Centroids for Q^2 and $\cos 3\delta$ for the low-lying states in ^{74}Ge.

References

[1] G. Gneuss *et al.*, Nucl. Phys. **A171**(1978) 449.
[2] K. Kumar *et al.*, J. Phys. **G4**(1978) 847.
[3] R. Lecomte *et al.*, Phys. Rev. **C25**(1982) 2812.
[4] B. Kotlinski *et al.*, Nucl. Phys **A519**(1990)646.
[5] R. Lecomte *et al.*, Phys. Rev. **C22**(1980) 1530.
[6] R. Lecomte *et al.*, Phys. Rev.**C22**(1980) 2420.
[7] R. Lecomte *et al.*, Phys. Rev. **C25**(1982) 2812.
[8] K.J. Weeks *et al.*, Phys. Rev. **C24**(1981) 703.
[9] P. D. Duval *et al.*, Phys. Lett. **124B**(1983) 297.
[10] A. Petrovici *et al.*, Nucl. Phys. **A483**(1988) 317.
[11] I. Deloncle *et al.*, Phys. Lett. **B 233**(1989) 16.
[12] T. Czosnyka *et al.*, Nucl. Phys. **A458**(1986) 123.
[13] K. Furuno *et al.*, Nucl. Instrum. Methods Phys. Res. **A421**(1999) 211.
[14] Y. Toh *et al.*, Nucl. Instrum. Methods Phys. Res.**A** (submitted).

2.7 IDENTICAL BANDS BETWEEN ^{153}Sm AND ^{155}Gd

T.HAYAKAWA, M.OSHIMA, Y.HATSUKAWA, J.KATAKURA, H.IIMURA,
M.MATSUDA, S.MITARAI[1], R.SHIMIZU[1], T.SHIZUMA[2],
M.SUGAWARA[3] and H.KUSAKARI[4]

The in-beam spectroscopy on N=91 isotones was carried out using the ^{12}C + ^{150}Nd reaction. The target was a self-supporting ^{150}Nd metallic foil enriched to 96.1 % with 2 mg/cm^2 thickness. Gamma-rays from excited states populated after the reaction were detected with an array of 11 HPGe detectors with BGO Compton suppressors and the Si-ball. The high-spin states of ^{153}Sm were populated through the ^{150}Nd (^{12}C, 2α1n) reaction. The $\nu i_{13/2}$ and $\nu h_{11/2}$ bands of ^{153}Sm were extended up to $33/2^+$ and $31/2^-$ respectively. Two new γ-rays were added on top of the unfavored band with $i_{13/2}$ configuration in ^{157}Dy. The identical bands of the yrast $\nu i_{13/2}$ configuration were found at the low-spin region between ^{153}Sm and ^{155}Gd. The ones of unfavored bands were also found between ^{155}Gd and ^{157}Dy. Here these nulcei have the same neutron number. Fig. 1 shows the energy differences, dE, of the corresponding γ-ray energies , which are subtractions of γ-ray energies in the lighter nucleus from those in the heavier nucleus.

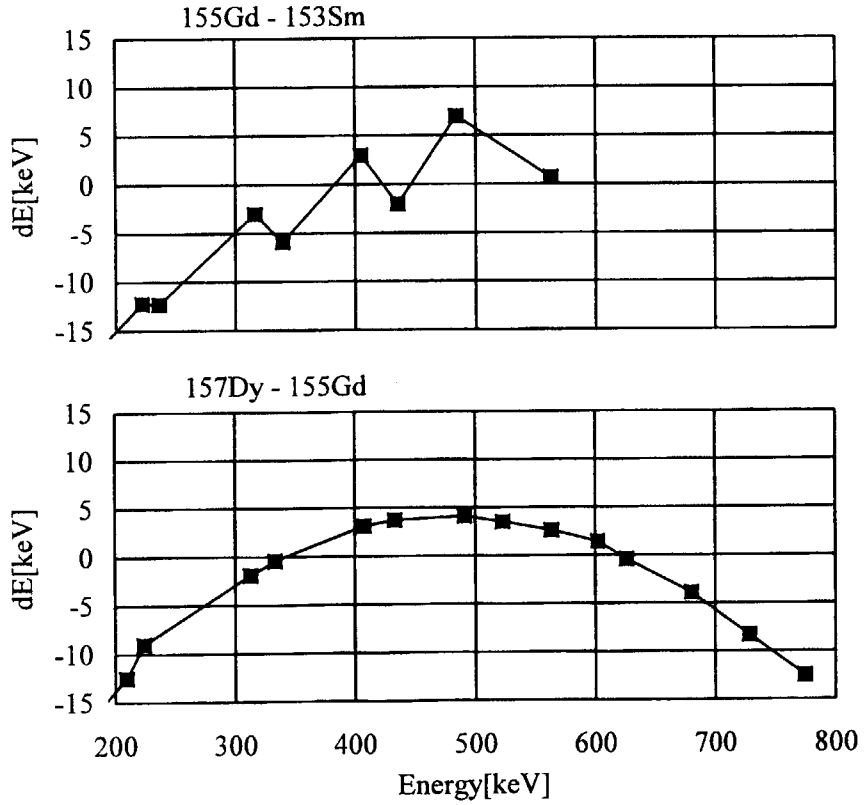

Fig. 1 Energy differences

[1]Kyushu University, Hakozaki, Hukuoka 812-8581, Japan
[2]University of Tsukuba, Tsukuba, Ibaraki 305-8577, Japan
[3]Chiba University, Inage, Chiba 263-8522, Japan
[4]Chiba Institute of Technology, Narashino, Chiba 275-8588, Japan

2.8 HIGH SPIN EXCITED STATES OF ^{154}Sm

H. KUSAKARI[1], M. OSHIMA, T. HAYAKAWA, M. SUGAWARA[2],
Y. TOH, Y. HATSUKAWA, J. KATAKURA and Y. SATO[1]

The nucleus ^{154}Sm with N=92 has very interesting features[1,2]. Excited states of ^{154}Sm have been investigated in Coulomb excitation experiment using a ^{90}Zr beam from JAERI tandem accelerator. Gamma-rays following Coulomb excitation of ^{154}Sm were measured in γ-γ coincidence mode with the Ge-detector array GEMINI. The incident energy of ^{90}Zr beam was 380 MeV. This energy is higher than the safe energy for usual Coulomb excitation experiments, but it is suitable for the purpose of the present experiment because of searching new levels with high spins. The ^{154}Sm target used in this experiment was isotopically enriched and thin metallic foil (2 mg/cm^2) with thick Au backing (5 mg/cm^2). Fig. 1 shows the gamma-ray spectra gated by the 596 keV transition (from 16+) and the transitions from 8+, 10+, 12+ and 16+ states. Analysis of the data in this experiment is in progress.

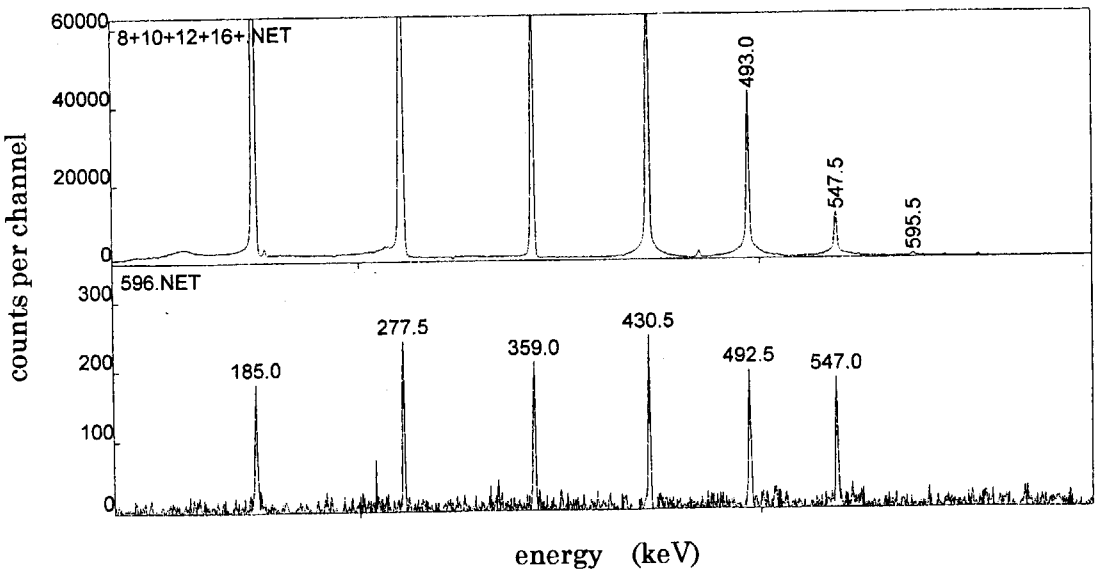

Fig. 1. Gated gamma-ray spectra in Coulomb excitation of ^{154}Sm with a 380 MeV ^{90}Zr beam.

References

[1] T. Morikawa et al., Zeitschrift fur Physik **A343** (1992) 373.

[2] C. W. Reich and R. G. Helmer, Nucl. Data Sheets **85** (1998) 171.

[1] Faculty of Education, Chiba University.

[2] Chiba Institute of Technology.

2.9 DECAY OF 9⁻ ISOMER IN ^{180}Ta BY COULOMB EXCITATION

H. KUSAKARI[1], M. OSHIMA, T. HAYAKAWA, M. SUGAWARA[2],
Y. HATSUKAWA, H. IIMURA and M. SUGIE[1]

The 75 keV 9⁻ state of ^{180}Ta is an isomer with an extremely long life of $T_{1/2} > 1.2 \times 10^{15}$ years, and it seems to have K = 9. Its decay to the 1^+ ground state or the 2^+ first excited state at 40 keV is strongly forbidden. Recent investigations in ^{180}Ta have been reported by Schlegel et al.[1], Schumann et al.[2] and Dracoulis et al.[3]. We have investigated the decay of 9⁻ isomer in ^{180}Ta by Coulomb excitation. The method of the present investigation is explained in Fig. 1. Radiation following the decay of the ground state fed by Coulomb excitation of the 9⁻ isomer of ^{180}Ta was measured. We got the excitation function of these cross sections using 205, 215, 225 and 235 MeV ^{58}Ni beams from the JAERI tandem accelerator. The target used in this experiment was isotopically enriched to 5.7 %. The enrichment of ^{180}Ta in the present target was 475 times higher than the abundance of ^{180}Ta in natural Ta (i.e. 0.012 %). Therefore, we could expect the enough reduction of the contribution from the reaction ^{181}Ta(^{58}Ni, ^{59}Ni)^{180}Ta. The yields of 54.6 keV X-rays ($K\alpha_2$) and 55.8 keV X-rays ($K\alpha_1$) of the daughter nucleus ^{180}Hf were measured, and the population of the ground state fed by the induced decay of the 9⁻ isomer of ^{180}Ta was obtained.

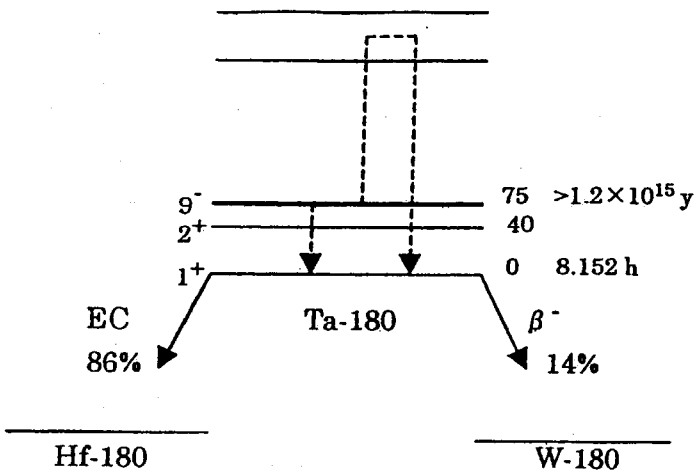

Fig. 1. Coulomb excitation of the 9⁻ isomer in ^{180}Ta and the decay to ^{180}Hf and ^{180}W.

[1] Faculty of Education, Chiba University.
[2] Chiba Institute of Technology.

The measurement of yields of 54.6 keV and 55.8 keV X-rays was repeated at the time interval of two hours, and they were checked to follow the decay curve with the half-life of 8.152 h for the ground state of ^{180}Ta. Similar measurements were done for bombardments of 205, 215,225 and 235 MeV ^{58}Ni beams.

We could obtain the absolute values of Coulomb excitation cross sections of 9$^-$ isomer using the above value of populations and also the values of beam intensities and target thickness. The preliminary result of the obtained excitation function is shown in Fig. 2. The errors shown in Fig. 2 are mainly from uncertainties in the absolute values of beam intensity and target thickness.

In the present Coulomb excitation, there are two possibilities for transitions from the 9$^-$ isomer: one is the direct feeding to the ground state or the 2$^+$ first excited state at 40 keV, and another is the transition via intermediate state. In the latter, we have to assume the weak K mixing between the 9$^-$ isomer and the relevant level. Farther investigation of the present experiment is in progress.

References

[1] C. Schlegel et al., Phys. Rev. **C50** (1994) 2198.
[2] M. Schumann et al., Phys. Rev. **C58** (1998) 1790.
[3] G.D. Dracoulis et al., Phys. Rev. **C58** (1998) 1444.

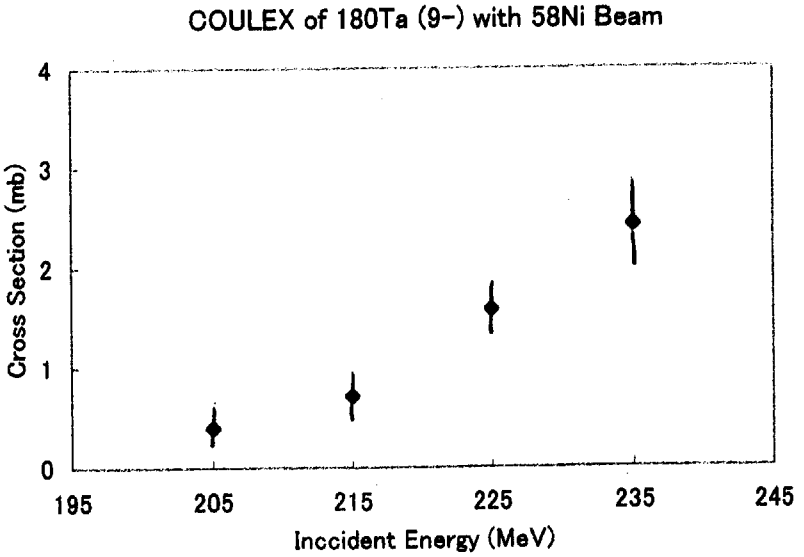

Fig. 2. Excitation function of the induced decay of the 9$^-$ isomer with ^{58}Ni beam.

2.10 ROTATIONAL BANDS OF ^{156}Gd

M. SUGAWARA[1], S. MITARAI[2], H. KUSAKARI[3], M. OSHIMA,
T. HAYAKAWA, Y. TOH, Y. HATSUKAWA, J.KATAKURA,
H.IIMURA, Y. H. ZHANG[4], M. SUGIE[3] and Y. SATO[3]

Nuclear deformations of Gd isotopes show a gradual transition from spherical shape in closed shell to a prolate deformation in neutron rich region. The nucleus of ^{156}Gd(N=92) belongs to the deformed region, and consequently exhibits a band structure with a ground state rotational band and several vibrational (β-, γ-, and octupole-) bands. However, the knowledge on the high-spin states was limited so far because ^{156}Gd is located in the neutron rich region, which means the lack of a suitable projectile and target combination for the ordinary (HI,xn) reaction.

The nucleus ^{156}Gd was produced with the reaction ^{150}Nd (^{13}C, α3n) using a 65 MeV ^{13}C beam. The target was a self-supporting ^{150}Nd metallic foil enriched to 96.1% with a thickness of 2 mg/cm^2. Gamma-rays from excited states populated after the reaction were detected with an array of 12 HPGe detectors with BGO Compton suppressors (GEMINI)[1] in coincidence with the particles detected by the Si-ball[2] made up of 20 detector segments.

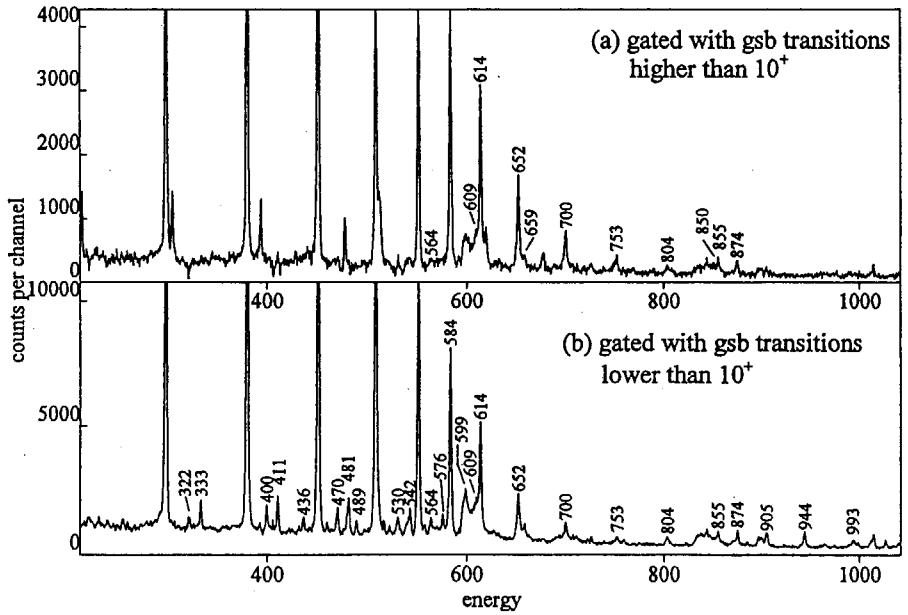

Fig.1 The gated spectra obtained by setting gates on the ground band transitions higher ((a)) and lower ((b)) than the 10^+ state.

[1]Chiba Institute of Technology
[2]Faculty of Science, Kyushu University
[3]Faculty of Education, Chiba University
[4]Institute of Modern Physics, P. R. China

Fig. 1 shows the gated spectra obtained by setting gates on the ground band transitions higher((a)) and lower((b)) than the 10^+ state. Gamma-ray energies are indicated on top of the peaks for some of the intra-band transitions and out-going transitions of side bands. It is seen that the side bands were populated in rather small intensities as compared with the ground band.

The level scheme for ^{156}Gd established in this experiment is shown in Fig. 2. We could extend the ground state band, γ- , and octupole-bands up to 26^+, 16^+, and 21^- states respectively. Additionaly a new band in the energy range from 2.5 to 5MeV was observed. Gamma-ray energies for the intra-band transitions within this band were found to differ by only one or two keV from those of one of the side bands in the isotone ^{158}Dy[3].

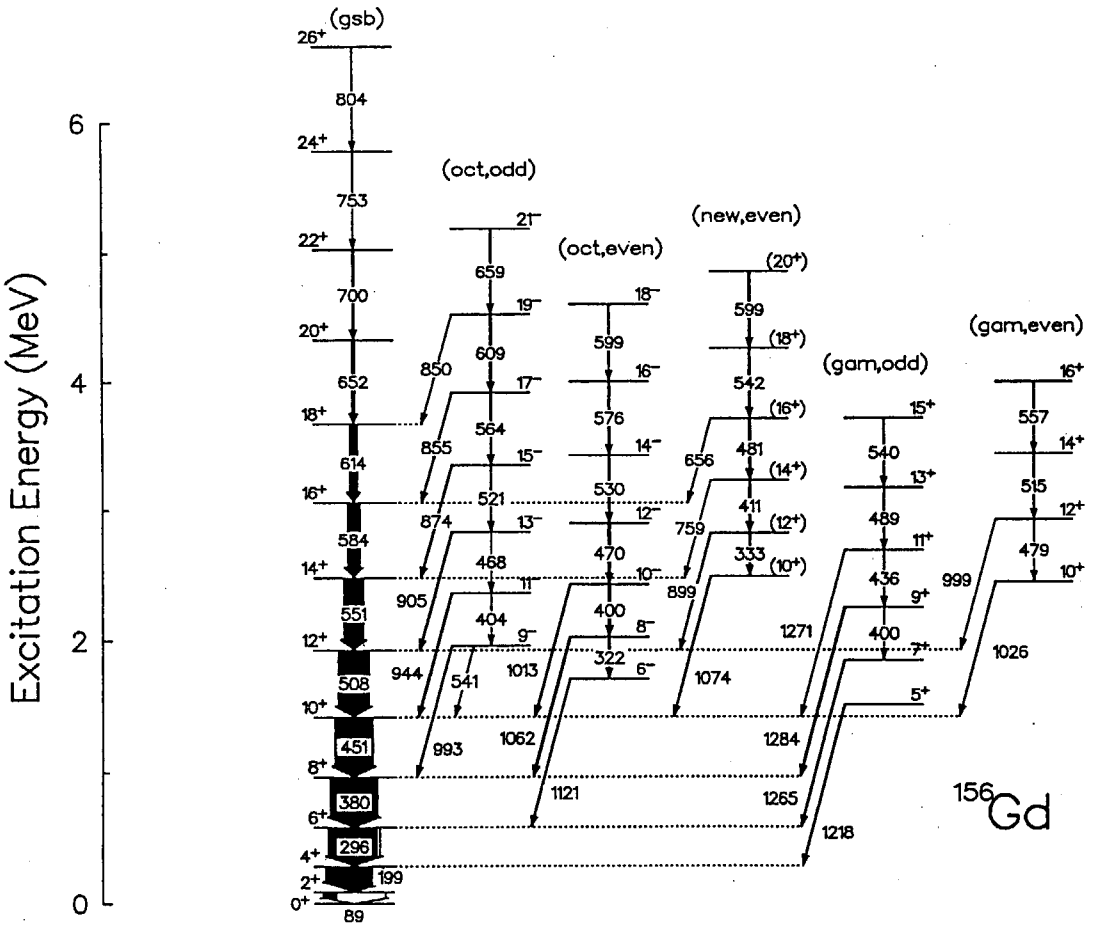

Fig.2 The level scheme for ^{156}Gd established in this experiment which is classified into several vibrational bands as labelled on top of the respective sequences.

References

[1] K. Furuno et al., Nucl. Instrum. Methods **A421**(1999)211.

[2] T. Kuroyanagi et al., Nucl. Instrum. Methods **A316**(1992)289.

[3] R. B. Firestone, V. S. Shirley, C. M. Baglin, S. Y. Flank Chu, and J. Zipkin, Table of Isotopes, Eighth Edition, Wiley Interscience, 1998

2.11 α DECAY OF ^{217}Th POPULATING EXCITED STATES IN ^{213}Ra

K. NISHIO, H. IKEZOE, S. MITSUOKA, J. LU

Experimental investigations of low-lying excited states for the N=125 isotones with even proton numbers near the ^{208}Pb core (^{207}Pb, ^{209}Po, ^{211}Rn and ^{213}Ra) are interesting because of the simplicity of the states at low excitation. The single-particle model predicts that the neutron-hole successively occupies the $3p_{\frac{1}{2}}$, $2f_{\frac{5}{2}}$ and $3p_{\frac{3}{2}}$ orbitals, dominating the configuration of the low-lying states. These states are populated by γ-transition following fusion reactions and by particle stripping and/or pickup reactions. Electron capture and α-decay [1-3] of a precursor also populate these states. The α-decay to the $J^{\pi} = \frac{5}{2}^{-}$ and $\frac{3}{2}^{-}$ excited states as well as the ground state in ^{207}Pb, ^{209}Po and ^{211}Rn have been investigated. On the other hand, for α-decay of ^{217}Th only the decay feeding the ground state in ^{213}Ra has been reported so far [2,4]. We have observed the ^{217}Th α-decay populating the low-lying two excited states in ^{213}Ra [5], which have expected spin and parity of $\frac{5}{2}^{-}$ and $\frac{3}{2}^{-}$, and the branching ratios to these states were determined. We established the excitation energy of the second excited state in ^{213}Ra for the first time.

We have performed ^{28}Si+^{198}Pt fusion reaction to produce ^{217}Th by $\alpha 5n$ channel. The ^{28}Si beam of 140 − 180 MeV was supplied from JAERI-tandem accelerator and used to bombard the rotating ^{198}Pt targets. The ^{198}Pt targets of 460 μg/cm^2 thickness were made by sputtering the enriched material of ^{198}Pt isotope (98%) on a 0.8 μm aluminum foil. The evaporation residues (ERs) emitted to the beam direction were separated in flight from the beam by the recoil mass separator (JAERI-RMS [6]). The separated recoils were implanted into a double sided position-sensitive strip detector (PSD; 73 × 55 mm^2). Two larger area timing detectors positioned at the upstream of the PSD supplied the time-of-flight signal of incoming particles, which separate ER implant events from the subsequent α-decay.

Figure 1(a) shows the typical energy spectrum of α-decay events obtained at beam energy of $E_{\mathrm{c.m.}}$=147.5 MeV. Alpha events in Fig.1(a) are correlated with the implanted ERs within 10 s, and the difference between the position of α-decay and that of implanted ER is less than (ΔX,ΔY)=(0.24, 0.34) mm. On the events appeared in Fig.1(a), we impose conditions that the successive α-decay have ^{213}Ra-character (daughter of ^{217}Th). Thus the chain ER-α_1-α_2 of interest has the time interval ΔT(ER-α_1) of less than 10 s, $0.274 \leq \Delta T(\alpha_1\text{-}\alpha_2) \leq 27.4$ min and $6.422 \leq E_{\alpha 2} \leq 6.831$ MeV. The result is shown in Fig.1(b), where the events measured at $E_{\mathrm{c.m.}}$=132.5 − 155.0 MeV are summed. The large peak noted by A is the α-decay of ^{217}Th feeding the graund state in ^{213}Ra. Events in E comes from the chain ER-^{215}Ac-^{211}Fr, and those in D from ER-^{216}Th-^{212}Ra chain. We consider that the clusters indicated by B and C correspond to the α-decay of ^{217}Th populating the excited states in ^{213}Ra. The E_{α} determined from B and C are 8.713(32)MeV and 8.429(32) MeV, respectively.

The α decay energy was transformed to the α-decay Q value Q_{α}, and the second excited levels in ^{213}Ra was obtained to be 834 keV for the first time. The first excitation energy was 544 keV, which is close to 546 keV obtained by γ-spectroscopy [7]. The branching ratio to these levels is shown in Fig.2. It is found from the systematics of low lying excited states shown in Fig.2 that : (1) the probability of yielding two excited states by α decay increases

with adding proton numbers, and (2) for the α decay of ^{215}Ra and ^{217}Th, decay to the $\frac{3}{2}^-$ state is favored rather than the $\frac{5}{2}^-$ state of the daughter nucleus, forming contrasts to the ^{211}Po α decay. This was explained by the shell-model of α-decay [8,5], where the relative reduced width for specific neutron-orbital and angular momentum has identical value for the nuclei shown in Fig.3. The increasing trend of the branching ratio with a proton number is demonstrated by the calculation, and the strength of populating the $\frac{3}{2}^-$ state is larger than that for the $\frac{5}{2}^-$ state in Z $\geq$86, which is consistent with the experimental results.

References

[1] L.J. Jardine, Phys. Rev. C **11** (1975) 1385.

[2] K. Valli and E.K. Hyde, Phys. Rev. **176** (1968) 1377.

[3] D.F. Torgensen and R.D. Macfarlane, Phys. Rev. C **2** (1970) 2309.

[4] R.B. Firestone, Table of Isotopes, edited by V.S. Shirley (Wiley, New York, 1996)

[5] K. Nishio, H. Ikezoe, S. Mitsuoka, J. Lu, Phys. Rev. C **61** (2000) 034309.

[6] H. Ikezoe *et al.*, Nucl. Instrum. Meth. A **376** (1996) 420.

[7] D.G. Raich *et al.*, Z. Phys. A **279** (1976) 301.

[8] J.O. Rasmussen, Alpha-, Beta-, and Gamma-Ray Spectroscopy, Vol.1 (North-Holland, Amsterdam, 1966) Chap.XI.

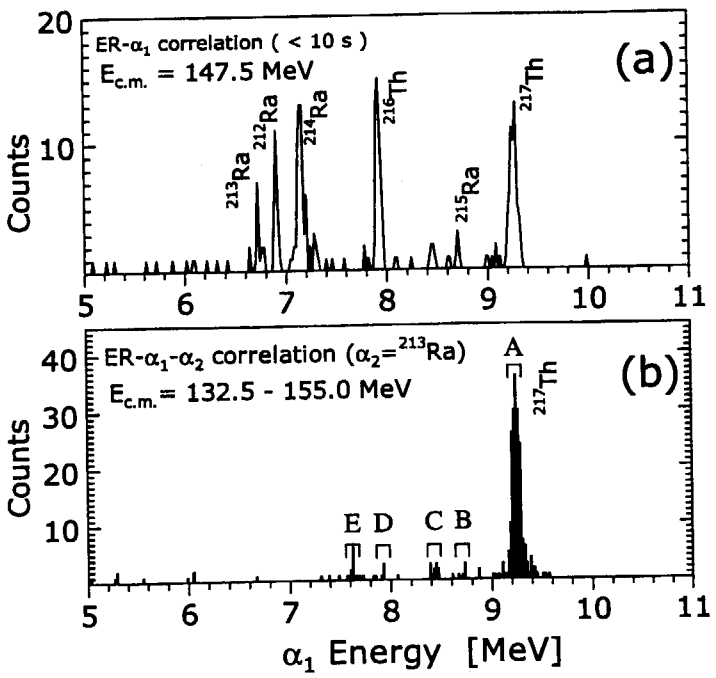

Fig.1. Energy spectrum of α-decay event.

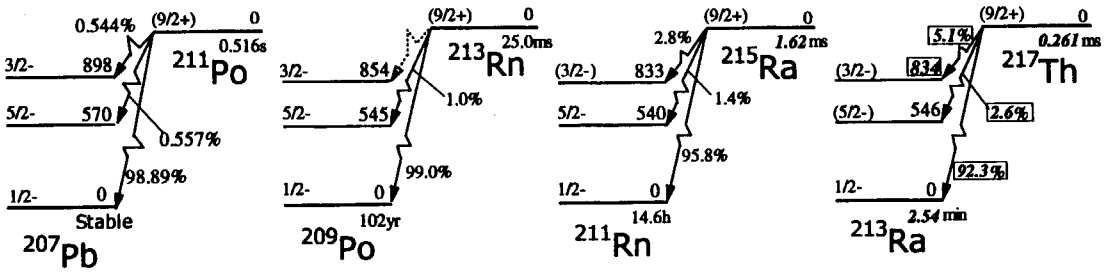

Fig.2. Low-lying states of N=125 isotones with even proton numbers near the ^{208}Pb core. Branching ratio to these levels populated by α-decay is also shown. Numerals indicated by the *italic* symbol represent the present results, in which the quantities in box represent the first results in this work. Other quantities are taken from ref.[4]. No data exits for the decay of ^{213}Rn populating the $J^{\pi} = \frac{3}{2}^{-}$ state in ^{209}Po.

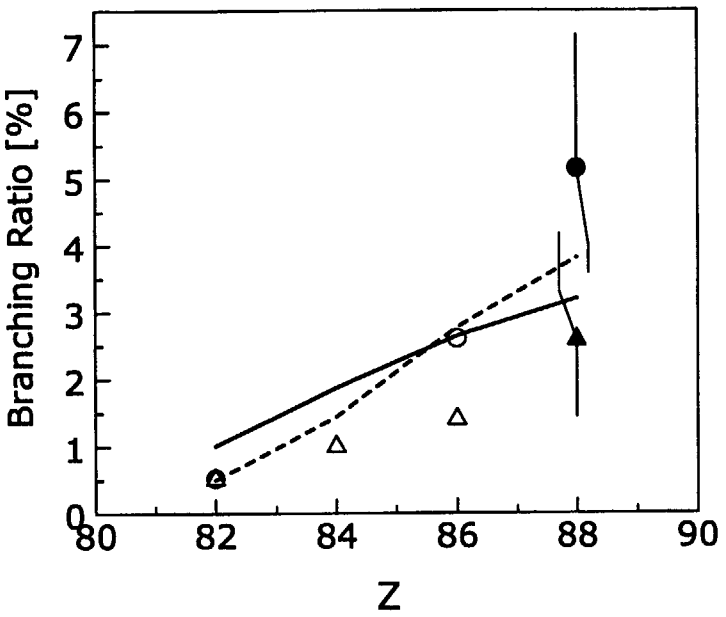

Fig.3. Branching ratio to $J^{\pi} = \frac{5}{2}^{-}$ and $\frac{3}{2}^{-}$ levels as a function of the proton number of daughter nucleus. Calculated results based on the shell-model of α-decay are shown by solid ($\frac{5}{2}^{-}$) and dashed ($\frac{3}{2}^{-}$) curves. Experimental results are shown by triangle ($\frac{5}{2}^{-}$) and circle ($\frac{3}{2}^{-}$), where the present results are shown by solid symbol with error bar.

2.12 HYPERFINE STRUCTURE AND ISOTOPE SHIFT MEASUREMENTS OF La ISOTOPES BY COLLINEAR LASER SPECTROSCOPY

H. IIMURA, Y. ISHIDA[1], M. KOIZUMI, T. SHIBATA, N. SHINOHARA, T. HORIGUCHI[2] and H.A. SCHUESSLER[3]

Collinear laser-ion-beam spectroscopy is superior to conventional spectroscopy methods because it provides mass separation and sub-Doppler resolution. In this work, we have used this technique to study hyperfine structure (HFS) and isotope shift (IS) of La isotopes (Z=57). The La isotopes are in a region of rapid transition from nuclei with nearly spherical shape (the singly magic ^{139}La) to nuclei that are soft towards deformation, presenting a good opportunity to test various nuclear models. There exist two naturally occurring La isotopes: the stable ^{139}La and the long-lived ^{138}La ($T_{1/2}$=1.05x10^{11}y). The nucleus ^{138}La is one of a few primordial odd-odd nuclei, and the natural abundance is very low (0.090%). So far, the HFS and IS of these nuclei were measured by means of Fabry-Pérot interferometer [1] and laser-rf double resonance technique [2]. However, these techniques are available only for LaI, and there is no IS data on LaII. In order to extract changes in nuclear mean-square charge radii from IS data on LaII, a detailed knowledge of the ionic structure of La is essential. Therefore, for later measurement of short-lived isotopes, we have measured the HFS and IS of several transitions in ^{138,139}LaII.

A tunable laser (Coherent 699-29) with rhodamine 110 dye was pumped by an Ar ion laser (Coherent INNOVA-100-20). A set up for polarization spectroscopy of $^{127}I_2$ was used to determine the absolute frequency. The relative frequency of spectral lines was calibrated by a confocal etalon with a free spectral range of 150 MHz (Burleigh CFT-500). The ^{138,139}La ions, part of which are in metastable levels, were produced by a surface ionization ion source. The ions were accelerated to 40 keV and mass-separated by a magnet. The intensity of the beam was typically 3-30 nA for ^{139}La. The metastable ions were excited to upper levels by a counter propagating laser beam. The interaction region was defined by a mesh tube, which was kept at -3 kV. Resonance was observed by detecting the fluorescence light from the upper level to levels close to the ground state. The fluorescence light was collected by an ellipsoidal mirror on to a cooled photomultiplier tube (Hamamatsu R2256). Stray light from the laser beam was suppressed by broad-band filters. Signals from the photomultiplier tubes were counted simultaneously during the laser frequency scanning, and recorded by using a personal computer.

Typical hyperfine spectrum for ^{139}LaII from the metastable $5d^2\ a^3P_2$ level to the $5d6p\ y^1D_2$ level (λ=548.4 nm) is shown in Fig.1. All the hyperfine components are well resolved and assigned as shown in Fig.1, where F quantum numbers are indicated in order of lower state(F')-upper state (F). The linewidth is approximately 80 MHz (FWHM). The spectra for ^{138}LaII were also obtained. From these spectra, the magnetic dipole constant A, the electric quadrupole constant B and the IS were derived. Further analysis including the comparison with the atomic-structure calculations is now in progress.

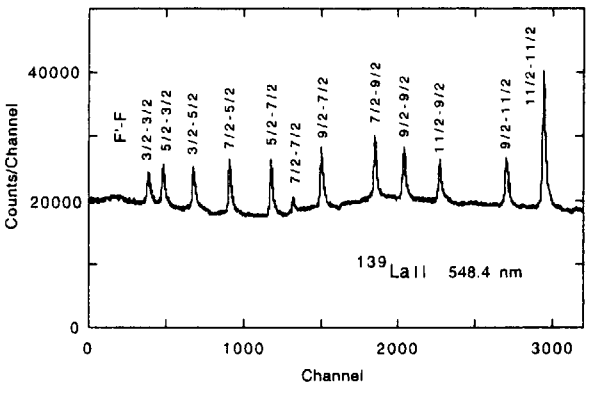

Fig. 1. Typical hyperfine spectrum of the transition a^3P_2-y^1D_2 (λ=548.4 nm) in ^{139}LaII.

References

[1] W. Fischer, H. H'hnermann and K. Mandrek, Z. Phys. 269 (1974) 245.
[2] W.J. Childs and L.S. Goodman, Phys. Rev. A20 (1979) 1922.

[1]High Energy Accelerator Research Organization
[2]Hiroshima International University
[3]Texas A&M University

2.13 EFFICIENCY CALIBRATION OF A Ge DETECTOR IN THE 0.1-11.0 MeV REGION

S. RAMAN[1], C. YONEZAWA, H. MATSUE, H. IIMURA and N. SHINOHARA

A paper on this subject will appear in Nuclear Instruments and Methods.

The creation of an accurate γ-ray detection efficiency curve for a Ge detector over a particular energy range is a straightforward proposition provided that suitable standards exist. Use of the $I\gamma$ values recommended in the IAEA-CRP report [1] can potentially lead to an uncertainty value of about 1-2% for a relative efficiency calibration covering the entire 100-2754 keV region. At the high-energy end, the last calibration point occurs at 2754 keV (from ^{24}Na). Above 2754 keV, however, it is relatively hard to find radionuclides suitable for efficiency calibrations. Extensions of the calibration to 3548 keV or 4807 keV can be achieved using ^{56}Co ($T_{1/2}$=77d) or ^{66}Ga (9.5h) sources, respectively. But the use of ^{66}Ga for precise efficiency calibration was left open only as a future possibility in the IAEA-CRP report. Not only were the uncertainties in the published $I\gamma$ values quite large, but also it was pointed out that the intensities of high-energy γ rays are systematically too small. In this work, the ^{12}C(n,γ) and ^{14}N(n,γ) reactions were used to extend an efficiency curve of a Ge detector to 10829 keV. Then this curve was used to determine the $I\gamma$ values of γ rays from the decays of ^{56}Co and ^{66}Ga and from the ^{35}Cl(n,γ) reaction.

An efficiency curve was constructed for a Ge detector located at the thermal-neutron beam line of the JRR-3M reactor. Active volume of this detector is 111 cm^3 (diameter 5.2 cm). It is surrounded by a bismuth germanate detector for Compton suppression. An initial series of measurements were made with standard radioactive sources of ^{60}Co, ^{88}Y, ^{133}Ba, ^{152}Eu, ^{207}Bi, ^{226}Ra and ^{228}Th. The radioisotopes ^{24}Na, ^{46}Sc, ^{56}Mn, ^{75}Se, ^{110}Ag^m and ^{124}Sb were produced next through neutron activation, and measurements were made using them. After completing the series with the radioactive sources, the study of the ^{12}C(n,γ) and ^{14}N(n,γ) reactions was begun. Each data set gave a segment of the efficiency curve, and then these segments were collapsed into a single curve. An overall uncertainty level of ±1.5% has been established for $0.5 \leq E\gamma \leq 3$ MeV. Above this energy, the standard themselves are not known to accuracies better than about ±1.0%. Therefore, the uncertainty level should be increased to ±2.0%. It has been explicitly demonstrated in this work that the IAEA-CRP data do form a consistent set.

The isotopes ^{56}Co and ^{66}Ga were produced by means of the ^{56}Fe(p,n) and ^{66}Zn(p,n) reactions. Metal foils of iron and zinc were bombarded with proton beams of energy 15 MeV. Our measured $I\gamma$ values for ^{56}Co are in excellent agreement with those recommended in the IAEA-CRP report, while our values for ^{66}Ga are not only consistent but also are more accurate than those given in the same report. The use of the ^{14}N(n,γ) reaction for efficiency calibrations is limited by the small capture cross section (80 mb), which implies a strong neutron source, relatively large amount of target material and long counting times. The ^{35}Cl(n,γ) reaction is favored by many researchers because the cross section is large (43.6 b). The ^{35}Cl(n,γ) reaction was restudied in this work. Our measured $I\gamma$ values are significantly different from those appearing in the IAEA-CRP report (which quotes the values obtained at the Petten reactor [2]) and slightly different from those appearing in the more recent ref. [3] (measurements made at the Mol reactor).

Research supported in part by the US Department of Energy under contract with Lockheed Martin Energy Research Corporation.

References

[1] X-ray and gamma-ray standards for detector calibration, IAEA-TECDOC-619, International Atomic Energy Agency, Vienna, 1991.
[2] A.M.J. Spits and J. Kopecky, Nucl. Phys. A264 (1976) 63.
[3] C. Coceva, A. Brusegan and C. van der Vorst, Nucl. Instr. and Meth. A378 (1996) 511.

[1]Physics Division, Oak Ridge National Laboratory

2.14 ACTIVATION ANALYSIS OF METEORITE SAMPLE BY USING MULTIDIMENSIONAL SPECTRUM METHOD

Y. HATSUKAWA, T. HAYAKAWA, Y. TOH, N. SHINOHARA, M. OHSHIMA

Feasibility of application method of the multidimensional γ-ray spectrum for neutron activation analysis was examined. Reference igneous rock (JP-1, JB-1a and JB-1) samples issued by the Geological Survey of Japan (GSJ) and the Allende meteorite reference sample were irradiated at a research reactor, and multiple γ rays from the produced radioisotopes via neutron capture reactions were measured using an array of twelve germanium detectors with BGO Compton suppressors, GEMINI.[1] Thirty elements were observed with no chemical separation.

The Allende sample[2] was analyzed as meteorite sample. These samples were already powdered and were not subjected to further pulverization. About 100 mg of each powdered samples was weighed and heat sealed doubly in small polyethylene bags (about 10 mm x 10 mm). Multiple γ rays from the radioisotopes produced by neutron capture reactions were measured with GEMINI.

For determination of trace elements observed in the Allende meteorite sample, quantitative determination of trace elements was carried out. The JB-1 sample which was irradiated and measured under the same conditions as the Allende meteorite sample was used as a reference sample. Obtained values of trace elements of the Allende sample are listed in Table 1. All of the values obtained in this study are in good agreement with the reference values. Moreover, γ-rays from ^{75}Se and ^{192,194}Ir were observed in the spectrum from the Allende meteorite sample in this study. However, we could not find any γ rays from ^{75}Se, and ^{192,194}Ir from JB-1 reference sample, so we are not able to determine quantities of selenium and iridium in the Allende meteorite sample by this method.

Reference

[1] Furuno, K., M. Oshima, T. Komatsubara, K. Furutaka, T. Hayakawa, M. Kidera, Y. Hatsukawa, M. Matsuda, S. Mitarai, T. Shizuma, T. Saitoh, N. Hashimoto, H. Kusakari, M. Sugawara, T. Morikawa., Nucl. Instr. and Meth. **A421** (1999) 211.

[2] Jarosewich, E.,. Claeke Jr., R. S., and Barrows, J.N., Smithonian Contributions to the Earth Sciences, **27**, (1987) 1.

Table 1 Result of Quantitative analysis of the Allende meteorite sample by using JB-1 as a reference standard.

Element	This work (ppm)	Previous data[2](ppm)
K	250±100	332±10
Sc	10.2±0.2	11±1
Ca	1.4±0.4 %	1.85±0.07 %
Ti	1200±400	900±10
Fe	23.8±1.6 %	23.57±0.80 %
Co	639±23	600±10
Ga	6.8±1.4	6±1
As	1.38±0.28	0.87- 3
Br	2.0±0.4	1.52 - 1.54
La	0.479±0.026	0.52±0.04
Sm	0.284±0.024	0.34±0.02
Eu	0.13±0.04	0.11±0.01
Tb	0.12±0.05	0.081±0.01
Yb-166	0.40±0.14	0.30±0.02
Yb-175	0.21±0.05	0.30±0.02
Lu	0.046±0.008	0.052±0.006
Hf	0.31±0.06	0.21±0.01
W	0.41±0.06	0.2 - 0.29

This is a blank page.

3. Nuclear Reactions

This is a blank page.

3.1 STRONG ENHANCEMENT OF MULTINUCLEON TRANSFER IN ^{58}Ni+ ^{58}Ni REACTION AROUND THE COULOMB BARRIER

Y.SUGIYAMA, S.HAMADA and A.YAMAZAKI[1]

It was predicted that the nuclear Josephson effect could be observed in pair-transfer reactions between superfluid nuclei near the Coulomb barrier, since the probability of pair-transfer could be enhanced by the coherent nature of the nuclear states in both nuclei[1]. Weiss pointed out from the semiclassical approach that multiple transfer of nucleon pair should be observed if Josephson currents could really exist[2]. In the collision of two nuclei around the Coulomb barrier, a differential cross section $\sigma_{tr}(\theta)$ of a transfer reaction is described well by the following semiclassical approach,

$$\sigma_{tr}(\theta)=<\sigma_{el}(\theta)> \times P_t(\theta) \times F(Q) \qquad (1)$$

where $<\sigma_{el}(\theta)>$ is elastic scattering cross section, $P_t(\theta)$ is transfer probability and F(Q) is a correction factor due to Q-value effect[3]. When we describe multinucleon transfer as a successive process, *x*-nucleon transfer probability of $P_x(\theta)$ can be approximated as

$$P_x(\theta)=(P_1(\theta))^x \quad . \qquad (2)$$

The enhancement of two-nucleon transfer probability ($P_2 > (P_1)^2$) was observed in many systems. However there were no clear evidences of multiple transfer of nucleon pair caused by Josephson currents. We could expect the enhancement of multi pair transfer e.g. $P_4 > (P_2)^2$ in four nucleon transfer if Josephson currents could exist.

So far we made systematic measurements of multinucleon transfer reactions between several Ni isotopes. We measured the cross sections up to four nucleon transfer reactions in the ^{58}Ni+^{58}Ni system. The experiment of the ^{58}Ni+^{58}Ni system was carried out at $E_{c.m.}$=110MeV by using the JAERI tandem accelerator and the heavy-ion magnetic spectrograph "ENMA". In order to identify the mass number we measured a time-of-flight (TOF) of the outgoing particle. For the backward angles from θ_{lab}=27.5° to 45°, we measured kinematic coincidences between the outgoing and recoiling particles with a position-sensitive surface-barrier detector. The coincidence measurement had the advantage that not only precise elastic scattering angular distributions were obtained but also the charge states q of the outgoing particles were clearly identified. An angular distribution of elastic scattering is shown in Fig.1. A fine oscillation originated from the symmetrization of the scattering amplitudes between two identical ^{58}Ni nuclei is observed at backward angles. The solid line is the result of the coupled-channels calculation including the first order couplings to inelastic excitations of collective 2_1^+ and 3_1^- states. The parameters of the optical potential and the couplings are listed in ref.[4].

Energy-integrated angular distributions for the transfer of one up to four particles are shown in Fig.2. Angular distributions show similar shapes for all transfer channels. From the considerations of the charge state distributions and of the Q-value effect, main channels of one-, two-, three- and four-particle transfer can be 1n, 2n, 2n+1p and 2n+2p, respectively. The transfer probability P_x obtained at θ=90° is shown in Fig.3 without the correction factor F(Q). The solid line in the figure is the result of the relation (2). Multinucleon transfer probabilities are enhanced strongly compared with the relation (2). Multiple transfer of nucleon pair P_4 is also enhanced strongly compared with the one obtained from the single pair transfer P_2. These results can suggest a possible existence of the nuclear Josephson effect in the ^{58}Ni+^{58}Ni system.

---

[1]Physics Department, Tohoku University

References

[1] V.I.Gol'danskii and A.I.Lapkin, Th. Eksp.Theor. Fiz.53(1967)1032.
[2] H.Weiss, Phys. Rev. C**19** (1979) 834.
[3] R.Kunkel, W. von Oertzen, B.Gebauer, H.G.Bohlen, H.A.Bosser, B.Kohlmeyer, F.Puhlhofer and D.Schull, Phys. Lett. **20**B (1988) 355.
[4] Y.Sugiyama, S.Hamada, T.Ikuta and A.Yamazaki, J. Phys. G **23** (1997) 1393.

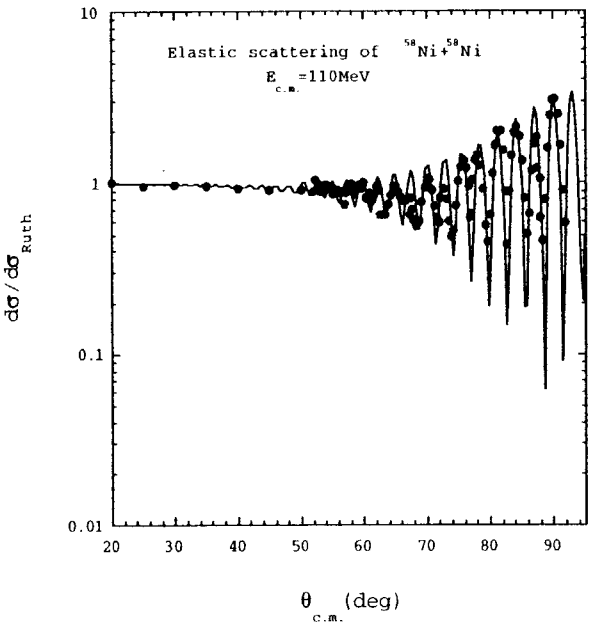

Fig.1 Angular distribution of elastic scattering. The solid line is the result of coupled-channels calculations.

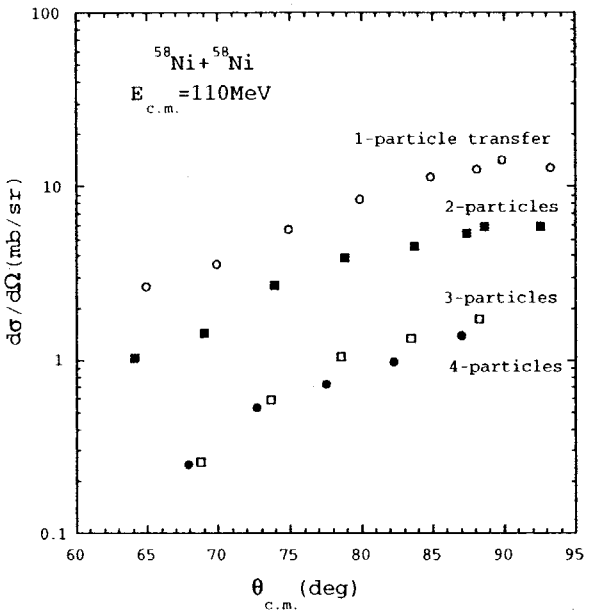

Fig.2 Energy-integrated angular distributions for the transer of one up to four particles.

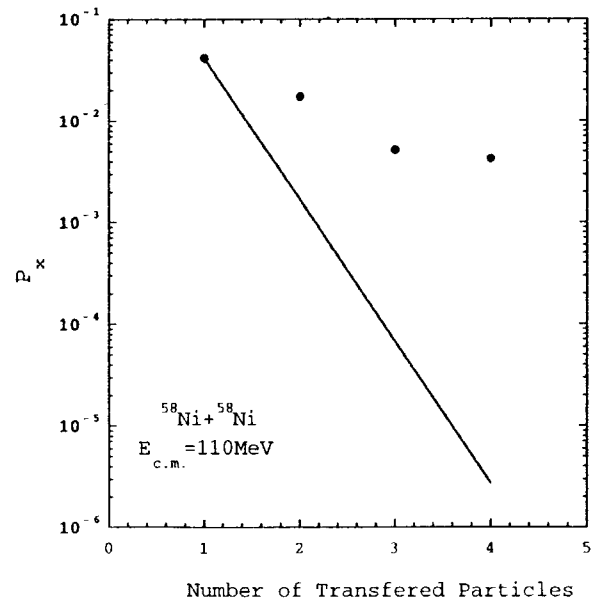

Fig.3 Transfer probability P_x obtained at $\theta_{c.m.}$=90° as a function of number of transfered particles. The solid line is the result of the relation (2).

3.2 SUB-BARRIER FUSION OF ^{64}Ni + ^{154}Sm

H. IKEZOE, S. MITSUOKA, K. NISHIO and J. LU[1]

In the previous measurement of evaporation residues in the reaction of ^{60}Ni + ^{154}Sm [1], we found that the fusion probability was dependent on the collision angle of the projectile ^{60}Ni with respect to the symmetric axis of the deformed target ^{154}Sm. The fusion at the tip of the deformed target ^{154}Sm was hindered by two to three orders of magnitude, while the fusion at the side of the ^{154}Sm nucleus was not hindered at all. This phenomenon was investigated by using ^{64}Ni beams instead of ^{60}Ni, to see how the neutron-rich projectile acts on the sub-barrier fusion especially at the tip collision.

^{64}Ni beams from the JAERI tandem accelerator were used to bombard a ^{154}Sm target of 350 μg/cm thickness. The evaporation residues were separated in flight from the primary beam by the JAERI recoil mass separator [2] and implanted into a double-sided position sensitive detector. The identification of each residue was achieved by observing the α decay events. The obtained cross section of each evaporation channel is shown in Fig.1 together with the predictions (solid lines) of the statistical model [3]. In the present reaction system, the fusion barrier height is varied as a function of the collision angle θ from 173.8 MeV at the tip collision (θ = 0) to 198 MeV at the side collision (θ = 90). The present data clearly show that the fusion is hindered at the energy region of E_{cm} < 200 MeV except a very low energy, while it agrees with the prediction at E_{cm} > 200 MeV. At the very low energy close to the barrier height in the tip collision, the fusion probability recovers. From the present data we could extract the extra-extra push energy as a function of the collision angle. Any extra-extra push energy is not needed at the side collision (70 < θ < 90), while the fusion at the collision angles 10 < θ < 70 requires the extra-extra push energy of about 20 MeV. The extra-extra push energy decreases to be 5 to 10 MeV at the collision angles θ < 10. The present result is consistent with the previous result obtained in the reaction of ^{60}Ni + ^{154}Sm except the case of the tip collision, where the obtained fusion cross section is reproduced by assuming the extra-extra push energy of 20 MeV.

References

[1] S. Mitsuoka et al., JAERI Tandem & V.D.G. Annual Report 1998, p.37.
[2] H. Ikezoe et al., Nucl. Instrum. and Meth. **A376** (1996)420.
[3] W. Reisdorf and M. Schädel, Z. Phys. **A343** (1992) 47.

[1]Institute of Modern Physics, Chinese Academy of Sciences, 730000 Lanzhou, China.

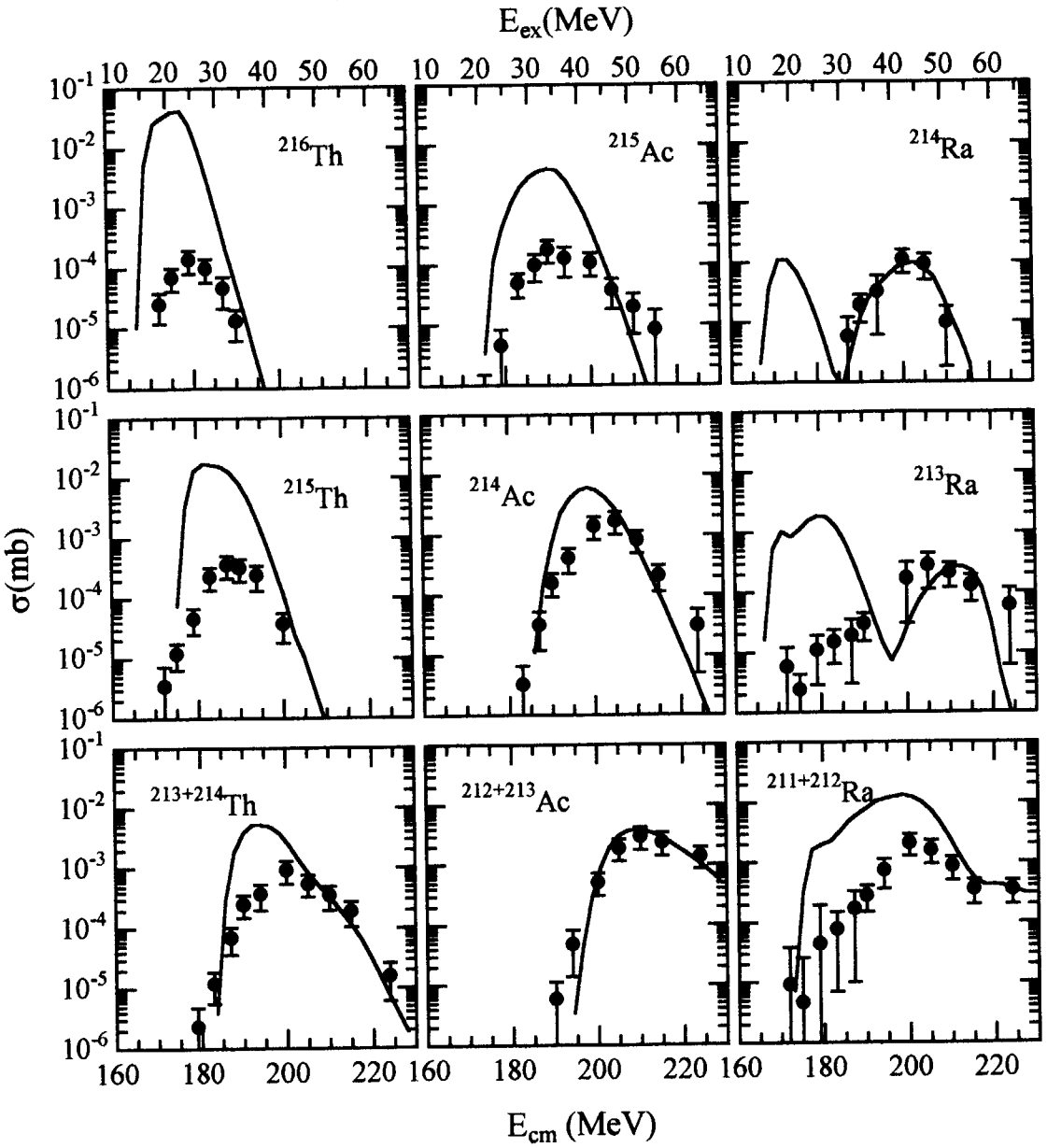

Fig. 1 Measured cross sections of evaporation residues in the ^{64}Ni+^{154}Sm reaction. The solid lines are the calculated results using the statistical model code HIVAP.

3.3 FUSION OF DEFORMED NUCLEI IN THE REACTIONS OF ^{76}Ge+^{150}Nd AND ^{28}Si+^{198}Pt NEAR THE COULOMB BARRIER

K. NISHIO, H. IKEZOE, S. MITSUOKA, J. LU

The synthesis of super heavy elements (SHEs) is one of the important topics in nuclear physics because it gives an insight into the shell stabilization in the vicinity of the double magic nucleus of Z=114 and N=184, without which such a heavy nucleus cannot exist due to the overwhelming repulsive Coulomb force. Recently, an evidence of producing new SHEs was reported [1][2]. Among the α-decay nuclei they have observed, however, there is no nuclei whose decay properties (energy and life-time) are known. Therefore, a further experimental study of synthesizing SHEs and measuring its α-decay properties is important. Production cross section of SHEs using hot- and cold-fusion reaction is extremely low, i.e., pico-barn range, making an investigation of SHEs very difficult. Other approaches of synthesizing SHEs proposed theoretically are the gentle fusion [3] and the hugging fusion [4] which use deformed nuclei as colliding partners. In these cases, there is a certain probability that the deformed target and projectile collide with each other with the symmetry axis being orthogonal, and this specific configulation is expected to lead a compound nucleus with a larger probability than the other configurations.

In order to investigate the effect of nuclear deformation on fusion process, we have measured the evaporation residue (ER) cross sections for ^{76}Ge+^{150}Nd [5]. We also measured the ER cross sections of the ^{28}Si+^{198}Pt system which forms the same compound nucleus and is expected to have no fusion hindrance, as well as the fission cross section that is well approximated to the fusion cross section. Two kinds of cross sections for ^{28}Si+^{198}Pt determined the parameters entering in the statistical model code (HIVAP) [6] which demonstrates the deexcitation of ^{226}U. Assuming that the statistical model code is applicable to the exit channel following the fusion of ^{76}Ge+^{150}Nd, we extracted the effect of nuclear deformation on the fusion process from the ER cross sections.

Measurements of ER cross sections following the fusion of ^{28}Si+^{198}Pt and ^{76}Ge+^{150}Nd were made by using ^{28}Si and ^{76}Ge beams supplied by the JAERI-tandem booster facility. The targets were made by sputtering the enriched material on a 0.8 μm thick aluminum foil. The thickness of the ^{198}Pt (enrichment of 98%) and ^{150}Nd (Nd_2O_3; enrichment of 92.5%) targets were 460 μg/cm^2 and 380 μg/cm^2, respectively. The evaporation residues emitted to the beam direction were separated in flight from the primary beams by the recoil mass separator (JAERI-RMS) [7]. The separated recoils were implanted into a double sided position-sensitive strip detector, and the nucleus for the specific evaporation channel was identified by observing the α-decay energy and life-time. Details of the detection method and data analysis are given elsewhere [5].

The evaporation residue cross sections for ^{28}Si+^{198}Pt are shown in Fig.1 as a function of c.m. energy, and are reasonably reproduced by the statistical model calculation (HIVAP). In this calculation, the spin distribution of the compound nucleus was determined by the coupled channel calculation of the fusion reaction ^{28}Si+^{198}Pt (CCDEF code [8]), which reproduced the fission cross section quite well (see Fig.1). The details of the calculation are found in [5]. Figure 2 shows the ER cross sections for ^{76}Ge+^{150}Nd. The dotted curve in this figure

is the HIVAP calculation coupled with the CCDEF code. Due to the large deformed shape of ^{150}Nd (β_2, β_4)=(0.358,0.107), the fusion barrier height varies with the collision angle of ^{76}Ge on ^{150}Nd and ranges between 184 MeV (tip) and 215 MeV (side). The channels of ^{225,224}U predicted in the calculation were not observed at all in the measurement and the upper limit lies far below the prediction, especially for ^{225}U. This indicates that there is a fusion hindrance when ^{76}Ge collides with the tip of ^{150}Nd. In $E_{\mathrm{c.m.}} > 210$ MeV, the measred data agrees reasonably with the calculation, indicating no fusion hindrance.

We estimated the extra-extra-push energy (E_{XX}) by imposing

$$E_{\mathrm{XX}}(r) = E_{\mathrm{XX0}} \frac{r - R_{\mathrm{side}}}{R_{\mathrm{tip}} - R_{\mathrm{side}}}, \tag{1}$$

where E_{XX0} is the extra-extra-push energy at the tip collision (r=R_{tip}). This comes from the assumption that the more the barrier distance is far away, the additional energy to drive the system into the compound nucleus shape scales with the distance between centers, r, at the Coulomb barrier. The calculation including $E_{\mathrm{XX}}(r)$ is shown by the solid curve in Fig.2, which was obtained with $E_{\mathrm{XX0}} = 13$ MeV, and is consistent with the measured data. Since the fusion is dominated by the side collision in $E_{\mathrm{c.m.}}$ >210 MeV, an extremely large E_{XX0} value also reproduced the experimental data. The 13 MeV should be interpreted as the lowest limit of E_{XX0}. The conclusion reached is the same with our previous work using ^{60}Ni+^{154}Sm fusion reaction. In this system, the extra-extra-push energy of 20 MeV was observed for the tip collision, whereas no fusion hindrance is suggested in the side collision [9].

References

[1] Yu.Ts. Oganessian, *et al.*, Phys. Rev. Lett. **83** (1999) 3154.

[2] V. Ninov, *et al.*, Phys. Rev. Lett. **83** (1999) 1104.

[3] W. Nörenberg, Proc. Int. Workshop on Heavy-Ion Fusion, Padva, Italy (1994)

[4] A. Iwamoto, P. Möller, J.R. Nix, and H. Sagawa, Nucl. Phys. **A596** (1996) 319.

[5] K. Nishio, H. Ikezoe, S. Mitsuoka, and J. Lu, Phys. Rev. C **62** (2000) 014602.

[6] W. Reisdorf and M. Schädel, Z. Phys. A **343** (1992) 47.

[7] H. Ikezoe, Y. Nagame, T. Ikuta, S. Hamada, I. Nishinaka and T. Ohtsuki, Nucl. Instr. Meth. A **376** (1996) 420.

[8] J.O. Fernández Niello, C.H. Dasso and S. Landowne, Comput. Phys. Commun. **54** (1989) 409.

[9] S. Mitsuoka, H. Ikezoe, K. Nishio, and J. Lu, to be published Phys. Rev. C

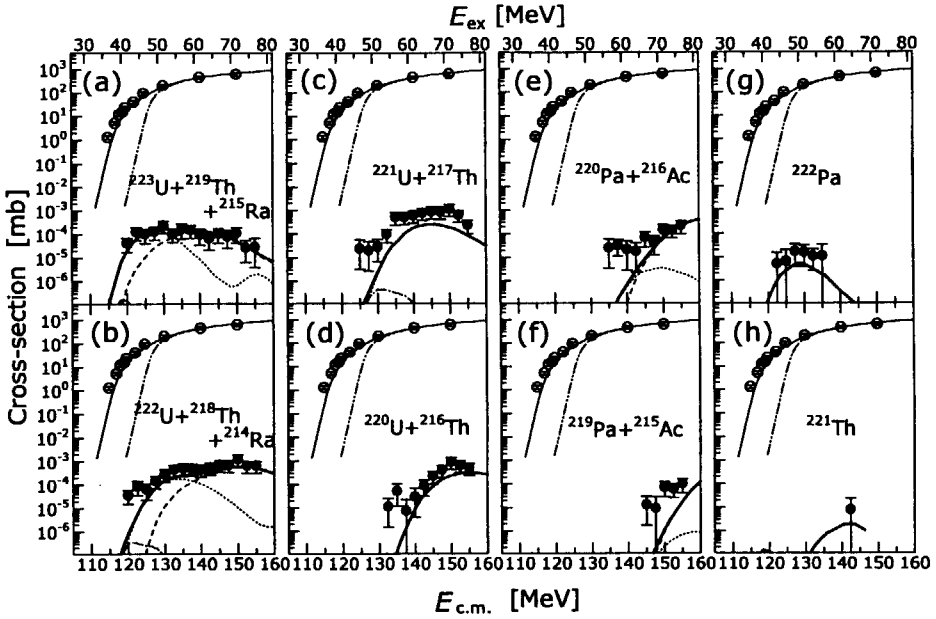

Fig.1. Fusion and evaporation residue cross sections for $^{28}Si+^{198}Pt$ as a function of c.m. energy. Excitation energy of the compound nucleus, E_{ex}, is also indicated. Experimental results of ER cross sections for the specific channel ((a) ~ (h)) are shown by solid circles with error bars. The thick solid curve is the results of the statistical model calculation (HIVAP code) coupled with the CCDEF code. For (a) ~ (f), the cross section includes the components noted in each portion of the figure, and the calculated cross sections of the constituent are show by the dash-dotted (uranium), dotted (thorium or protactinium) and dashed (radium or actinium) curves. Open circles with error bars plotted in every sections are the measured fission cross section. The calculated fusion cross section based on the coupled channels calculation (thin solid) and the one-dimensional barrier penetration model (thin dash-dot-dotted) are also shown.

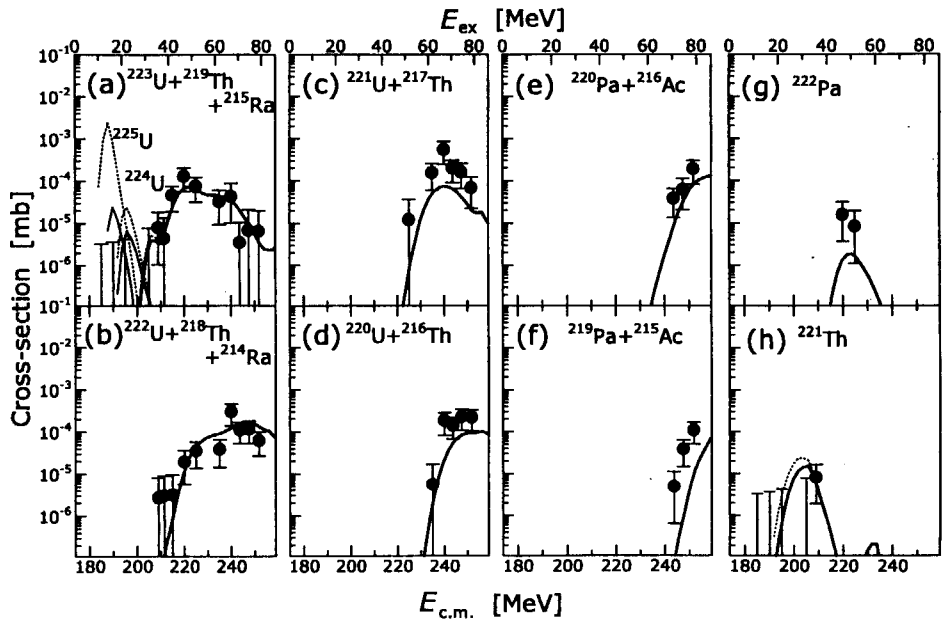

Fig.2. Evaporation residue cross sections for $^{76}Ge+^{150}Nd$ as a function of c.m. energy. Experimental results of ER cross sections for the specific channel ((a) ~ (h)) are shown by solid circles with error bars. In (a) and (h), the upper limit of the ER cross section is indicated with the style of error bar. The dotted curve is the results of the statistical model calculation (HIVAP code) coupled with the CCDEF code assuming no fusion hindrance. One obtains the solid curve when the extra-extra-push energy of Eq.(1) is adopted in the fusion process.

3.4 COMPARATIVE STUDY OF FUSION PROBABILITY BETWEEN ^{82}Se+^{nat}Ce AND ^{76}Ge+^{150}Nd NEAR THE COULOMB BARRIER

K. NISHIO, H. IKEZOE, S. MITSUOKA, J. LU

In our previous measurement of evaporation residue cross section for ^{76}Ge+^{150}Nd [1], we found that there is more than 13 MeV extra-extra-push energy (E_{XX}) for the system to fuse together when the projectile ^{76}Ge collides at the tip of the deformed ^{150}Nd nucleus. On the contrary, for the side collision having more compact configuration than the tip collision, no fusion hindrance was observed. The peculiarity of the fusion process inherent in the fusion of deformed nucleus would be clear when one compares its fusion probability with that for the fusion reaction using spherical nuclei. So, we have measured the evaporation residue cross sectios for ^{82}Se+^{nat}Ce having Z_1Z_2 value of 1972, which is close to ^{76}Ge+^{150}Nd (1920). Measurement was made by using ^{82}Se beams supplied by the JAERI-tandem booster facility. The experimental method and data analysis were similar to that described in [1].

Evaporation residue (ER) cross sections for ^{82}Se+^{nat}Ce are shown in Fig.1 as a function of c.m. energy. We have obtained the fusion probability weighted by the angular momentum l from

$$P_{fus}(E_{c.m.}) = \frac{\sum_c \sigma_{er,c}(E_{c.m.})}{\pi\lambda\!\!\!^{-2} \sum_l (2l+1) \sum_c w_{er,c}(E_{c.m.}+Q, l)}, \quad (1)$$

which involves in the numerator the sum of the measured evaporation residue cross section $\sigma_{er,c}$ over the available channel c. The survival probability against fission for the specific evaporation channel c, $w_{er,c}$, is a function of the excitation energy $E_{c.m.}+Q$(reaction Q-value) and the angular momentum. This was calculated by the HIVAP code [2] using parameters in [1] except the slight modification of the fission barrier scaling factor. Since the angular momentum contributing to the evaporation residue cross section is limited to the small value ($\langle l\rangle$=6$\sim$8 $\hbar$), the P_{fus} in this case can be approximated to the fusion probability of the central collision. The obtained result of P_{fus} for ^{82}Se+^{nat}Ce is shown in Fig.2 by solid circles as a function of $E_{c.m.}$ normalized to the Bass barrier V_{Bass}. Below $E_{c.m.}/V_{Bass} = 1.1$, the P_{fus} sharply decreases with lowering the bombarding energy, exhibiting the curve peculiear to the massive system having fusion hindrance [3]. This fusion probability is compared to the barrier penetrability of the Hill-Wheeler formula,

$$T(E, V_{Bass}) = \left[1 + \exp\left\{\frac{2\pi}{\hbar\omega_B}(V_{Bass} - E)\right\}\right]^{-1}, \quad (2)$$

shown by the dotted curve in Fig.2. The systematics of P_{fus} obtained for the massive and near symmetric fusion [4] tells that the fusion barrier height can be expressed by the Gaussian distribution of mean value $V_{Bass} + E_{XX}$ and standard deviation σ_B. With this assumption, we obtained (E_{XX},σ_B)=(27, 10) MeV for ^{82}Se+^{nat}Ce as the best fit parameters, which were close to the predicted value (21, 8.2) MeV [4]. The obtained fusion probability was adopted to determine the spin distribution of the compound nucleus, with which the HIVAP calculation was made to demonstrate the measured ER cross sections. The results are shown in Fig.1, which agrees with the experimental cross sections.

The open circles in Fig.2 are the fusion probability for ^{76}Ge+^{150}Nd, and compared to the prediction of [4] (dash-dotted curve). The prediction underestimates the experimental data

in $1.00 < E_{\mathrm{c.m.}}/V_{\mathrm{Bass}} < 1.10$, and fails to reproduce the P_{fus} of ^{76}Ge+^{150}Nd. Since the ^{150}Nd is largely deformed, the $E_{\mathrm{c.m.}}/V_{\mathrm{Bass}}$ (V_{Bass}=209 MeV) value varies from 0.88 and 1.02 as a function of the colliding angle of ^{76}Ge against the symmetric axis of ^{150}Nd (see Fig.3). The nearly constant P_{fus} =1 above V_{Bass} shows that there is no fusion hindrance in the side collision of θ_{coll} >50°.

References

[1] K. Nishio, H. Ikezoe, S. Mitsuoka, and J. Lu, Phys. Rev. C **62** (2000) 014602.

[2] W. Reisdorf and M. Schädel, Z. Phys. A **343** (1992) 47.

[3] C.-C. Sahm *et al.*, Nucl. Phys. **A441** (1985) 316. J.G. Keller *et al.*, Nucl. Phys. **A452** (1986) 173.

[4] A.B. Quint *et al.*, Z. Phys. A **346** (1993) 119.

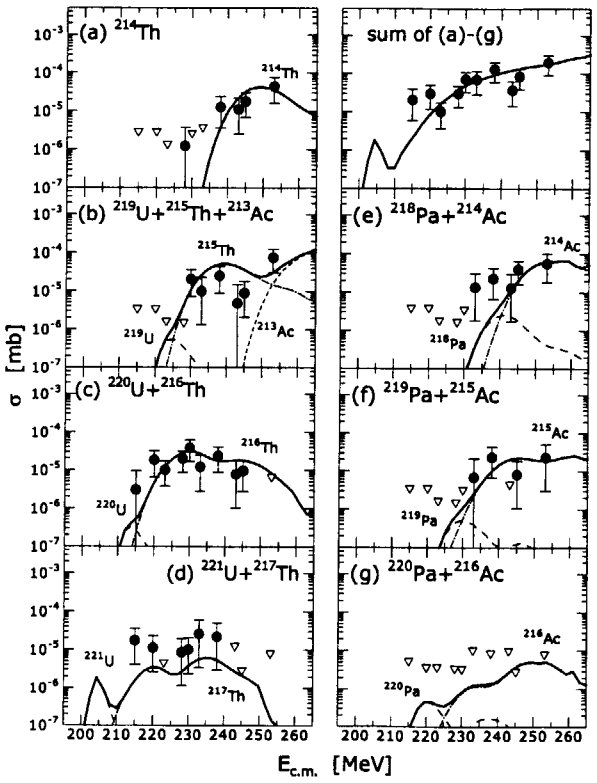

Fig.1. Evaporation residue cross sections for ^{82}Se+$^{\mathrm{nat}}$Ce.

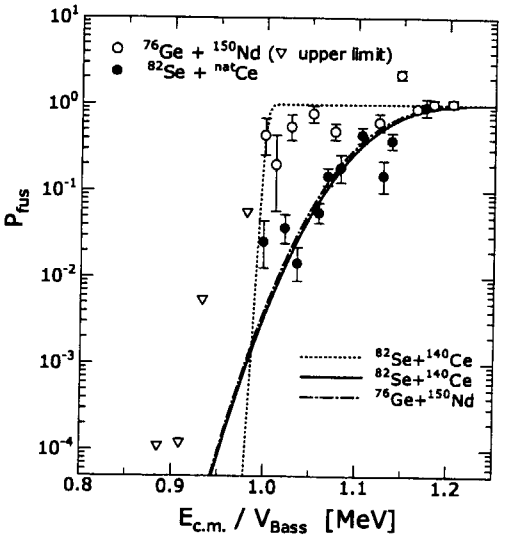

Fig.2. Fusion probability, P_{fus}.

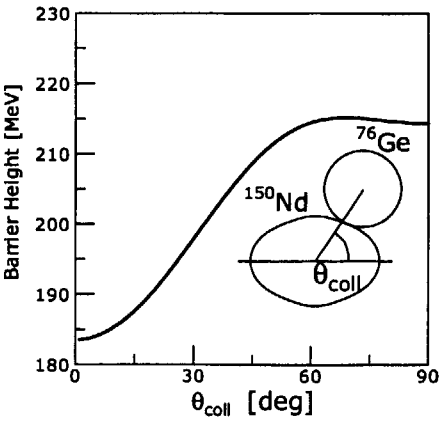

Fig.3. Fusion barrier height as a function of colliding angle for ^{76}Ge+^{150}Nd.

3.5 MEASUREMENT OF MASS YIELD DISTRIBUTIONS IN PROTON-INDUCED FISSION OF MINOR ACTINIDES

N. SHINOHARA, Y. HATSUKAWA, M. OSHIMA, Y. TOH, J. KATAKURA, S. IWAMOTO, K. NISHIO, Y. NAGAME, K. TSUKADA and I. NISHINAKA

Fission product yields of minor actinides have been the subject of interest, because they are essential data in management of radioactive waste from nuclear power plants. Although there are a lot of data on the fission of uranium and plutonium nuclides, the number of measured data on minor actinides is limited [1]. In the present study, the fission product yields of 25- and 30-MeV proton-induced fission of ^{237}Np and ^{248}Cm were measured by γ-ray spectrometry in order to determine the mass yield distributions from the measured values.

Figure 1 shows a γ-ray spectrum of the fission products in the ^{237}Np + p (30 MeV) reaction. Several fission products can be observed in this study and data analysis is now in progress. Measurement of the fission product yields in the proton-induced fission of ^{241}Am and ^{243}Am is planned in the next beam time of the tandem accelerator.

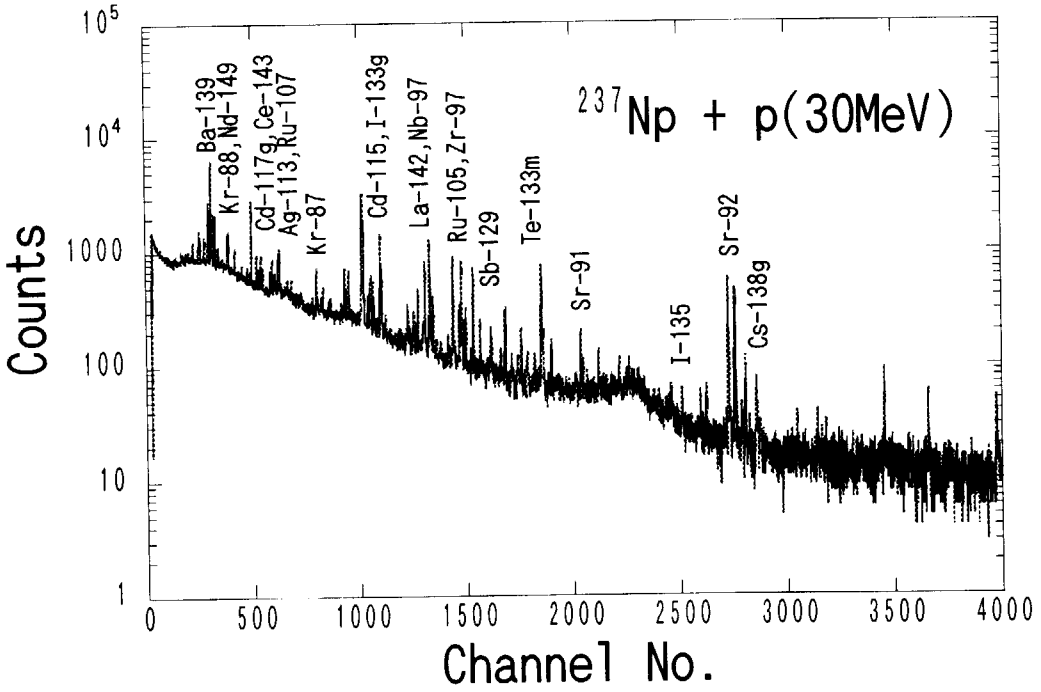

Fig. 1. Gamma-ray spectrum of the fission products produced by the ^{237}Np + p (30 MeV) reaction.

Reference

[1] Z. Qin et al., Radiochim. Acta **84** (1999) 115.

3.6 MASS AND ENERGY DISTRIBUTIONS OF FRAGMENTS IN THE PROTON-INDUCED FISSION OF URANIUM ISOTOPES

S. GOTO[1], I. NISHINAKA, Y. NAGAME, I. ICHIKAWA, K. TSUKADA, M. ASAI, H. HABA, S. MITSUOKA, K. NISHIO, M. SAKAMA[2], Y. L. ZHAO[2], K. SUEKI[2], H. NAKAHARA[2], M. TANIKAWA[3], K. TAKAMIYA[4], Y. HAMAJIMA[5], D. KAJI[1], and H. KUDO[1]

In the low-energy fission of actinides, it has been demonstrated that there exist at least two independent deformation paths; one leads to a symmetric elongated scission conifguration, and the other leads to a compact scission configuration with reflection asymmetry [1]. From the detailed analysis with respect to the asymmetric mass distributions in the proton-induced fission of ^{232}Th, ^{238}U, ^{244}Pu, and ^{248}Cm, it has been found that the lighter side of the heavier asymmetric mass distributions converges on $A = 126$–128, on the other hand, the heavier side of those distributions broadenes with the fissioning nucleus mass number. Those features of the asymmetric mass distribution would be caused by the shell structure of the fragments: heavy fragments with $Z = 50$ and the $N = 50$ shell structure of the complementary light fragments. If the systems with different N/Z are studied, it is expected that the features of the asymmetric mass distribution will become different from those in the above systems because the fragment mass number corresponding with $Z = 50$ and $N = 50$ changes. Thus, to study the relation between the asymmetric mass distribution and the shell structure of the fragments systematically, the fragment mass and total kinetic energy distribution in the proton-induced fission of uranium isotopes, ^{233,235,238}U ($N/Z = 1.52, 1.54, 1.57$), were measured precisely.

Each uranium isotope target (^{233}U: 70 μg/cm^2, ^{235}U: 130 μg/cm^2, ^{238}U: 20 μg/cm^2) on 0.1 μm Ni backing foils was bombarded with 13 and 15 MeV proton beams at the JAERI tandem accelerator. The average beam current was 300–500 nA. Fission fragment velocities were measured by the double time-of-flight (TOF) method. Each start and stop detector of the TOF1 telescope placed at $\theta_{lab} = 50°$ was composed of a carbon foil and a microchannel plate detector (MCPD). A Si surface barrier detector (SSD) was located behind the stop MCPD to measure stop and energy signals. The TOF2 telescope was set around $\theta_{lab} = 128°$ at the opposite side of TOF1 to detect complementary fragments. The start and stop signals of TOF2 were delivered with MCPD and a thin plastic scintillator (10 μm thickness), respectively. The flight path of each telescope was about 96 and 110 cm with solid angles of 0.16 and 4.56 msr, respectively. More than 2×10^5 fission coincidence events were accumulated in each run.

From the measured velocities of the complementary fragments, the mass and the total kinetic energy (TKE) of the fragments were determined. Details of analysis were described in ref. [1]. Figure 1 shows the heavy fragment mass yield distributions of each uranium system

[1]Department of Chemistry, Niigata University
[2]Department of Chemistry, Tokyo Metropolitan University
[3]Department of Chemistry, The University of Tokyo
[4]Research Reactor Institute, Kyoto University
[5]Department of Chemistry, Kanazawa University

at $E_p = 13$ MeV as preliminary result. It is found that the peak position shifts to heavier mass number with the fissionig nucleus mass number in uranium isotopes. More detailed analysis and discussion inclusive of TKE distributions is now in progress.

References

[1] Y. Nagame, *et al*, Phys. Lett. B**387** (1996) 26.

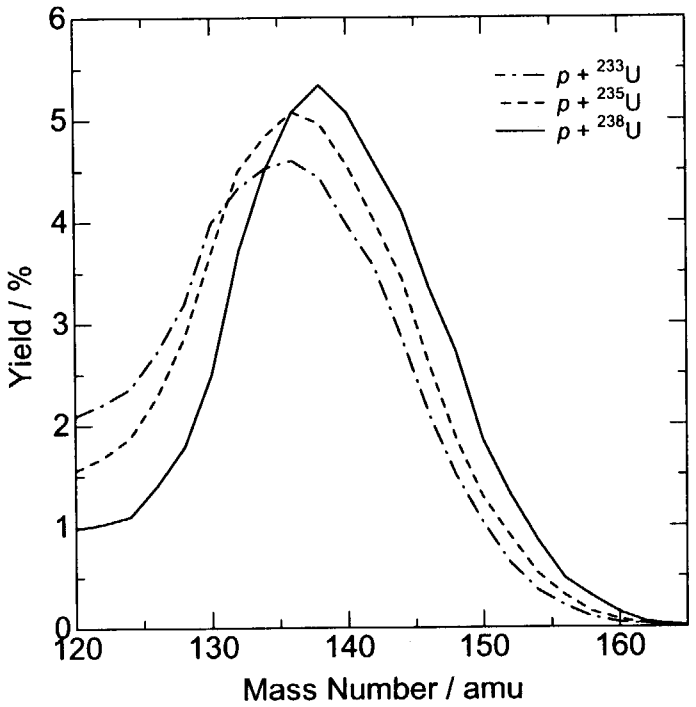

Fig. 1. Heavy fragment mass distributions of the 13 MeV p + ^{233,235,238}U systems.

3.7 STARTUP OF TRANSACTINIDE CHEMISTRY IN JAERI

H. HABA, K. TSUKADA, I. NISHINAKA, M. ASAI, M. HIRATA, S. ICHIKAWA, Y. NAGAME, S. GOTO[1], T. KANEKO[1], H. KUDO[1], A. YOKOYAMA[2], A. TOYOSHIMA[2], Y. SHOJI[2], A. SHINOHARA[2], M. SAKAMA[3], Y. OURA[3], and M. SCHÄDEL[4]

Investigation of chemical properties of the transactinide elements is one of the most interesting and challenging subjects in nuclear chemistry, because deviations in chemical properties from periodicities based on lighter homologues in the periodic table are expected as a consequence of the strong relativistic effects. We first intend to produce element 104, rutherfordium (^{261}Rf) by using the JAERI tandem accelerator, and to perform its chemical experiment in aqueous systems. In the last two years, we have developed a gas-jet coupled target system for production of the transactinide elements and a rotating wheel system for measurement of their α and spontaneous fission (SF) decays. Recently, we have successfully produced ^{261}Rf for the first time in Japan.

The isotope ^{261}Rf has been produced by the ^{248}Cm(^{18}O,5n) reaction. A target chamber coupled to the gas-jet transport system was set in a glove box for handling the radioactive ^{248}Cm target. The ^{248}Cm target of 590 μg/cm^2 in thickness and 5 mm in diameter was prepared by the electrodeposition of $Cm(NO_3)_3$ in 2-propanol onto a 2.1 mg/cm^2 thick beryllium backing foil. The target contained Gd (39.3%-enriched ^{152}Gd) of 35 μg/cm^2 in thickness to produce Hf isotopes. The 112.0-MeV $^{18}O^{6+}$ beam passed through a Havar vacuum window (2.0 mg/cm^2), the helium cooling gas (0.09 mg/cm^2), the beryllium target backing, and finally entered the target material at 99.4 MeV. The average $^{18}O^{6+}$ beam intensity was 200 pnA, and the production rate of ^{261}Rf was estimated to be 0.53 atom/min using the cross section data of 5 nb [1]. The recoiling products attached to KCl aerosol generated by sublimation of KCl powder at 620 °C were continuously transported through a Teflon capillary (2.0 mm i.d., 20 m long) and deposited on polypropylene foils of 240 μg/cm^2 in thickness and 20 mm in diameter at the periphery of an 80-position stainless wheel of 80 cm in diameter. The transport yield was deduced to be about 50% based on the production of ^{165}Hf by the Gd(^{18}O,*x*n) reaction. The wheel was stepped at 30-s time interval to position the foils between six pairs of Si PIN photodiodes. Each detector had an active area of 18 x 18 mm^2 and a counting efficiency of approximately 40% for α particles was achieved. The α-particle energy resolution was about 30 keV full width at half maximum (FWHM) for the top detectors and about 150 keV FWHM for the bottom detectors. All events were registered in an event-by-event mode. The sum of α-particle spectra measured in the six top detectors in a 3.9-h irradiation is shown in Fig. 1. In the α-energy range of 8.05–8.35 MeV,

[1] Department of Chemistry, Faculty of Science, Niigata University

[2] Department of Chemistry, Graduate School of Science, Osaka University

[3] Department of Chemistry, Graduate School of Science, Tokyo Metropolitan University

[4] Gesellschaft für Schwerionenforschung

α lines from 78-s ^{261}Rf (8.28 MeV) [2, 3] and its daughter 25-s ^{257}No (8.22, 8.27, 8.32 MeV) [2] are clearly shown. No contributions from other nuclides were found in this energy window of interest, though there exist several α lines originating from Po, At, Rn, and Fr nuclides which were produced from Pb impurities in the target material. A total of 84 events were registered both in the top and bottom detectors in this energy window, including 18 time-correlated α pairs. Based on these time-correlated events, the half-life values of 55±26 s and 23±6 s were evaluated for ^{261}Rf and ^{257}No, respectively, and they are reasonably consistent with the reported values [2, 3] within the associated errors.

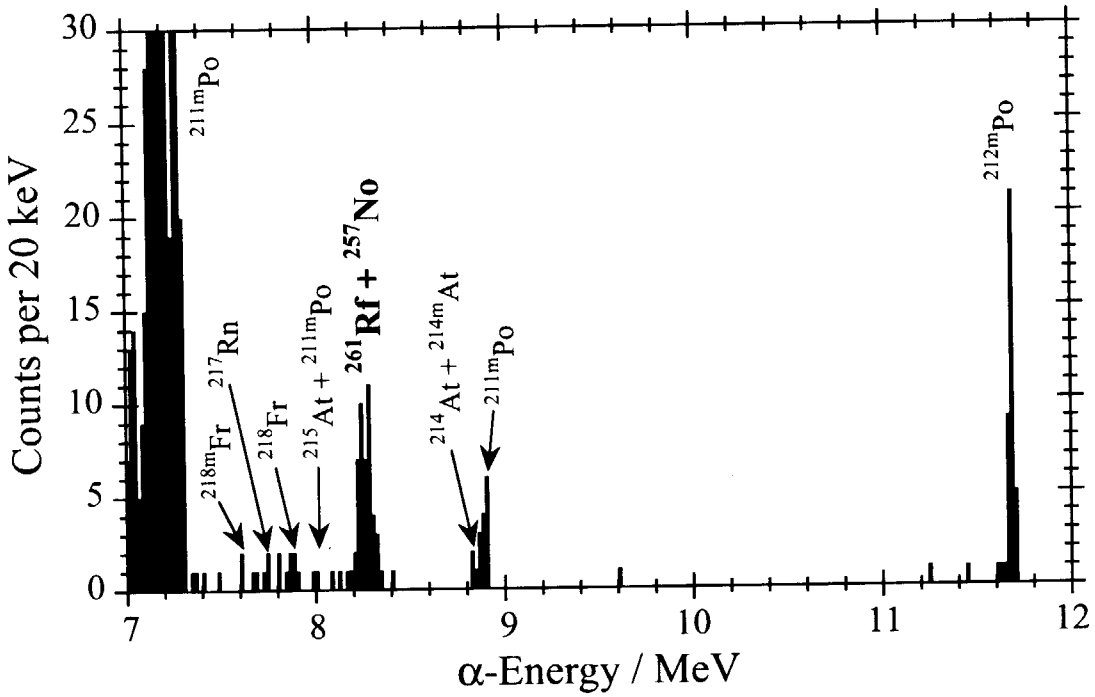

Fig. 1. Sum of α-particle spectra measured in the six top detectors.

Very recently, element 105, dubnium (^{262}Db), was also produced in the ^{248}Cm(^{19}F,5n)^{262}Db reaction at the $^{19}F^{7+}$-beam energies of 106.1 and 102.9 MeV. About 30 time-correlated α pairs of 34-s ^{262}Db [2] and its daughter 3.9-s ^{258}Lr [2] were observed in a 3-d irradiation. The cross section value was preliminarily deduced to be about 1 nb at both energies, though it was four times higher than that by Dressler *et al.* [4] at 106.5 MeV (0.26 nb). The production rate of ^{262}Db is expected to be 0.2 atom/min with the beam intensity of 300 pnA, which motivates us to perform chemical experiments of Db in the near future.

References

[1] A. Ghiorso *et al.*: Phys. Lett. **32B**(1970)95.

[2] R. B. Firestone: *Table of Isotopes*, 8th ed., John Wiley and Sons, Inc., New York (1996).

[3] B. Kadkhodayan *et al.*: Radiochim. Acta **72**(1996)169.

[4] R. Dressler *et al.*: Phys. Rev. C **59**(1999)3433.

3.8 PRODUCTION OF ^{111}In BY PROTON IRRADIATION AND RELATIVE INTENSITY DETERMINATION OF THE 171 AND 245 keV GAMMA-RAYS

H. MIYAHARA[1], N. MARNADA[2], K. IKEDA[2], N. HAYASHI[2], Y. KATOH[2], S. ICHIKAWA, K. TSUKADA, I. NISHINAKA

Usually, there are a few standard sources for efficiency calibration in the energy region between 150 and 200 keV, and ^{75}Se, ^{166}Ho, ^{169}Yb and ^{182}Ta are the candidates for them. ^{75}Se (119 d) emits the 198.6 keV γ-rays, but the emission probability is only 1.5%, and ^{182}Ta (114 d) has similar feature. On the other hand, ^{169}Yb (32 d) emits 177.2 keV γ-rays with probability of 21.75% and 198.0 keV with 35.14%. However, it is difficult to obtain the sources with known activities and it does not emit γ-rays with energy of 200 to 400 keV to normalise the relative efficiency by using other standard sources, for examples, ^{133}Ba or ^{152}Eu. ^{166}Ho (1200 y) is more suitable nuclide that emits 184.4 keV γ-rays with emission probability of 72.58% together with 280.5 and 410.9 keV γ-rays with 29.49 and 11.20%, respectively.

Another candidate is ^{111}In that emits the 171.3 and 245.4 keV γ-rays with high emission probabilities in spite of short half-life. ^{111}In decays by electron capture with half-life of 2.8047(4) d [1]. Evaluated emission probabilities for the 171.3 and 245.4 keV γ-rays are very precise, namely, 0.9066(25) and 0.9409(6), respectively [1]. The high accuracy of emission probabilities for both γ-rays is attractive as a standard source for efficiency calibration of γ-ray detector. However, these values have not been directly determined by measurement. The decay scheme is very simple, and the transitions of 171.3 and 245.4 keV are cascade and the probabilities are almost 100%. The accuracy of γ-ray emission probabilities can be determined from the accuracy of the internal conversion coefficients, because the internal conversion coefficients are relatively large, namely 0.103(3) and 0.0628(7). The purpose of this study is to ascertain experimentally the relative γ-ray intensity with small uncertainty.

^{111}In can be produced by the ^{111}Cd(p,n) and ^{112}Cd(p,2n) reactions and natural Cd foil was used as a target. Therefore, ^{114}In (49.51 d) was also generated by the ^{114}Cd(p,n) reaction. Thin Cd foil with thickness of 25 μm was irradiated by 13 MeV protons. Since the foil evaporated and adsorbed on Al foil enveloped it, the Al foil was dissolved in HCl solution and In sources were prepared on thin VYNS foils. Fig. 1 shows an example of γ-ray spectrum. The measurement was carried out at about a week after irradiation. The 190.27 keV peak by ^{114}In is clearly observed and the ratio of disintegration rate for ^{114}In to ^{111}In was estimated to be about 2.2% at the end of proton irradiation.

The measurements of γ-ray intensity were carried out by a 4πβ pressurised proportional counter, HPGe detector with relative efficiency of 23%, and coincidence apparatus of a two-dimensional data-acquisition system [2]. The γ-ray detection efficiencies were calibrated by measuring the peak areas of the γ-ray spectra and the disintegration rates of standard sources of ^{57}Co, ^{133}Ba, ^{134}Cs and ^{152}Eu. The γ-ray emission probabilities adopted for these standard sources are the evaluated values taken from an IAEA standards report [3]. The obtained data were corrected for

[1] Department of Radiological Technology, School of Health Sciences, Nagoya University

[2] Department of Nuclear Engineering, Graduate School of Engineering, Nagoya University

cascade summing effect by using total detection efficiency curve containing the result of ^{60}Co. A fourth-order polynomial function was used to fit the logarithms of the energy and corrected efficiency values below 800 keV by a method of least squares incorporating a covariance matrix. The detection efficiencies for the 171.3 and 245.4 keV γ-rays of ^{111}In were evaluated from the estimated standard deviations from the fitting function.

The present relative γ-ray intensities and other evaluated values are shown in Table 1 for comparison. The data was mean of the final results for six sources that were corrected also for cascade summing effect. Our result agrees with the other values within the uncertainty. This source can be used for efficiency calibration together with other source such as ^{152}Eu that is commercially obtained with known activity and emits 244.7 keV γ-rays with emission probability of 7.53%. Agreement means only correctness of the ratio of internal conversion coefficients due to its definition, but does not show the correctness of the absolute γ-ray intensities. Future problem in this study is absolute determination of γ-ray emission probabilities.

References

[1] V.P. Chechev, BNM-CEA/DTA/LPRI-Table de Radionucleides (1999).

[2] H. Miyahara, S. Kitaori, Y. Nozue and T. Watanabe, Appl. Radiat. Isot. **40** (1989) 343.

[3] IAEA, IAEA-TECDOC-619, Vienna (1991).

[4] J. Blachot, Nucl. Data Sheets, **77** (1996) 299.

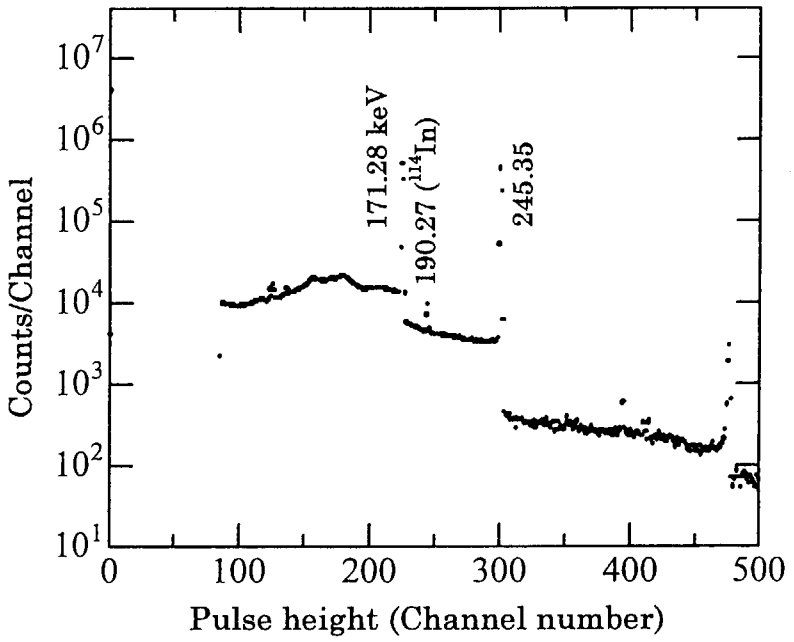

Fig.1. Example of gamma-ray spectrum of ^{111}In. The 190.27 keV peak means the presence of ^{114}In.

Table 1 Relative gamma-ray intensities from ^{111}In

Energy (keV)	Nucl. Data Sheets [4]*	BNM-CEA/DTA/LPRI[1]	Present result
171.28	96	96.35(28)	96.14(24)
245.35	100	100	100

* : Uncertainty is not evaluated

3.9 STUDY OF ACTINIDE METALLOFULLERENES

K. SUEKI[1], K. AKIYAMA[1], Y.L. ZHAO[1], M. SAKAGUCHI[1], M. KATADA[1], K. KIKUCHI[1], H. NAKAHARA[1], K. TSUKADA, Y. NAGAME

For elements in actinides, there were no reports showing a successful production or isolation of actinide metallofullerenes under ambient condition. In this work, we improved and established a reliable method for synthesizing and isolating actinide encapsulated metallofullerenes.

The actinide elements, Am, Np and U were prepared using ^{6}Li beams provided from the Tandem accelerator to bombard onto the metal ^{238}U targets via the reactions of ^{238}U (^{6}Li, 4n) ^{240}Am, ^{238}U (^{6}Li, αn) ^{239}Np and ^{238}U (^{6}Li, pα2n) ^{237}U. The irradiated metal U-foils were dissolved in concentrated nitric acid. The ^{237}U and ^{239}Np were in tern isolated from fission products (FPs) and ^{240}Am using an anion exchange resin method. The Am were then separated from the FPs by a cation resin exchange. The prepared actinide elements were quantitatively added into 0.5 g lanthanum nitrate solution and adsorbed into a 10 mm diameter porous carbon rod. It was heated to 800 °C for about 5 hours in a He gas flow, and then used as an anode electrode for fullerene production by an arc discharge method with a dc current of 110 A under a He atmosphere of 400 Torr. For comparison with known metallofullerenes, the FPs (^{153}Sm, ^{143}Ce) were added into the carbon rod. The soot produced by the arc discharge was recovered by CS_2 solvent, and a crude product containing all such species as hollow fullerenes (C_{60}, C_{70} etc.) and metallofullerenes were extracted from the soot. A part of crude that was dissolved into toluene and was injected into a Buckyprep HPLC column with toluene as the mobile phase. The elution rate was 3.2 *ml*/min. The other was injected into a 5PBB HPLC column with toluene as the mobile phase, the flow rate being 6.0 *ml*/min. The species from the HPLC column was on-line monitored using a UV detector at 340 nm and off-line X, γ-ray measurements of eluate fraction (2min) by a LEPS detector. The amount of each element going to any fraction of each chemical step was determined using low background X, γ-ray spectrometry.

The production yield for actinide elements to form metallofullerene compounds is 0.1 % and it is as high as Lanthanide's. Figure 1 shows the elution curves from the 5PBB HPLC column, the elution peaks of Am, Np and U are observed about 50 min of retention time. It gives the same retention time with that of the Ce@C_{82}. Figure 2 shows those from the Buckyprep HPLC column, the peaks of Am, Np and U are observed about 60 min of retention time. It also gives the same retention time with the Ce@C_{82}. The results of two elution curves indicate a successful

[1]Department of Chemistry, Tokyo Metropolitan University

production of new actinide encapsulated fullerenes.

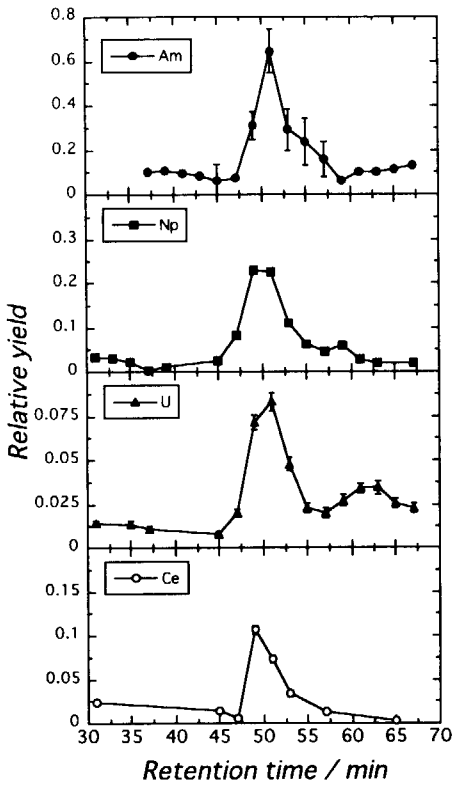

Fig. 1. The elution curves of radiotracers (^{237}U, ^{239}Np, and ^{240}Am) from a 5PBB column.

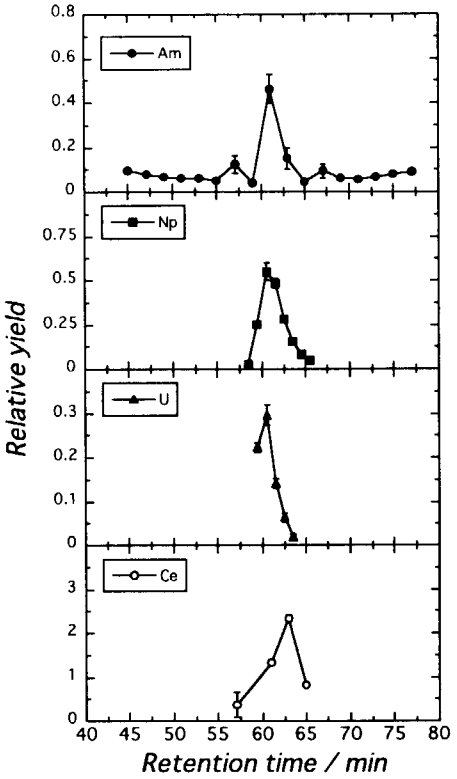

Fig. 2. The elution curves of radiotracers (^{237}U, ^{239}Np, and ^{240}Am) from a Buckyprep column.

4. Nuclear Theory

This is a blank page.

4.1 QMD SIMULATION OF EXPANDING NUCLEAR MATTER

S. CHIKAZUMI, [1] T. MARUYAMA, K. NIITA, S. CHIBA, A. IWAMOTO

The study of nuclear matter has been undertaken concerned with several topics in nuclear physics. In particular, the phase transition of nuclear matter is an attractive topic. Our target is the nuclear matter with homogeneous expansion [1]. On the basis of quantum molecular dynamics (QMD) [2] simulation, we investigate the expanding nuclear matter as a model to study multi-fragmentation in heavy ion collision.

To simulate infinite system with collective motion, we introduce an extended periodic boundary condition [3] with QMD. In terms of molecular dynamics, homogeneous expansion means that any pair of two particles has relative momentum proportional to its distance. We control this ratio by one parameter h as follows.

$$\mathbf{P} = h\frac{\mathbf{R}}{\rho_0^{-\frac{1}{3}}}P_F, \tag{1}$$

where P_F is the Fermi momentum at ρ_0 (saturation density). Before we give this collective motion to the system, we prepare the nuclear matter with a certain temperature T at ρ_0. After that, we give the above collective momentum to each nucleon. From ρ_0 to $0.05\rho_0$, we perform the time evolution of expanding matter and investigate how the fragmentation occurs in expanding matter. We perform this time evolution 1000 times for each (h, T) and examine fragment mass distribution at the final state. Our main purpose is to investigate how this distribution depends on (h, T).

Figure 1 shows the fragment mass distribution for the initial temperature $T = 30$ (MeV). The parameter h describing the expanding velocity is set at $h = 0.1, 0.5, 1.0$ and $h = 2.0$ respectively. Notice the abscissa is semi-log scale. The linear shape under this scale means that the fragment yield decreases exponentially as a function of fragment size. Furthermore, the slope depends on h. Namely, the slope becomes steeper as h increases. This results are consistent with the data of heavy ion collision with large radial flow [4].

Figure 2 shows the same data as above, but the abscissa is changed into log-log scale. This time only $h = 0.1$ has linear shape. The linear shape in log-log scale refers the power law which is thought to describe the occurance of the second-order phase transition. This power law behavior is similar to the data of spectator fragmentation [5]. However, the power law in expanding system can not be explained by any models assuming thermal equilibrium, because the system is completely non-equilibrium in expanding matter. We tried the same calculation for the initial temperature $T = 5$ (MeV). This is clearly lower than typical critical temperature. Nevertheless, we also get the power law for $h = 0.1$. We can conclude that the system with power law is not necessarily a signature of critical state occurring in thermal equilibrium.

[1]Institute of Physics, University of Tsukuba

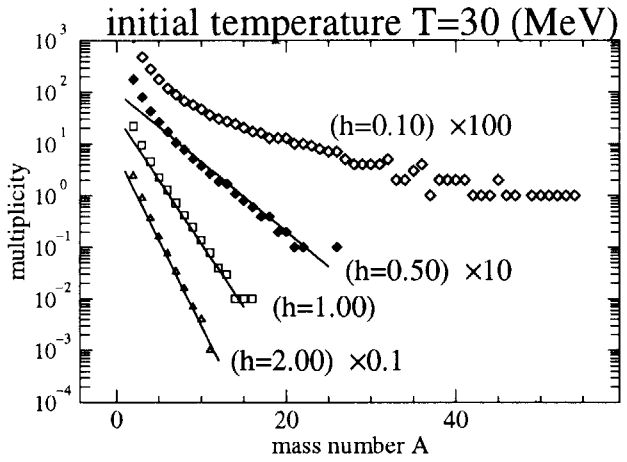

Figure 1: The fragment mass distribution for initial temperature $T = 30$ MeV and $h = 0.1, 0.5, 1.0$ and $h = 2.0$ in semi-log scale.

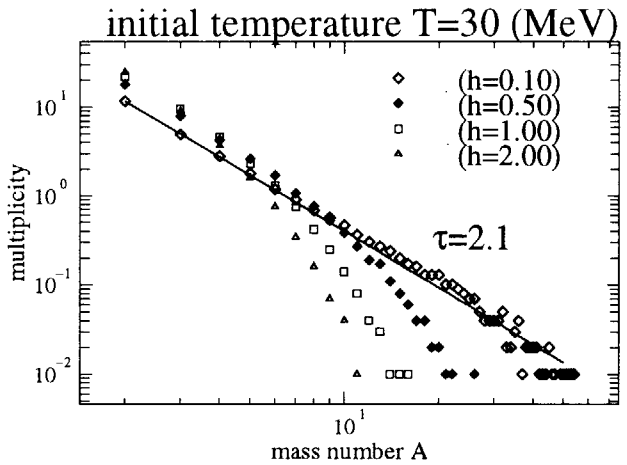

Figure 2: The fragment mass distribution in log-log scale. The data used in this figure is same as Figure 1.

References

[1] S. Chikazumi, T. Maruyama, K. Niita and A. Iwamoto, Physics Letters, **B476** (2000) 273.
[2] T. Maruyama, K. Niita, K. Oyamatsu, T. Maruyama, S. Chiba, and A. Iwamoto, Physical Review, C**57** (1998) 655.
[3] B. L. Holian and D. E. Grady, Physical Review Letters **60** (1988) 1355.
[4] W. Reisdorf et al, Nuclear Physics, **A612** (1997) 494.
[5] J. B. Elliot et al, Physics Letters, **B418** (1998) 34.

4.2 MASSES OF NUCLEI IN STRONG MAGNETIC FIELDS

V.N. KONDRATYEV [1], T. MARUYAMA and S. CHIBA

Transitional metals of iron series are well known [1] to represent the mostly bound nuclei at laboratory conditions. The associated magic numbers are determined by the pronounced shell-closure related to the minima of shell-oscillations in nuclear masses. As we have found recently [2] the magnetic field B can modify dramatically shell-correction components of binding energies leading to a change of nuclear magics. The predominant mechanism of such a modification can be interpreted as a phase-shift in shell-oscillations originating from a field dependent interference of contributions coming from majority- and minority-spin energy levels. Figure 1 demonstrates the shell-correction energy at various values of $b = \mu_N B/\omega$ with the nuclear magneton μ_N and $\omega = A^{-1/3}41$ MeV for nuclei of mass numbers A in the vicinity of the stability line.

For neutrons (fig. 1(a)) this effect is entirely given by the Pauli-type paramagnetic response. As a consequence, the neutron shell-correction energy displays almost periodic behavior as a function of the magnetic field strength.

The proton magnetic response is determined by the relationship between spin- and orbital-magnetism. Apart from a shift of the magic numbers the magnetic field enhances the proton shell-effect due to a reinforcement of the degeneracy of spin-down levels. As demonstrated in figs. 1(b) and (c) such an enhancement is particularly pronounced when the level splitting induced by the interaction of the orbital-magnetic-dipole moment with a field is comparable to the spin-orbit coupling.

Therefore, nuclear magic numbers corresponding the vicinity of the stability line depend on the magnetic field and are changed considerably (fig. 1(d)) at the strength scale $B \sim 10^{16} - 10^{17}$ G relevant, e.g., for supernovas and neutron stars. At such a field strength the nuclear magics of the iron region are shifted towards smaller mass numbers.
As a matter of fact, the nuclear level density represents an important ingredient to the prediction of nuclear reaction cross sections. Therefore, our analysis indicates possible dependence of the nuclear reaction (e.g. s- and r-processes) rates on the magnetic field implying a variety of the nucleosynthesis scenario.

We note finally that similar modification of magic numbers can show up in e.g. atomic clusters suggesting a possibility for laboratory tests of the predicted phase-shift of shell-

[1]on leave from: *Institute for Nuclear Research, 47, Pr.Nauki, Kiev, 252028 Ukraine*

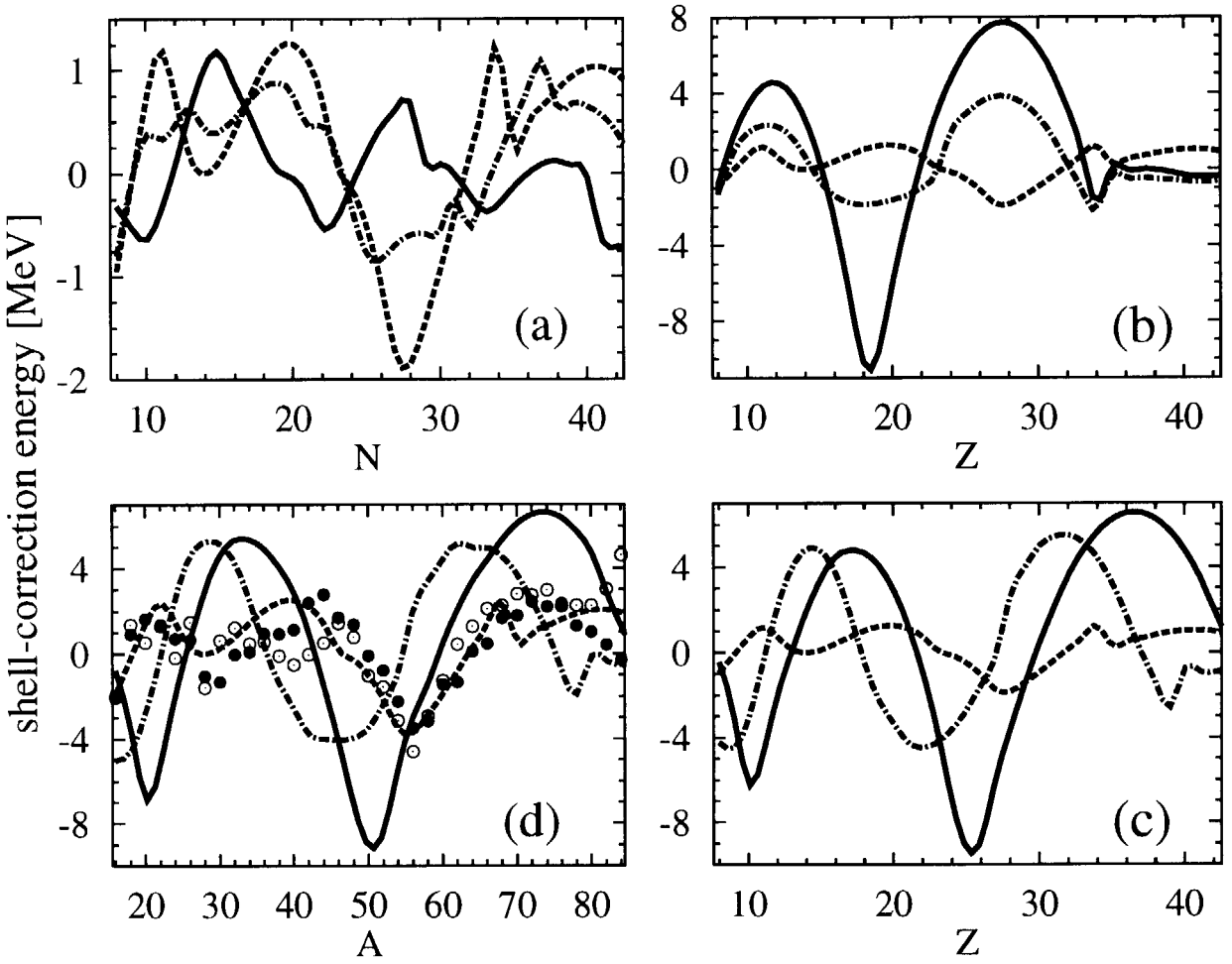

Figure 1. The shell-correction energy versus the nucleon number with spin-orbit coupling and $b = 0$ (dashed line), 0.1 (dashed-dotted line), and 0.2 (solid line). (a) shows the neutron contribution, (b) and (c) display the proton shell energy without and with the Pauli magnetism, (d) represents the total shell-correction energy of symmetric nuclei ($N = Z = A/2$), with the full circles indicating the deviation of the experimental masses from the liquid drop model prediction (cf. [1]), and the open circles displaying the results of ref. [3]. oscillations.

References

[1] A. Bohr and B.R. Mottelson, *Nuclear Structure* (Benjamin, NY, 1969).

[2] V.N. Kondratyev, T. Maruyama, and S. Chiba, JAERI-Research 99-065 (1999); Phys. Rev. Lett. **84** (2000) 1086.

[3] P. Möller, J.R. Nix, W.D. Myers, and W.J. Swiatecki, At. & Nucl. Data Tables **59** (1995) 185.

4.3 FRAGMENTATION MECHANISM REFLECTING THE CLUSTER STRUCTURE OF ^{19}B

H. TAKEMOTO, H. HORIUCHI[1] and A. ONO[2]

We investigate how clustering structure of the neutron dripline nucleus, ^{19}B, is reflected in the heavy-ion reaction. We compare ^{19}B fragmentation with ^{13}B fragmentation in ^{14}N-target reactions calculated by antisymmetrized molecular dynamics (AMD) [1] where ^{13}B which is the neutron closed shell nucleus has no clustering feature in its structure, while ^{19}B which is the neutron drip-line nucleus has a well developed cluster structure in its ground state. The clustering structure of the ^{19}B nucleus is predicted by the molecular orbital model [2] and the AMD model [3], but has not yet been confirmed experimentally.

Clustering structure of the ^{19}B nucleus is reflected as the "dynamical" cluster breakup of the ^{19}B nucleus into He and Li isotopes in its fragmentation. As is shown in Fig. 1(a), there is the abundance of He and Li isotopes in ^{19}B fragmentation compared with in ^{13}B fragmentation at the end of dynamical processes in the ^{14}N-target reaction at 35 MeV/nucleon. From Fig. 1(c), we can see that most of these He and Li isotopes are produced simultaneously in ^{19}B fragmentation by reflecting its cluster structure, while most of Li isotopes are produced with the emission of H isotopes in ^{13}B fragmentation [4]. However, if we consider statistical decay of excited fragments produced during dynamical processes, most of He and Li isotopes are produced simultaneously in both ^{13}B and ^{19}B fragmentation, as is shown in Fig. 1(d).

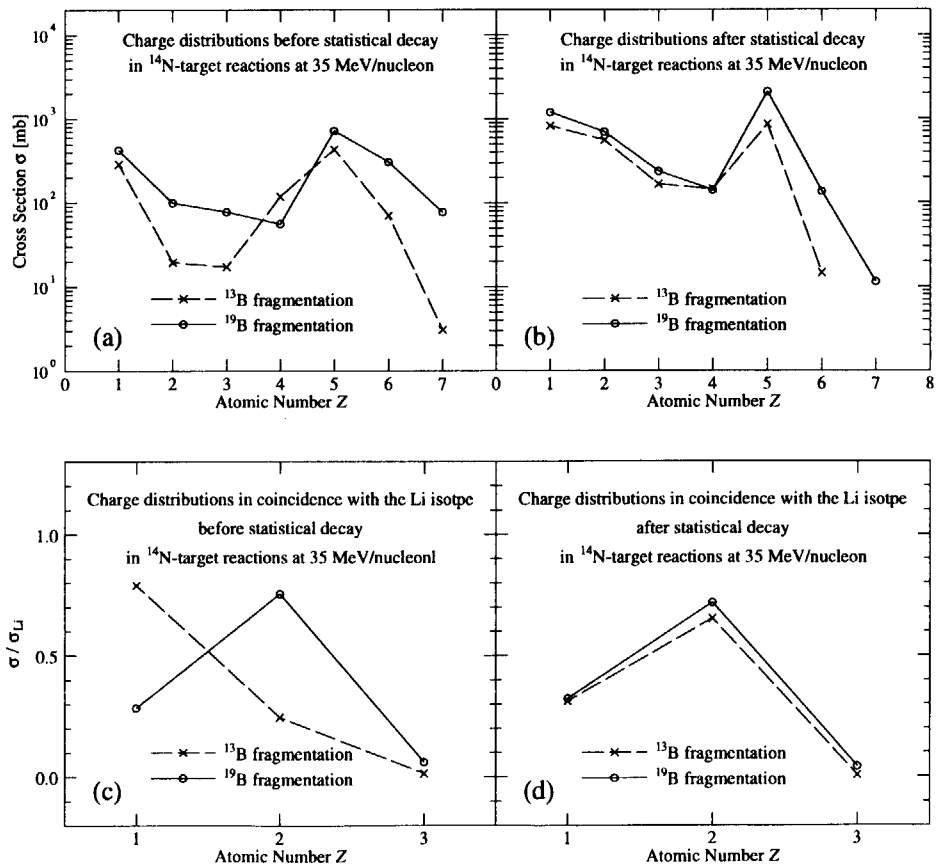

Fig. 1 (a) and (b) show charge distributions before and after statistical decay, respectively, and (c) and (d) show charge distributions in coincidence with the Li isotope before and after statistical decay, respectively. Solid and broken lines indicate those from ^{19}B and ^{13}B fragmentation in ^{14}N-target reactions at 35 MeV/A, respectively.

[1]Department of Physics, Kyoto University
[2]Department of Physics, Tohoku University

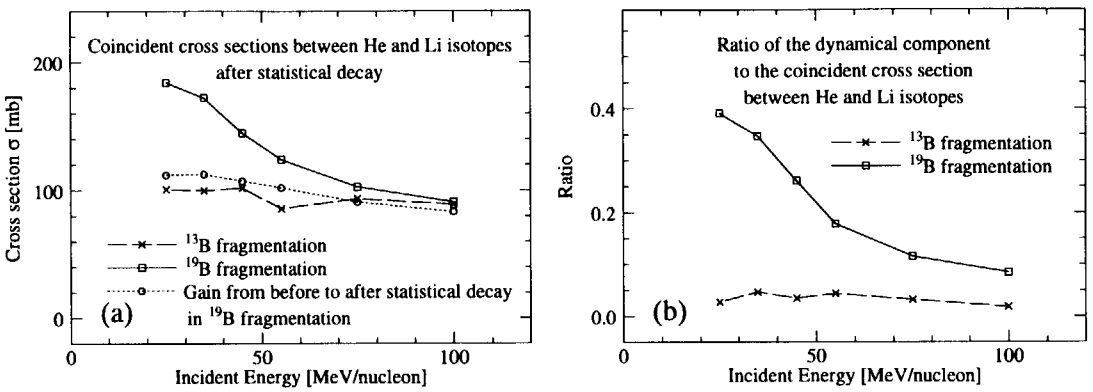

Fig. 2 (a) Incident-energy dependence of coincident cross sections between He and Li isotopes after statistical decay. (b) Ratios of coincident cross sections between He and Li isotopes at the end of dynamical processes to that after statistical decay. Solid and broken lines indicate ^{19}B and ^{13}B fragmentation, respectively, and the dotted line in (a) indicates the gain of the coincident cross section in ^{19}B + ^{14}N reactions from before to after statistical decay.

The coincident cross section between He and Li isotopes after statistical decay in ^{19}B fragmentation decreases with the incident energy increasing, while that in ^{13}B fragmentation is independent on the incident energy, as is shown in Fig. 2(a). The coincident cross section in ^{19}B fragmentation is about twice as large as that in ^{13}B fragmentation at 25 MeV/nucleon. As the incident energy increases, its difference becomes small, and they are almost the same at 100 MeV/nucleon. By comparing the gain of the coincident cross section in ^{19}B fragmentation from before to after statistical decay, which is indicated by the dotted line in Fig. 2(a), with the coincident cross section in ^{13}B fragmentation, we see that they are almost the same. Here the simultaneous production of He and Li isotopes in ^{13}B fragmentation is mainly due to statistical decay processes, as is shown in Fig. 2(b) which displays ratios of coincident cross sections between He and Li isotopes at the end of dynamical processes to those after statistical decay. Therefore we find that the larger value of the coincident cross section between He and Li isotopes in ^{19}B fragmentation than that in ^{13}B fragmentation at low incident energies is due to the "dynamical" cluster breakup of the ^{19}B nucleus by reflecting the cluster structure of the ^{19}B nucleus. As the incident energy increases, the dynamical component of simultaneous production of He and Li isotopes in ^{19}B fragmentation decreases, which is shown in Fig. 2(a), and the coincident cross sections become almost the same in ^{13}B and ^{19}B fragmentation at 100 MeV/nucleon, that is to say, the cluster structure of the ^{19}B nucleus is not reflected in its fragmentation at high incident energies.

From these results, we suggest that it is possible to examine the cluster structure of the ^{19}B nucleus in its ground state experimentally by using fragmentation mechanism, in particular, by using a coincident experiment between He and Li isotopes. AMD calculations indicate that if we observe the larger value of the coincident cross section between He and Li isotopes in ^{19}B fragmentation than that in ^{13}B fragmentation, this is due to the "dynamical" cluster breakup of the ^{19}B nucleus by reflecting the cluster structure of the ^{19}B nucleus. We stress here that it is important to verify such a clustering structure as the ^{19}B nucleus experimentally since such a structure is expected to be a new aspect in neutron-rich nuclei.

References

[1] A. Ono, H. Horiuchi, T. Maruyama and A. Ohnishi, Prog. Theor. Phys. **87** (1992) 1185.
[2] M. Seya, M. Kohno and S. Nagata, Prog. Theor. Phys. **65** (1981) 204.
[3] Y. Kanada-En'yo and H. Horiuchi, Phys. Rev. C **52** (1995) 647.
[4] H. Takemoto, H. Horiuchi and A. Ono, Prog. Theor. Phys., **101** (1999) 101.

5. Atomic Physics, Solid State Physics and Radiation Effects

This is a blank page.

5.1 HIGH-RESOLUTION ZERO-DEGREE ELECTRON SPECTROSCOPY (VI)

M. IMAI[1], M. SATAKA, S. KITAZAWA, K. KAWATSURA[2], K. KOMAKI[3], H. SHIBATA[4], H. TAWARA[5], T. AZUMA[6], Y. KANAI[7] and Y. YAMAZAKI[3,7]

The method of zero-degree electron spectroscopy has been applied to study collision dynamics of highly charged ions colliding with gaseous and solid targets, as well as to study highly excited ions in spectroscopic point of view. We have been studying Na-like or Mg-like Sc ions [1,2], Na-like S ions [2,3] formed via collisions with He target, and from Li-like to C-like Si ions [4,5] formed via collisions with C foil. These spectroscopic results have found to be useful also as a test for precise calculations of the energies of the Rydberg states [6], which joins another important subject of collision dynamics; formation of doubly excited states via correlated or uncorrelated electron capture [7,8]. As for collision dynamics inside solid, zero-degree electron spectroscopy proved to be an excellent tool, and electron capture, loss and/or excitation processes occurring within or at the exiting surface of solids have been studied measuring Auger, C-K, or cusp electrons [9–11]. We have devoted to measuring Coster-Kronig (C-K) electrons from Be-like configuration $1s^22p(^2P_{3/2}°)nl \rightarrow 1s^22s(^2S_{1/2})\varepsilon l'$ or $1s^22p(^2P_{1/2}°)nl \rightarrow 1s^22s(^2S_{1/2})\varepsilon l'$ of S^{12+} ions excited through He or C-foil target, studying the difference of the l-distribution between gas and solid phase targets [12,13], or the dependence of the l-distribution on foil thickness or projectile charge state [14]. We present here our latest results of Auger spectra for 2.0 MeV/u S^{5+} and 2.5 MeV/u S^{7+} colliding with He target, and of C-K spectra for 2.5 MeV/u S^{7+} and S^{13+} ions penetrating through C-foil targets.

The present experiment has been performed at HIR2–2 beam line of the Tandem Accelerator at JAERI, Tokai. As the experimental apparatus have already been presented previously [1–5,12–14], only the major parameters are given here. Measured are the electrons emitted from sulfur projectile passing through He-gas or C-foil target. A beam of 2.0 MeV/u S^{5+} or 2.5 MeV/u S^{7+} was provided by the accelerator and was guided directly into the target for S^{5+} or S^{7+} injection cases. As for S^{13+} collisions, a fraction of the primary S^{7+} beam was selected by switching magnet after passing a post stripper foil. Electrons emitted from the projectile were energy analyzed by a tandem electrostatic analyzer at zero degrees. Electron energies observed are from 0 to 160 eV. Two spectra corresponding to the low and the high energy wings of the cusp are obtained from measured spectrum by converting the laboratory frame spectrum in projectile rest frame, resulting in the energy resolution of ~0.1 eV at lower region and of ~0.5 eV around 40 eV.

In fig.1, shown are the electron energy spectra, transformed into projectile rest frame, for 2.0 MeV/u S^{5+} and 2.5 MeV/u S^{7+} ions colliding with He-gas target. The appearance and the nonexistence of Auger transitions for S^{5+} and S^{7+} injection, respectively, are well reproduced by compiled wavelength table [15], except some shift of electron energies for S^{5+} ions. In fig.2, the C-K electron energy spectra for 2.5MeV/u S^{7+} and S^{13+} passing through C-foils of various thickness (3–10 μg/cm^2) are shown, together with the calculated values of the electron energy for some initial configurations [6]. It can be seen that C-K electrons from S^{7+} collision have different distribution in both intensity and energy, while those from S^{13+} collision form similar spectra, although the autoionizing Rydberg configuration is formed by attaching continuum electron to Li-like core at the exiting surface of the foil anyway. In the S^{7+} collision, the attached electron is possibly the one which was once lost into continuum from projectile bound states

[1] Department of Nuclear Engineering, Kyoto University
[2] Department of Chemistry and Materials Technology, Kyoto Institute of Technology
[3] Graduate School of Arts and Sciences, University of Tokyo
[4] Research Center for Nuclear Science and Technology, University of Tokyo
[5] Department of Physics, Kansas State University
[6] Institute of Applied Physics, University of Tsukuba
[7] The Institute of Physical and Chemical Research (RIKEN)

and having traveled inside the solid. The increasing intensity shows the increasing number of quasi-free electrons in train with projectile, and the change of energy distribution can be attributed to its l-enhancement through multiple collisions inside solid, as has been shown theoretically [16] for $1s^2 2p5l \rightarrow 1s^2 2s\varepsilon l'$ transition of 1.5 MeV C^{2+} ion [10]. In the S^{13+} collision, on the other hand, the autoionizing Be-like state is formed by electron capture from target upon exiting surface, which makes no dependence on foil thickness in the electron spectra.

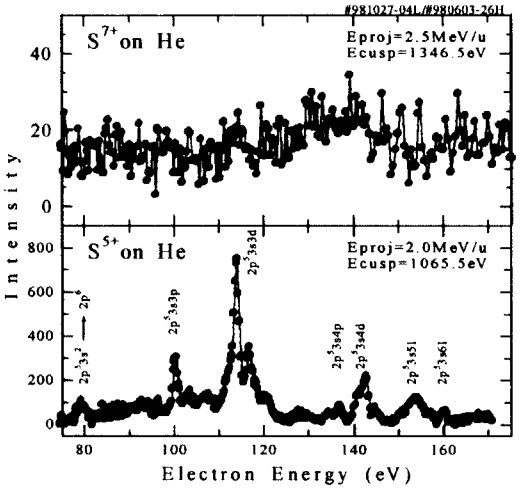

Fig.1. Electron energy spectra, transformed into projectile rest frame, for 2.0 MeV/u S^{5+} and 2.5 MeV/u S^{7+} ions colliding with He-gas target.

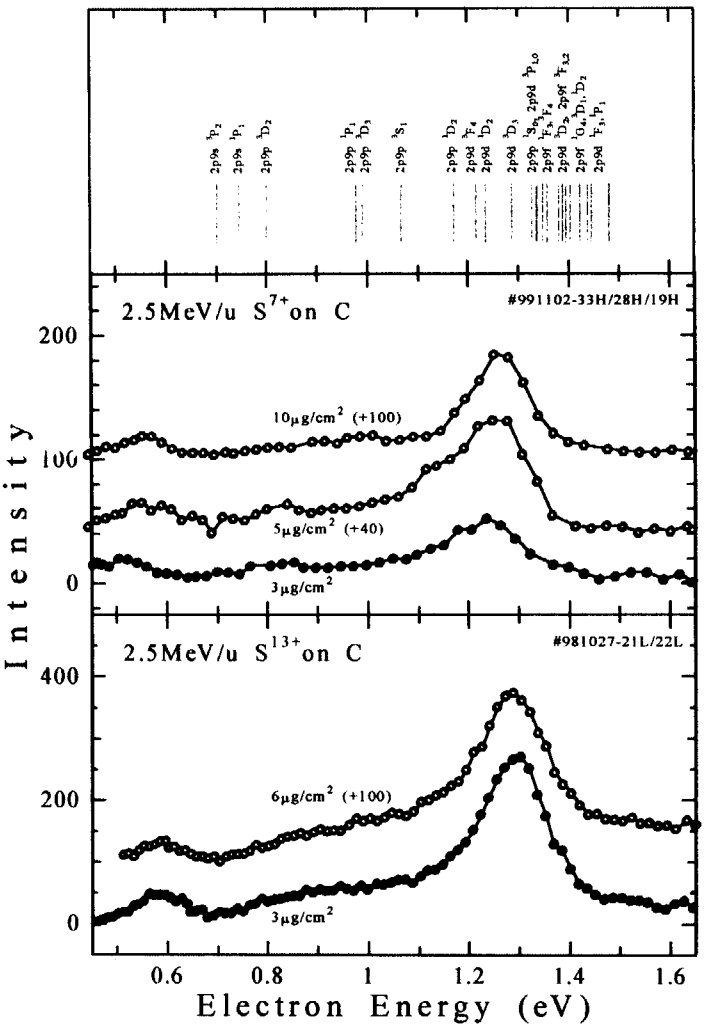

Fig.2. Electron energy spectra from Coster-Kronig transition $1s^2 2p(^2P_{3/2}°)9l \rightarrow 1s^2 2s(^2S_{1/2})\varepsilon l'$ of Be-like states formed through 2.5 MeV/u S^{7+} or S^{13+} ions colliding with C-foil targets. The uppermost indicators show calculated energy values [6].

References

[1] M. Sataka *et al.*, Phys. Rev. **A44** (1991)7290.
[2] K. Kawatsura *et al.*, J. Electron Spectr. and Relat. Phenomena **88–91**, (1998) 83.
[3] K. Kawatsura *et al.*, Nucl. Instrum. Methods **B53**, (1991) 421.
[4] M. Imai *et al.*, Physica. Scripta **T73**, (1997) 93.
[5] K. Kawatsura *et al.*, J. Electron Spectr. and Relat. Phenomena **88–91**, (1998) 87.
[6] I. Yu. Tolstikhina *et al.*, Physica Scripta **54**, (1996) 188.
[7] M. Barat and P. J. Roncin, J. Phys. **B25**, (1992) 2205.
[8] B. Sulik *et al.*, Phys. Rev. **A52**, (1995) 387.
[9] N. Stolterfoht *et al.*, Phys. Rep. **146**, (1987) 315.
[10] Y. Yamazaki *et al.*, Phys. Rev. Lett. **61**, (1988) 2913.
[11] Y. Yamazaki, Nucl. Instr. Meth. **B96**, (1995) 517.
[12] K. Kawatsura *et al.*, Nucl. Instrum. Methods **B48**, (1990) 103.
[13] K. Kawatsura *et al.*, Nucl. Instrum. Methods **B124**, (1997) 381.
[14] M. Imai *et al.*, Nucl. Instrum. Methods **B67**, (1992) 142.
[15] V. Kaufman and W. C. Martin, J. Phys. Chem. Ref. Data **22**, (1993) 279.
[16] J. Burgdörfer and C. Bottcher, Phys. Rev. Lett. **61**, (1988) 2917.

5.2 EMISSION OF SECONDARY IONS FROM CONDUCTIVE MATERIALS BOMBARDED WITH HEAVY IONS

T. SEKIOKA[1], M. TERASAWA[1], M. SATAKA and S. KITAZAWA

The importance of the electronic excitation effect in materials has been attracting great interest. We have been studying the secondary ions mass spectra from thin conductive solid targets irradiated with heavy ion beams from the JAERI tandem accelerator at the energy region where the electronic stopping power is dominant. There have been few researches on the electronic excitation effect in the conductive materials, because it has been believed that electronic excitation in the conductive materials is rapidly neutralized by free electrons.

The Cu foil target of 1000Å thickness evaporated on C-foils of 10μg/cm^2 were irradiated with high energy heavy ions beam from the tandem accelerator. The secondary ions ejected from the front surface of the target were collected by a time of flight (TOF) mass spectrometer by applying an acceleration voltage of −500V and detected by an electron multiplier. Secondary electrons from the backside of the target were detected by another electron multiplier and this signal was used as the start signal of the TOF. The projectiles were 100, 150 and 200 MeV Au^{12+} ions, 240 MeV Au^{14+} ions and 300 and 320 MeV Au^{25+} ions.

Figure 1 shows the yield of the secondary ions of Cu^+ normalized by the counts of secondary electron signal as a function of the electronic stopping power. The values of the electronic stopping power are obtained from Ziegler's table [1] by TRIM. As can be seen in the figure, the secondary ion yield increases remarkably above an electronic stopping power of 3keV/Å. The solid line in the figure represents the slope of $(dE/dx)^2$ for the eye guide. The strong dependence of the secondary ion yield from conductive materials on the electronic stopping power suggests that even in the conductive materials, the electronic excitation effects play an important role in the secondary ion sputtering. The $(dE/dx)^2$ dependence of the secondary ion yield suggests the importance of Coulomb repulsion between ionized target atoms in the high electronic excitation region.

In order to confirm the electronic excitation effect in conductive materials irradiated by high-energy heavy ions, it is highly desirable to measure the total sputtering yield. As most part of the sputtered particles is neutral, we are planning to develop a spectrometer for the measurement of secondary neutral particles in the near future.

References

[1] J.F.Ziegler, Stopping Cross-Sections for Energetic Ions in All Elements, Vol.5, Pergamon Press (1980).

[1] Faculty of Engineering, Himeji Institute of Technology

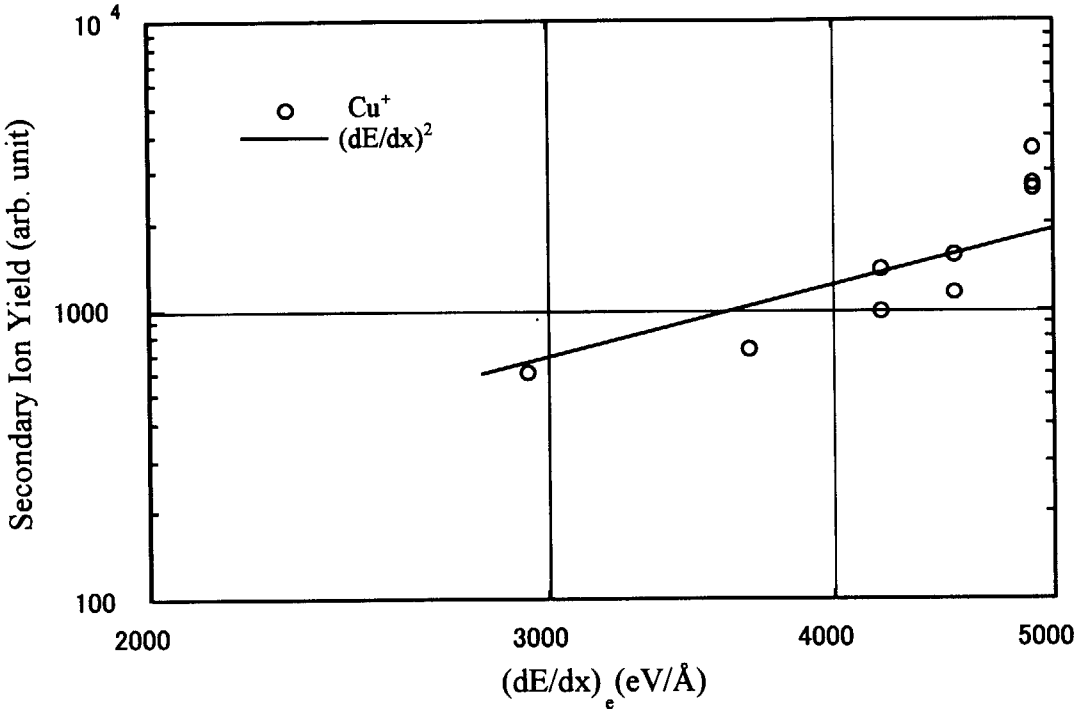

Fig. 1. The yield of the secondary ions of Cu^+ normalized by the counts of secondary electrons signal as a function of the electronic stopping power. The values of the electronic stopping power are obtained by Ziegler's table [1] (TRIM). The solid line represents the slope of $(dE/dx)^2$ for the eye guide.

5.3 RELATIONSHIP AMONG FLUX DEPINNING, PHASE TRANSITION AND IRREVERSIBILITY IN DISORDERED HIGH T_c SUPERCONDUCTORS

T. KISS

One of the significant features of HTS is its complicated magnetic phase diagram. It is originated from the competition among at least three different kinds of energies, i.e., 1) the elastic energy of flux line lattice (FLL), U_e, 2) the thermal energy, U_t, and 3) the pinning energy, U_p. The FLL melting transition observed in the magnetically reversible state for weakly pinned HTS is mostly determined by the competition between U_e and U_t [1]. The transition associated with the dimensional crossover of FLL, which is observed in low magnetic field in the low temperature region for a Bi-2212 superconductor, is determined by U_e and U_p [2]. The so-called vortex glass-liquid (GL) transition [3] is analogously expected to be determined by the competition between U_t and U_p. However, the concepts among the thermal flux depinning, the GL phase transition and the irreversibility are still confused. In this study, from detail measurements of electric field (E) vs. current density (J) curves in a YBCO film over a wide range of magnetic field (B) and temperature (T), we investigated the influence of flux pinning and its statistic properties on the GL phase transition and irreversibility.

We reported that the probability density function of J_c in a random pin medium is increased in proportion to the power of the distance from the percolation limit [4]. Then the transport properties can be described by a simple expression as follows [5].

$$E(J) = \rho_{ff} \int_0^J [(J_c - J_{cm})/J_0]^m dJ_c \quad for \quad J \geq J_{cm} \tag{1}$$

where J_{cm} is the percolation threshold, J_0 is the scale parameter, m is the power index determinig the shape of distribution and ρ_{ff} is the flux flow resistivity in the uniform flow. It was shown that the minimum value of J_c, that is J_{cm}, as well as the typical value J_k ($=J_{cm}+J_0$) are both scaled as a function of reduced magnetic field as in the similar form of conventional superconductors.

$$J_{cm(k)}B = A\,B_{GL(k)}(T)^{\zeta}\left(\frac{B}{B_{GL(k)}}\right)^{\gamma}\left(1-\frac{B}{B_{GL(k)}}\right)^{\delta} \tag{2}$$

where B_{GL} (B_k) is the transition field determined by the criterion J_{cm}=0 (J_k=0). A, ζ, γ, and δ are pin parameters characterizing the pinning mechanism.

The GL transition seems to be supported by the iso-therm scaling of the observed E-J curves. However, the scaling will also be explained by the present model as well. One major difference is that the scaling indices will be influenced strongly by the pinning properties whereas they depends mainly on the dimensionality in the phase transition theory. The static index ν and the dynamic index z are related directly to the pin parameter δ and the statistic parameter m as follows.

$$\upsilon = \frac{1}{2}\delta, \tag{3}$$

$$z=2m+1. \tag{4}$$

When the uniformity of the sample was enhanced, we

Department of Electrical and Electronic Systems Engineering, Kyushu University

obtained very sharp *E-J* curves even in YBCO HTS film. The parameter *m* extracted from the measured *E-J* curves using the statistic model reached as high as 5.4 which corresponds to z=11.8. Using the magnetic field dependent *E-J* curves, we examined the macroscopic pinning force density, $J_{cm}B$, then the pin parameter δ in (2) was deduced to be 1.32. The iso-therm scaling of the *E-J* curves for the constant magnetic field of 8.0T was shown in Fig. 1. It can be seen the scaling indices z and ν agreed well with the prediction of (3) and (4), respectively. Notice that the value of z is extremely large to be explained within the framework of the phase transition theory [3]. These results strongly suggest that the scaling is influenced by the sharp distribution of the pinning strength.

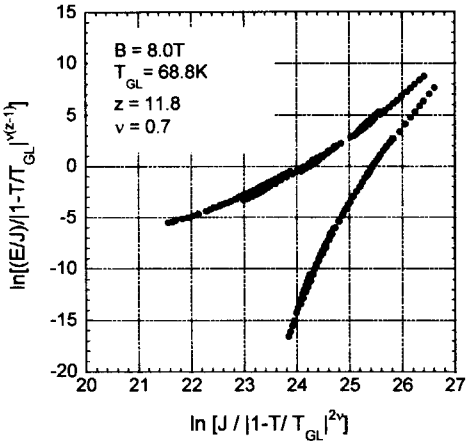

Fig. 1. Iso-therm scaling of *E-J* curves observed in a YBCO film in the temperature range of 54.0K to 74.2K under a constant magnetic field of 8.0T.

Based on the consideration of thermodynamic properties of the macroscopic pinning force density and its distribution, we can formulate the nonlinear *E-J* characteristics in a wide (*B*, *T*)-plane by eqs. (1) and (2). From that relationship, we can estimate iso-*J* lines for an electric field criterion E_c as shown in Fig. 2, where E_c was chosen to be 10^{-3} V/m as an example. The material parameters were determined by the measurements for a YBCO film. It can be seen that the irreversibility field is identified as one of the iso-*J* lines depending on the criterion. The relationship between B_{GL} and B_{irr} can be determined if we determine the criteria E_c and J_{c0}.

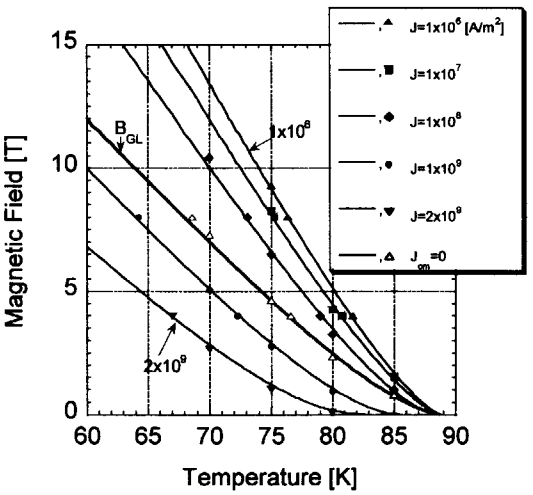

Fig. 2. Iso-*J* curves in a YBCO film for the criterion of E_c=10^{-3}V/m. The markers are measured data whereas the lines are the theory [5].

The influence of flux pinning on the vortex glass-liquid (GL) phase transition and irreversibility in HTS has been examined on the bases of systematic measurements of electric field (*E*) vs. current density (*J*) curves in YBCO thin films. It has been shown that the GL transition is identical to the thermal depinning determined by the minimum value of macroscopic pinning strength. The iso-therm scaling of the *E-J* characteristics are directly related to the pinning natures. The irreversibility line can be described as an iso-*J* line governed by the statistic pin distribution. If we determine the criteria for the irreversibility line, we can describe the irreversibility line based on the depinning line. The essential physical quantity, therefore, can be attributed to the flux depinning.

References

[1] T. Matsushita, *Physica C* **214** (1993) 100-106.

[2] T. Matsushitaet al., *Supercond. Sci. Technol.* **11** (1998) 925-928.

[3] D. S. Fisher, M. P. A. Fisher and D. A. Huse, *Phys. Rev. B* **43** (1991) 130-159.

[4] K. Yamafuji and T. Kiss, *Physica C* **290** (1997) 9-22.

[5] T. Kiss et al., *Supercond. Sci. Technol.* **12** (1999) 1079–1082.

5.4 THE EFFECTS OF PRIMARY IONIZATION IN ION-IRRADIATED OXIDE SUPERCONDUCTORS

N. ISHIKAWA, A. IWASE, Y. CHIMI, O. MICHIKAMI[1],
H. WAKANA[1] and T. KAMBARA[2]

It is customary to analyze the effect of electronic excitation induced by ion-irradiation in terms of the electronic stopping power, S_e, which is defined as the energy transferred from an incident ion to electrons of the target per unit ion-path length. However, in some insulating materials such as $Y_3Fe_5O_{12}$, even for the same electronic stopping power, diameter of the amorphized region has been found to vary depending on the velocity of the incident ions (so-called the velocity effect)[1]. Our recent study has shown that the velocity effect is observed also in ion-irradiated oxide superconductors $EuBa_2Cu_3O_y$ (EBCO) [2,3]. The existence of the velocity effect shows that the electronic stopping power is not a good scaling parameter. In this work, we have found a much better scaling parameter for describing the defect production process through the *in-situ* measurements of ion-fluence dependence of the normal-state resistivity and the superconducting temperature in oxide superconductor $EuBa_2Cu_3O_y$ irradiated with various heavy ions in a wide energy range of 90MeV-3.84GeV.

Thin films of oxide superconductor EBCO were prepared on MgO substrates by dc magnetron sputtering. The films were c-axis oriented and the thickness of the films was about 0.3 μ m. The samples were irradiated with high energy heavy ions; 120MeV $^{35}Cl^{8+}$, 150MeV $^{45}Sc^{10+}$, 90MeV $^{58}Ni^{6+}$, 125MeV $^{79}Br^{10+}$, 90MeV $^{127}I^{9+}$, and 200MeV $^{197}Au^{13+}$ from the tandem accelerator at JAERI-Tokai (Japan Atomic Energy Research Institute, Tokai Research Establishment), and 0.71GeV $^{84}Kr^{11+}$, 3.54GeV $^{136}Xe^{31+}$, and 3.84GeV $^{181}Ta^{37+}$ from the ring cyclotron at RIKEN (The Institute of Physical and Chemical Research). The irradiation temperature was fixed at 100K in order to investigate the change in normal-state resistivity and to minimize the thermal annihilation of irradiation-induced defects. The resistivity was measured at 100K *in situ* as a function of ion-fluence. The superconducting transition temperature, T_c, was

[1] Faculty of Engineering, Iwate University.

[2] Atomic Physics Laboratory, The Institute of Physical and Chemical Research (RIKEN).

defined as the temperature at which the resistivity became a half of the normal-state resistivity. The transition temperature before irradiation, T_{co}, was ranged between 87.5K and 91.1K. The samples were irradiated up to the ion-fluence, Φ_{total}, at which the resistivity at 100K became 2.4 times larger than that before irradiation, ρ_o. Then, the sample was cooled down, and $T_c(\Phi_{total})$ was measured. The change in T_c due to irradiation, ΔT_c, was defined as $\Delta T_c \equiv T_{co} - T_c(\Phi_{total})$.

Increase in normal-state resistivity and decrease in T_c were observed for all irradiations. $\Delta\rho/\rho_o$ represents the normalized resistivity change, where $\Delta\rho = \rho(\Phi) - \rho_o$ is the resistivity change due to irradiation, $\rho(\Phi)$ the resistivity as a function of ion-fluence, and ρ_o the resistivity before irradiation. Such normalization is convenient to eliminate the sample dependence of irradiation effects as can be found in refs.4 and 5. $[d(\Delta\rho/\rho_o)/d\Phi]_{\Phi\to 0}$ and $(\Delta T_c/T_{c0})/\Phi_{total}$ are the simplest quantities characterizing the defect production per unit ion-fluence. The *initial* slope is adopted for the analysis of resistivity change because it represents the effect of the first incoming ion, and the interaction between the incident ions and the defects already produced by other ions is ruled out. Figure 1 shows that both $[d(\Delta\rho/\rho_o)/d\Phi]_{\Phi\to 0}$ and $(\Delta T_c/T_{c0})/\Phi_{total}$ cannot be scaled with S_e. Figure 2 shows that both quantities are scaled with the primary ionization rate (dJ/dx), which is the number of atoms primarily ionized by an incident ion per unit path length[6,7]. This result indicates that the primary ionization rate should be the alternative parameter for describing the defect production via electronic excitation and that the defect production is triggered by Coulomb repulsion of ionized atoms.

References

[1] A. Meftah, F. Brisard, J.M. Costantini, M. Hage-Ali, J.P. Stoquert, F. Studer and M. Toulemonde, Phys. Rev. B**48** (1993) 920.

[2] N. Ishikawa, Y. Chimi, A. Iwase, H. Maeta, K. Tsuru, O. Michikami, T. Kambara, T. Mitamura, Y. Awaya and M.Terasawa,Nucl. Instrum. Methods B **135**(1998) 184.

[3] N. Ishikawa, Y. Chimi, N. Kuroda, A. Iwase and T. Kambara, Physica Scripta **T80** (1999)559.

[4] B. Hensel, B. Roas, S. Henke, R. Hopfengärtner, M. Lippert, J. P. Ströbel, M. Vildić and G. Saemann-Ischenko: Phys. Rev. B **42** (1990) 4135.

[5]D.Bourgault, S. Bouffard, M. Toulemonde, D. Groult, J. Provost, F. Studer, N.

Nguyen and B. Raveau: Phys. Rev. B **39** (1989) 6549.

[6]H.A. Bethe, Ann. Phys. **5** (1930) 325.

[7]R.L. Fleischer, P.B. Price, R.M. Walker and E.L. Hubbard, Phys. Rev. **156** (1967) 353.

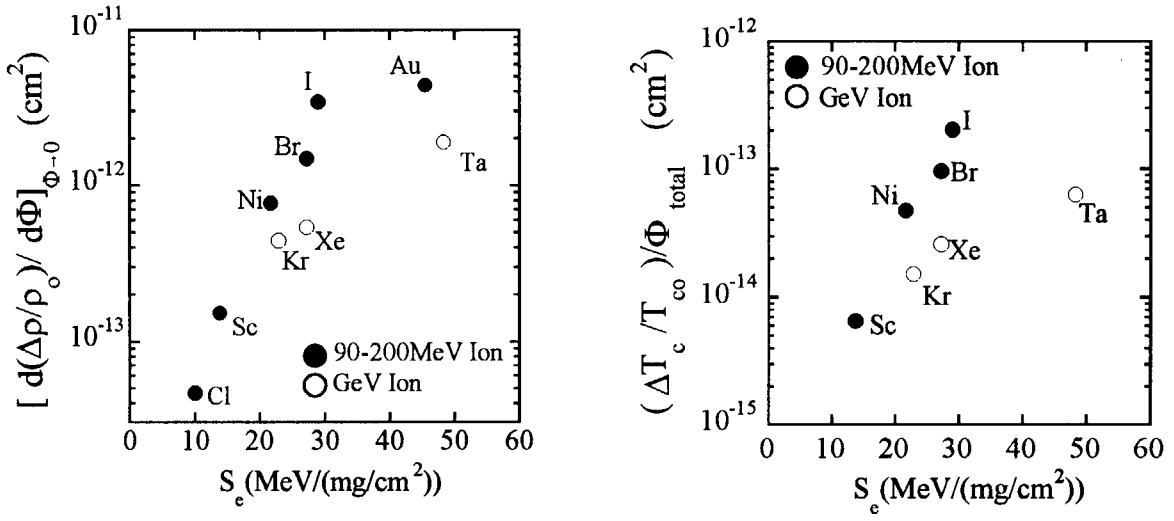

Fig.1. $[d(\Delta\rho/\rho_o)/d\Phi]_{\Phi\to 0}$ and (Δ T$_c$/T$_{co}$)/ Φ_{total} plotted against the electronic stopping power.

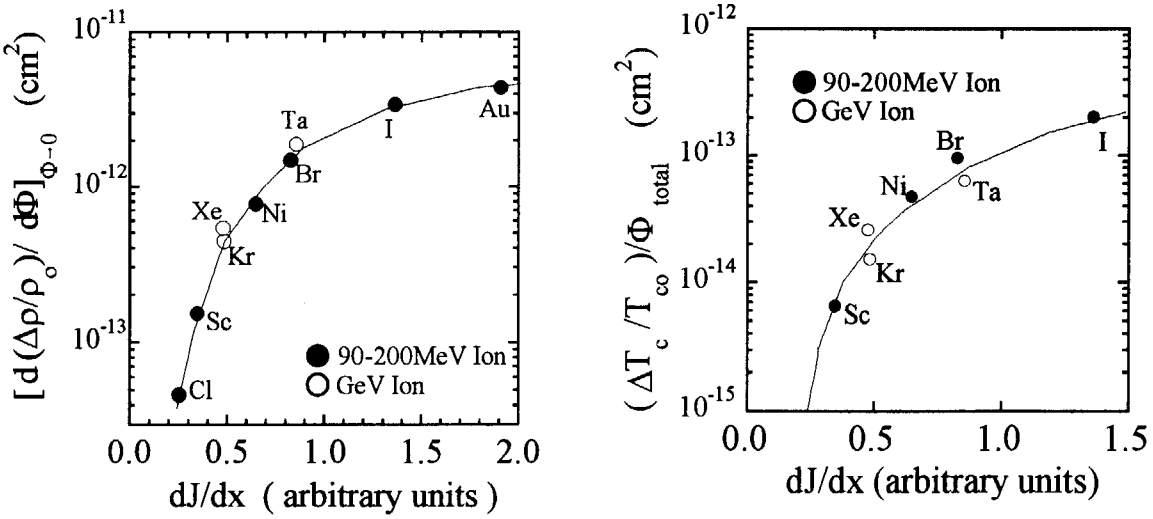

Fig.2. $[d(\Delta\rho/\rho_o)/d\Phi]_{\Phi\to 0}$ and (Δ T$_c$/T$_{co}$)/ Φ_{total} as a function of the primary ionization rate.

5.5 TRACK FORMATION IN HIGH-T_c SUPERCONDUCTOR BY HIGH-ENERGY HEAVY ION IRRADIATION

M. SASASE, S. OKAYASU, H. KURATA AND K. HOJOU

High energy heavy ions dissipate most of their energies in solids through the electronic excitation. Through this process, ions produce columnar defects in high-T_c superconductors [1]. In the formation of the columnar defects, it has been considered that the electronic stopping power (S_e) mainly affects the track morphology. However, some research groups found that the S_e was not only key parameter and ion velocity also plays a very important role in the formation of the columnar defects[2, 3]. In the present experiments, we have investigated the influence of the ion velocity on the track formation under the fixed S_e value. The relationship between the track size which is obtained from transmission electron microscope (TEM) observation, and the ion velocity has been discussed.

$Bi_2Sr_2CaCu_2O_x$ (Bi-2212) single crystals has been irradiated with 180 MeV Au^{12+} and 600 MeV I^{29+} at JAERI-Tokai tandem accelerator. The velocities of the ions were 1.32 x 10^9 cm/s and 3.02 x 10^9 cm/s, respectively. The each sample was irradiated to the fluence of 2.0 x 10^{10} ions/cm^2. The ions were irradiated parallel to the c-axis of the samples.

Fig. 1 shows the S_e values for Au^{12+} and I^{29+} for Bi-2212, calculated from TRIM code [4], as a function of ion energy/amu. The solid circles show the S_e values for 180 MeV Au^{12+} and 600 MeV I^{29+}. As shown in Fig. 1, S_e for both ions have almost the same value (=23 keV/nm).

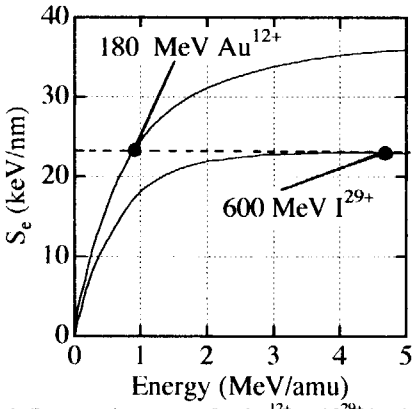

Fig. 1. S_e versus ion energy for Au^{12+} and I^{29+} ion in Bi-2212.

Fig. 2 shows the size distribution of the columnar defects induced by Au^{12+} and I^{29+} ions. On the basis of TEM observations, most of the tracks consist of continuous columns, and the most probable diameters are 13 nm for Au^{12+}, 6.5 nm for I^{29+}, respectively. These results reveal that irradiated ions which have lower ion-velocity produce larger tracks under the fixed S_e. It can be considered that the local deposited energy per unit volume becomes larger for the lower ion velocity even though S_e is constant.

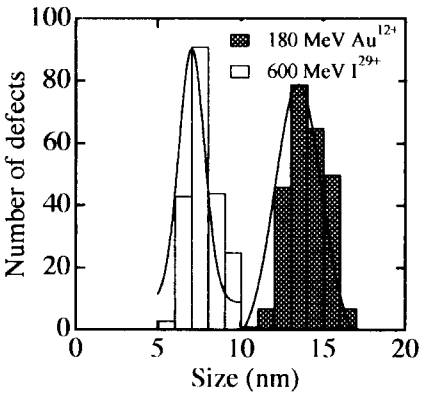

Fig. 2. Size distribution of the columnar defects induced by $Au^{12+}$and I^{29+} in Bi-2212.

Acknowledgement

The authors would like to thank Drs. A. Maeda and Y. Tsuchiya for preparing high-T_c superconductor single crystals.

Reference

[1] For example, M. Toulemonde, S. Bouffard and F. Studer, Nucl. Instrum. Method, **B91**(1994) 108.
[2] A. Meftah, F. Brisard, J. M. Constantini, M. Hage-Ali, J. P. Stoquert, F. Studer and M. Toulemonde et. al., Phys. Rev. **B48**(1993)920.
[3] N. Ishikawa, Y. Chimi, N. Kuroda, A. Iwase and T. Kambara, Physica Scripta. **T80**(1999) 559-561
[4] J. F. Ziegler : Handbook of Stopping Cross Section for Energetic Ions in All Elements (Pergamon, New York, 1980).

5.6 OBSERVATION OF VORTICES AND COLUMNAR DEFECTS BY LORENTZ MICROSCOPY

K. HARADA[1,2], H. KASAI[1], O. KAMIMURA[1], T. MATSUDA[1,2], A. TONOMURA[1,2], S. OKAYASU, M. SASASE, J. SHIMOYAMA[2,3], K. KISHIO[2,3] and K. KITAZAWA[2,3]

It is considered that columnar defects which are produced by penetration of high energy heavy ions are one of the most effective pinning centers for high-T_c superconductors [1]. However, the direct and dynamical experimental confirmation is difficult. Only scanning tunneling microscopy has succeeded to show the static condition [2] and Bitter decoration has showed as replica [3]. Lorentz microscopy with a 300-kV field-emission electron microscope has succeeded to observe each single vortex and their dynamics by TV rate [4], and the pinning effect by columnar defects was observed semi-macroscopically in our previous work [5].

One of our present target is simultaneous observation of single vortex and columnar defect, and the observation of their dynamical interactions. When applied magnetic field is above a several gauss (G), the vortex density in the material is about an order of 1.0×10^{8} vortices/cm^2 which is too much to observe the interaction vortices with pinning centers, because interaction force between vortices is stronger and dominant in the phenomena. In order to achieve the purpose, we had to reduce the ion dose to the order of the magnitude 1.0×10^{6} ions/cm^2 and control it precisely at first. A slit shutter system in the ion beam line of the tandem accelerator at the Japan Atomic Energy Research Institute (JAERI) was developed. By changing the width of the slit, we can easily chose fast shutter speed from 0.7×10^{-3} to 1.0×10^{-1} s and hence control the ion dose to an order of 1.0×10^{5} ions/cm^2 .

A single crystalline of $Bi_2Sr_2CaCu_2O_{8+\delta}$ (Bi-2212) was grown by the standard floating-zone technique and annealed at 800 ℃ for 3 days to be oxygen over-doped whose critical temperature T_c was about 85.5 K [6]. The Bi-2212 thin films of thickness about 200 nm with a 100 × 100 μm^2 uniform area were prepared by cleaving as specimens for transmission electron microscopy (TEM) [5]. The specimen was set on a low-temperature stage tilted 45° both to the incident electron beam and to the external magnetic field, which was applied parallel to the electron beam. After cleaving the thin films for TEM observation, columnar defects with density of 3.1×10^{5} ions/cm^2 were induced by 240-MeV Au^{+14} ion irradiation parallel to the c-axis of Bi-2212.

Figure 1 shows an image by putting together four adjacent electron micrographs and covered a wide area of the thin film. Arrowheads on the image indicate the locations of columnar defects whose size were about 10 nm in diameter. Almost all of the defects were counted.

[1]Advanced Research Laboratory, Hitachi Ltd., Hatoyama, Saitama 350-0395,
[2]Department of Chemistry, University of Tokyo, Bunkyou -ku, Tokyo 113-8656,
[3]CREST, Japan Science and Technology Corporation (JST), Kawaguchi, Saitama 332-0012

Vortices with black and white contrast feature at 4.5 K in the same region of Fig. 1 are shown by Lorentz micrograph in Fig. 2. Wide dark lines were bend contours which confirmed that the specimen was a single crystal and slightly bent in the microscope. The grain boundaries and/or steps are shown by lines in both micrographs. With comparison between the two micrographs, it is difficult to say each vortex was pinned by the column, because the defects in the Lorentz micrographs were invisible.

We shall examine how to improve the defect contrast in Lorentz images by changing the irradiation angles to the specimen. And we are planed to observe how the vortices are pinned by the column, and their dynamical behaviors by Lorentz microscopy on the next step.

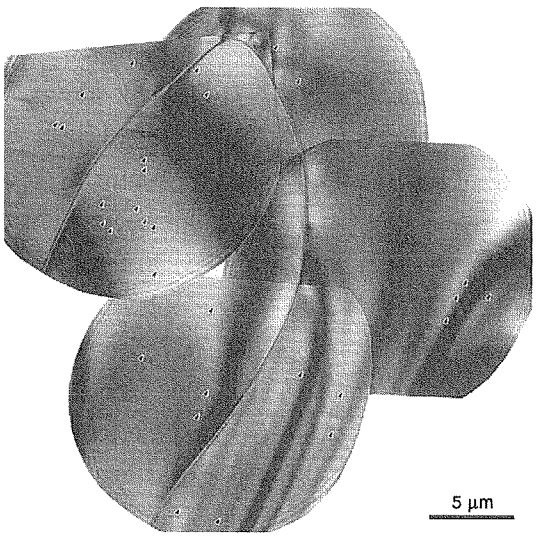

Fig. 1. Electron micrographs of Bi-2212.

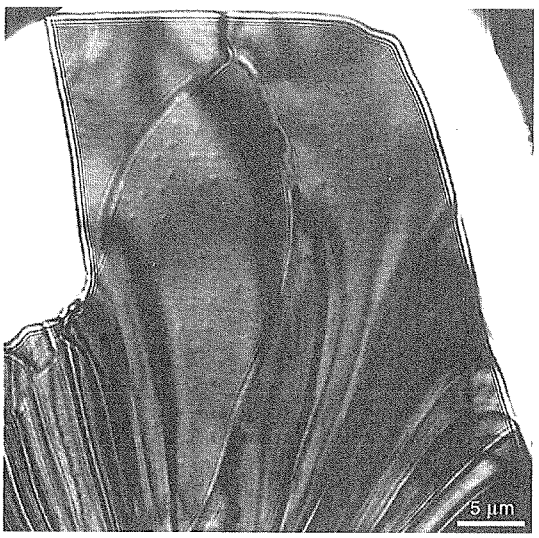

Fig. 2. Lorentz micrograph at 8 G and 4.5K.

References

[1] S. Oakayasu, Y. Kazumata, I. Tanaka and H. Kojima, Physica **B 194-196** (1994) 1881.
[2] S. Behler, S. H. Pan, P. Jess, A. Baratoff, H. -J. Güntherodt, F. Lévy, G. Wirth and J. Wiesner, Phys. Rev. Lett. **72** (1994) 1750.
[3] H. Dai, S. Yoon, J. Liu, R. C. Budhani and C. M. Lieber, Science **265** (1994) 1552.
[4] A. Tonomura, H. Kasai, O. Kamimura, T. Matsuda, K. Harada, J. Shimoyama, K. Kishio and K. Kitazawa, Nature **397** (1999) 308-309.
[5] K. Harada, H. Kasai, O. Kamimura, T. Matsuda, A. Tonomura, S. Okayasu amd Y. Kazumata, Phys. Rev. Lett. **71** (1996) 9400-9405.
[6] Y. Kotaka, T. Kimura, H. Ikuta, J. Shimoyama, K. Kitazawa, K. Yamafuji, K. Kishio and D. Pooke, Physica **C 235-240** (1994) 1529-1530.

5.7 STAIR-STEP COLUMNAR DEFECTS IN ION-IRRADIATED Bi-2212

D.X. HUANG[1], Y. SASAKI[1], S. OKAYASU and K. HOJOU

Bi-2212 single crystals irradiated by 75-MeV B were investigated using transmission electron microscopy. Defects with stair-step morphology were observed in the samples. Such defects usually exist in the area where the density of the ion energy deposited is lower than that required for producing cascade defects. The analyses of the defect microstructure and the location of the defects in the target material indicate that this kind of defects is neither simple cracks nor ordinary irradiation-induced defects.

Figure 1 shows a stair-step defects observed in the Bi-2212 irradiated with 75-MeV B. Figure 2 (b) is an enlarge of area A in Fig. 1. The morphology of this defect can be characterized as follows. (1) Near the bombarded surface, the defects looks like a columnar defects with a size of about 3nm, which can be clearly seen in Fig. 2 (b). Then, the defect appears as many short amorphous column steps with an increasing column diameter ranged from 3 nm to 9nm. The short column steps are connected with each other head -to tail along the c direction of Bi-2212 crystal, but separated by a shift on a-b plane with a distance from several nanometers to several tens nanameters. The first short column step is also connected head-to tail with the long column near the sample edge. (2) Following the short amorphous column steps, the defect morphology changes to several long column steps. The two long column steps are connected in the same way as the two short column steps described above. As shown by the white arrow in Fig. 1, the orientations of two neighboring column steps, planar defects along a-b crystal plane can be found. The whole stair-step defect is about 1.2 μm long in the c direction and the total shifted distance the a-axis is about 0.6 μm. Figure 2 (a) is the enlarged image of the stair-step defect observed at area A in Fig. 2 (b), which shows the detailed relationship between two neighboring short column steps. The front column step terminates at the Ca plane of the Bi-2212 crystal and the following column step starts from the same Ca plane. No defect can be observed between two column steps.

The morphologies of stair-step defects look like cracks on first sight. However, in the Bi-2212 single crystal the Bi-double layer has weakest bonding and thus the crystal is easily cleaved along this layer. Therefore, a crack on the a-b crystal plane should most likely lie between the Bi double layer. As shown in Fig. 2 (b), however, the crystal plane connecting two steps of stair-step defects is always Ca-plane. Based on this mentioned above, therefore, we conclude that the stair-step defects are not cracks.

The formation mechanism of stir-step defects may be very special, which is much different from the usual irradiation-induced defects. In the 75-MeV boron-irradiated Bi-2212 crystal, a rough estimation made using a high-energy extended EDEP-1 code indicates that the dE/dx of incident boron ions in the whole penetration depth region is less than 8 keV/nm. From the viewpoint of the ion energy deposition in the target material, such small values of dE/dx are not enough for introducing any visible defects in

[1] R & D Laboratory, Japan Fine Ceramics Center

the target. Cross-sectional TEM observations also confirm that there are no any defects in whole samples induced by 75-MeV boron ions. This means that stair-step defects are not usual irradiation-induced defects. The forming mechanism should be much different from the usual irradiation-induced defects and may connect with some specific physic process during ion irradiation.

New type defects, which we term stair-step columnar defects, have been observed in Bi-2212 single crystals irradiated with 75-MeV B ions. Such defects were not found in the same kind of target material before ion irradiation. From the microstructure and the location in the target material, it can be excluded that the defect is a kind of crack. Moreover, such defects are usually observed in areas with a very low ion-energy-deposition density, in which the incident ions usually can not generate any visible defects in the target crystals. Therefore, we do not think that they are produced by a direct ion-target interaction. The detail mechanism for the formation of the stair-step defects needs to be further investigated.

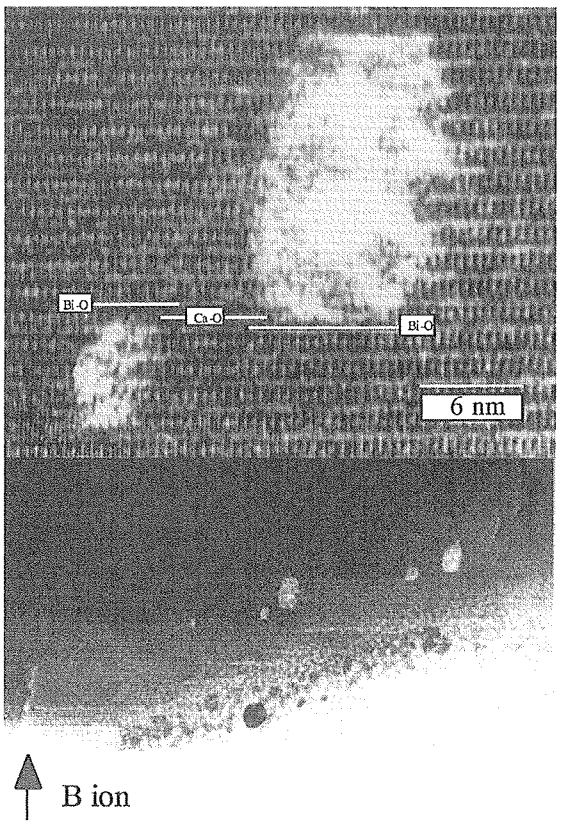

Fig. 1. Low magnification image showing complete stair-step defects in the Bi-2212 single crystal irradiated by 75-MeV B ions.

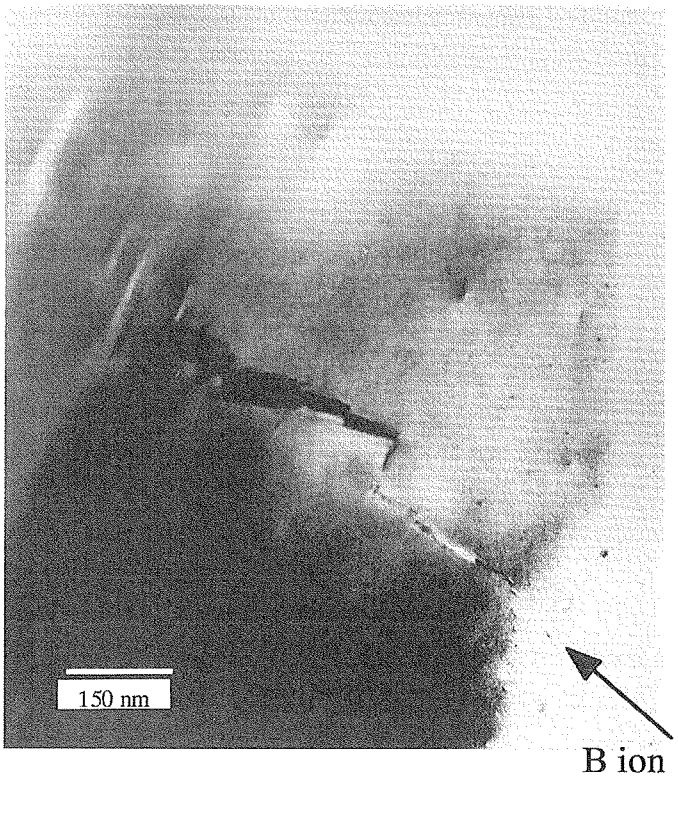

Fig. 2. (a) Enlarged image of area A in Fig. 2 (b) showing the microstructural details in the area between two short columnar steps.

5.8 ANOMALOUS MAGNETIZATION BEHAVIOR IN THE VORTEX LIQUID STATE IN $Bi_2Sr_2CaCu_2O_{8+\delta}$ WITH COLUMNAR DEFECTS

K. KIMURA[1], R. KOSHIDA[1], S. OKAYASU, M. SATAKA, Y. KAZUMATA[2], W.K. KWOK[3], G.W. CRABTEREE[3], and K. KADOWAKI[1,4]

Weak irreversible behavior was found in magnetization curves in the vortex liquid state above the irreversibility line, H_{irr}, but below a characteristic field, H_F, in as-grown $Bi_2Sr_2CaCu_2O_{8+\delta}$ single crystals and in columnar defected ones by using a SQUID magnetometer. H_F was also determined by temperature sweep measurements, and is strongly influenced by disorders in the samples. With increasing the number of columnar defects H_F systematically shifts higher temperature and field region. These results strongly suggest existence of a disorder-induced new phase between H_{irr} and H_F.

Magnetization measurements have been performed in $Bi_2Sr_2CaCu_2O_{8+\delta}$ single crystals with and without columnar defects by using a SQUID magnetometer (Quantum Design). RSO (Reciprocal Sample Option) method was used with parameters of the frequency 4 Hz and the amplitude 1 cm. $Bi_2Sr_2CaCu_2O_{8+\delta}$ single crystals were grown by the traveling solvent floating zone technique. Columnar defects were introduced into the crystals from the same batch by the heavy-ion irradiation (B_Φ = 0.005, 0.01, 0.02, 0.05, 0.1 T, 0.2, 0.5, 1 T).

Fig.1 (a) shows a set of magnetization hysteresis (*M-H*) curves of an as-grown $Bi_2Sr_2CaCu_2O_{8+\delta}$ single crystal. In the higher temperature region above 45 K magnetization jump associated with the first-order vortex lattice melting transition (represented by H_m) can be observed. In the lower temperature region below 40 K ($\sim$ the critical point, T_{cr}) the magnetization jump is no longer observed, but instead, a weak irreversible behavior below H_F can clearly be seen in the vortex liquid state above the irreversibility line (the second-order vortex glass transition line), H_{irr}, where main hysteresis almost closes (see Fig. 1 (a)). Such a behavior was also observed in all as-grown crystals we measured. H_F as well as H_{irr} can be determined more clearly by temperature-sweep measurement. A series of *M-T* curves is shown in Fig.1 (b), where magnetization steps are clearly observed in the reversible region in *M-T* curves at T_F (H), which corresponds quite well to H_F (T) determined from *M-H* curves.

In order to study the nature of the region in the vortex liquid state between H_{irr} and H_F we have checked several as-grown samples with different disorder level and different sizes, and columnar defected ones with B_Φ = 0.005 – 1 T. The weak pinning region between H_{irr} and H_F persists even in the sample with B_Φ = 1 T, and the essential features of both *M-H* and *M-T* curves above H_{irr} are qualitatively the same in all samples. H_F in two as-grown crystals, pure one and slightly disordered one, are plotted together with H_{irr}, H_m and the second peak field, H_{sp}, in *H-T* phase diagram in Fig.2 (a). In the slightly disordered sample the magnetization hysteresis area is larger than that in the pure sample, and magnetization jump denoting the first-order transition is no longer detected below 60 K. It is noted that H_F is strongly influenced by disorders and always lies below T_{cr} in as-grown samples we have measured. It appears that H_m splits into H_{irr} and H_F at T_{cr}. The weak pinning phenomena between H_{irr} and H_F may be a result of the second-order transition. It is also noted that H_F as well as H_{irr} does not depend on the sample size, which supports the interpretation that these phenomena is intrinsic in the vortex system. Fig. 2 (b) illustrates the *H-T* phase diagram of samples with

[1]Institute of Materials Science, University of Tsukuba
[2]Nihon Advanced Technology Corporation
[3]Materials Science Division, Argonne National Laboratory
[4]CREST, Japan Science and Technology Corporation (JST)

columnar defects of B_Φ = 0, 0.01, 0.02, 0.2, 0.5, and 1 T. H_F as well as H_{irr} shifts systematically to the higher temperature and the higher field region with increasing the number of columnar defects. This indicates that the weak pinning region between H_{irr} and H_F becomes more stable with disorders increased, and H_F may merge into the first-order transition line in the ideal crystal in the pure limit. It is intriguing to correlate these phenomena with the recent theoretical predictions, where the vortex-loop unbinding [1, 2] or defects [3] cause phase transitions.

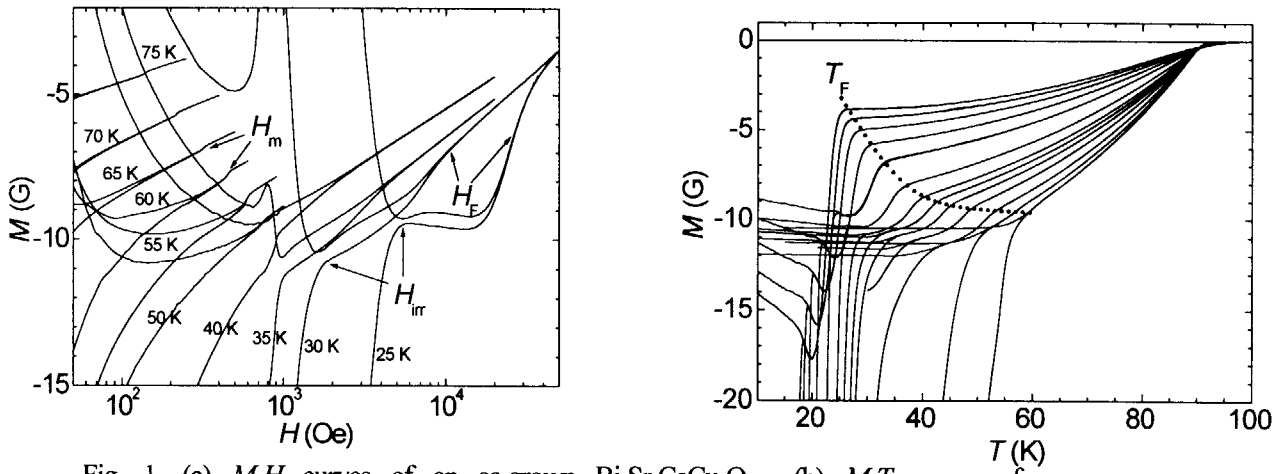

Fig. 1. (a) *M-H* curves of an as-grown $Bi_2Sr_2CaCu_2O_{8+\delta}$. (b) *M-T* curves of an as-grown $Bi_2Sr_2CaCu_2O_{8+\delta}$ (H= 0.03, 0.04, 0.07, 0.1, 0.2, 0.3, 0.5, 1, 2, 3, 4, and 5 T).

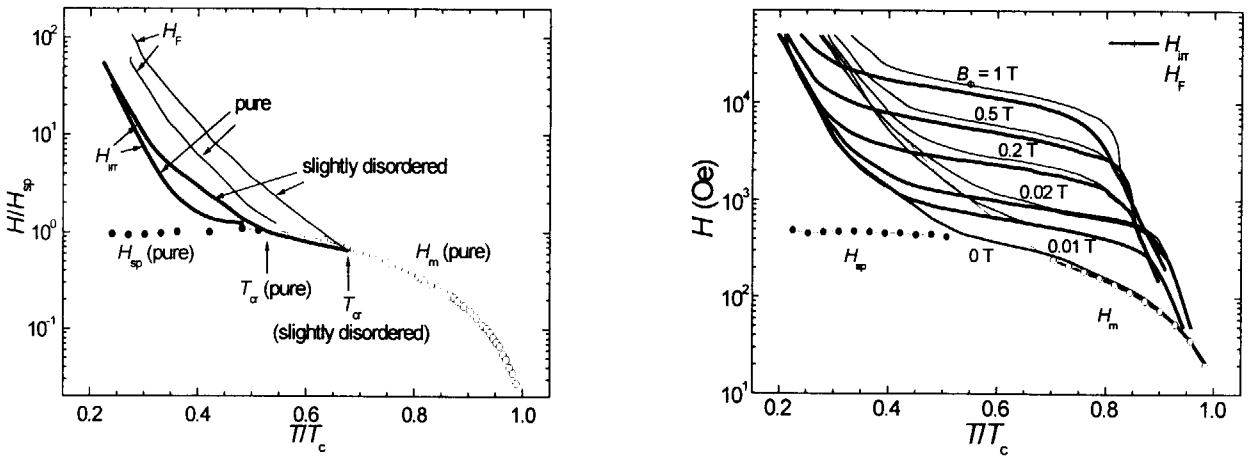

Fig. 2. (a) *H-T* phase diagram of two as-grown. T_α represents the critical point. (b) *H-T* phase diagram of with columnar defects (B_Φ = 0, 0.01, 0.02, 0.2, 0.5, and 1 T).

References

[1] Z. Tesanovic, Phys. Rev. **B 59** (1999) 6449

[2] A. K. Nguyen and A. Sudbo, EuroPhys. Lett. **46**, (1999) 780

[3] M. J. W. Dodgson, V. B. Geshkenbein, and G. Blatter, Phys. Rev. Lett. **83**, (1999) 5358

5.9 STUDY OF INTERLAYER COUPLING IN IRRADIATED $Bi_2Sr_2CaCu_2O_{8+\delta}$ SINGLE CRYSTAL BY MEANS OF JOSEPHSON PLASMA RESONANCE

I. KAKEYA [1], R. NAKAMURA[1], K. KADOWAKI[1],
S. OKAYASU, M. SATAKA, Y. KAZUMATA

Josephson plasma resonance (JPR) is a powerful tool to sense the interlayer coupling of adjacent CuO_2 superconducting layers quantitatively [1]. Several authors measured JPR in $Bi_2Sr_2CaCu_2O_{8+\delta}$ (BSCCO) with columnar defects (CD) and discussed two vortex states divided by characteristic magnetic fields depending upon those irradiation doses B_ϕ [2]. We present here experimental results of JPR in BSCCO with several doses of CD, and give a phenomenological picture which may represent the interlayer coupling quantitatively and universally.

We measured JPR for four single crystals with different doses of B_ϕ = 0.2, 0.5, 1, 2 T. Single crystals were grown by the traveling solvent floating zone method and irradiation of 650MeV I^{28+} ion was performed by a tandem accelerator at Japan Atomic Energy Research Institute (JAERI). For microwave measurements, we employed a cavity perturbation method with a cavity resonator at the rectangular TE_{102} mode (resonant frequency: 34 GHz). The resonance curves were obtained by sweeping external magnetic field generated by a split-pair superconducting magnet, and rotated at the center of it by a high precision goniometer.

The observed resonance shows considerable dependence upon temperature and irradiation doses. The plots of the resonance field as a function of the external field angle at several temperatures in samples of B_ϕ =0.2 and 1 T are represented in Fig. 1. The global features are summarized that the drastic rise near $\theta = 0$ ($\mathbf{H} \parallel ab$) observed in pristine samples is less significant at lower temperature in sample with denser dose. Temperature dependence of the resonance field for $\mathbf{H} \parallel c$ is shown in Fig. 2. The resonance field at a given temperature is largely enhanced as the irradiation dose increases. The temperature dependence shows takeoff below $T^* \simeq 80$ K, which is almost independent of CD doses. The results lead to the qualitative understanding that the interlayer coupling of BSCCO is drastically enhanced by introducing CD below T^*.

In order to describe such a change of interlayer coupling at T^* quantitatively, we apply a general scaling function to the angular dependence of the resonance field, that is,

$$H_{\rm res}(\theta) = \frac{H_{\rm res}(90^\circ)}{\sqrt{\sin^2\theta + \gamma_{\rm eff}^{-2}\cos^2\theta}}. \qquad (1)$$

This equation is quite general to describe anisotropic physical parameters such as field penetration depth inside superconductors [3], gyromagnetic (g-) factor of magnetic ions and nuclel. Here, $H_{\rm res}(\theta)$ represents the resonance field at arbitrary angle θ, and $\gamma_{\rm eff}$ is a temperature dependent effective anisotropy parameter, which renormalizes the effects of the vortex states in wider temperature region. The agreement between the experimental results and Eq. (1) is excellent except in

[1]Institute of Materials Science, University of Tsukuba.

the vicinity of $\theta = 0$ as shown in Fig. 1.

$\gamma_{\rm eff}$ for all samples are plotted as a function of temperature in Fig. 2 (open symbols). It is clear that $\gamma_{\rm eff}$ value has little temperature dependence below T^*, whereas it sharply increases above T^* and approaches the value for pristine sample. The behavior of $\gamma_{\rm eff}$ suggests that the interlayer vortex-vortex correlation grows rapidly in the irradiated samples with decreasing temperatures and it develops fully at T^* below which the anisotropy of the vortex state essentially no longer changes. This behavior can be interpreted by a picture that the pancake vortex are confined into CD below T^* and they are excited thermally to the almost freely movable state above T^*, which is independent of irradiation doses. This means that the confinement of the vortex into CD is governed by the nature of the single particle excitation.

In conclusion, we succeeded in setting a quantitative description of interlayer coupling in the vortex liquid state by JPR in irradiated BSCCO single crystals. By using the effective anisotropy parameter, we may describe microscopic vortex state with a single parameter.

This work has been supported by Core Research for Evolutional Science and Technology, Japan Science Technology Cooperation.

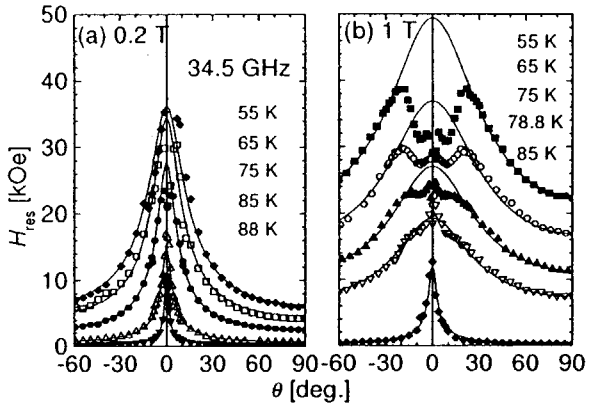

Fig. 1: Angular dependence of the resonance field $H_{\rm res}$ in samples of B_ϕ = (a) 0.2 and (b) 1 T. Solid lines are given by Eq. (1) with $\gamma_{\rm eff}$ being a unique fitting parameter.

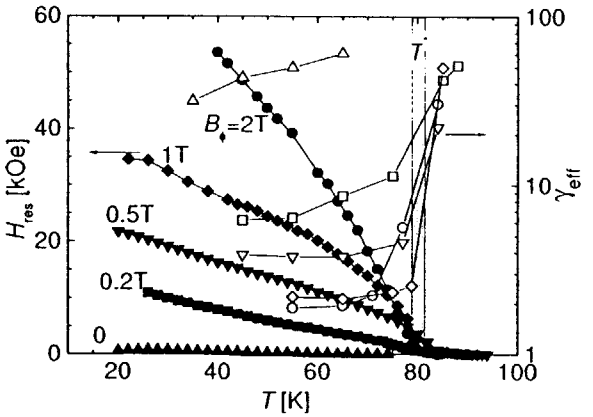

Fig. 2: Temperature dependence of the resonance field (solid) and the effective anisotropy parameter $\gamma_{\rm eff}$ (open) for all samples. The same shape of symbols means the result obtained in the identical sample. Hatched area indicates the threshold temperature T^*, and the solid lines are drawn for the eyes.

References

[1] O. K. C. Tsui *et al.*, Phys. Rev. Lett., **73** (1994) 724. L. N. Bulaevskii, M. P. Maley, and M. Tachiki, *ibid.*, **74** (1995) 801; Y. Matsuda *et al.*, *ibid.*, **75** (1995) 4512.

[2] T. Hanaguri *et al.*, Phys. Rev. Lett., **78** (1997) 3177; M. Kosugi *et al.*, *ibid.*, **79** (1997) 3763.

[3] M. Tinkham, *Introduction to Superconductivity, second edition*, McGraw-Hill, Inc. 1996.

5.10 PINNING PROPERTY CHANGE OF HIGH-ENERGY HEAVY-ION IRRADIATED $Bi_2Sr_2CaCu_2O_{8+x}$ SINGLE CRYSTALS DUE TO THERMAL ANNEALING

K.OGIKUBO[1], T.TERAI[1], S.OKAYASU and K.HOJOU

Particle-beam irradiation is one of the most effective methods to introduce strong pinning centers into high-T_c superconductors. In particular, high-energy heavy-ion irradiation is expected to produce columnar defects, which give very large pinning force for the vortices parallel to the defects. The size and the number of columnar defects as flux pinning centers can be changed by thermal annealing treatment after irradiation. This treatment is quite effective for the improvement of the superconducting properties in some cases for neutron irradiated specimens [1], because the superconducting properties are strongly affected by the defect structure in materials. In some cases, it is considered that some overlapped defect clusters make complex defects due to thermal annealing. In this study, we show the experimental results on the properties of the superconductors irradiated with high-energy heavy-ions (200 MeV Au^{13+} or 510 MeV Kr^{20+}) and annealed at high temperature.

$Bi_2Sr_2CaCu_2O_{8+x}$(Bi-2212) single crystals were prepared by the floating-zone method. Their size was 1 mm × 1 mm × 50 μm (c-axis). All of the specimens were annealed at 1073 K for 72 h in air and were quenched to room temperature in advance. The specimens were irradiated with 200 MeV Au^{13+} ions using a tandem accelerator at Tokai Research Establishment, JAERI (Japan Atomic Energy Research Institute). In addition, the results were compared with the ones on the irradiation with 510 MeV Kr^{20+} ions using an AVF cyclotron accelerator at Takasaki Radiation Chemistry Research Establishment, JAERI. The irradiation temperature was room temperature. The fluences were 5×10^{10} cm^{-2} and 1×10^{11} cm^{-2} for Au irradiation and 5×10^{10} cm^{-2} and 5×10^{11} cm^{-2} for Kr irradiation. After the irradiation, the specimens were annealed in air at 673 K for 1 h to 6 h. Magnetization hysteresis curves were measured by using a vibrating sample magnetometer (VSM) at 20 K, 40 K and 60 K as a function of applied magnetic field parallel to the c-axis. The critical current density J_c in a-b plane was calculated from the magnetization hysteresis curve using the extended Bean's model[2].

The ion-fluence dependence of J_c is shown in Fig.1. In the case of 200 MeV Au irradiation, J_c once increased at the fluence of 5×10^{10} cm^{-2} and J_c decreased at 1×10^{11} cm^{-2}. On the other hand, in the case of 510 MeV Kr irradiation, J_c increased monotonically with the fluence up to 5×10^{11} cm^{-2}. Fig.2 shows the annealing time dependence of J_c for 200 MeV Au-irradiated specimen (5×10^{10} cm^{-2}) and 510 MeV Kr-irradiated specimens (5×10^{10} cm^{-2} and 5×10^{11} cm^{-2}). For the specimen irradiated with Au ions to the fluence of 5×10^{10} cm^{-2}, J_c did not change even by thermal annealing up to 6 h. On the other hand, J_c once decreased by 1 h annealing, and slightly increased due to annealing above 3 h for the specimen irradiated with Kr ions to the fluence of 5×10^{10} cm^{-2}, while J_c gradually decreased with annealing time for the specimen irradiated with Kr ions to the fluence of 5×10^{10} cm^{-2}.

[1]Department of Quantum Engineering and Systems Science, The University of Tokyo.

In order to elucidate the reason of this different behavior of J_c between Au irradiation and Kr irradiation, the electronic stopping power of both ion species in Bi-2212 was calculated using TRIM (SRIM96) code, as shown in Table 1. It is expected that the diameter of columnar defects produced by Kr irradiation is smaller than that by Au irradiation, because Kr irradiation gives lower electronic stopping power and the diameter of a columnar defect depends on the electronic stopping power of the incident ion [3]. Therefore, it is considered that the area occupied by columnar defects in a-b plane for Kr irradiation is lower than that for Au irradiation at the same fluence.

Table 1 Electronic stopping power in Bi-2212

ion species	maximum stopping power
200 MeV Au^{13+}	30 keV/nm
510 MeV Kr^{20+}	17 keV/nm

This consideration is supported by the change of J_c due to thermal annealing after irradiation shown in Fig.2. In case of Au irradiation which makes the columnar defects of a larger diameter, J_c did not change by thermal annealing. This means that the columnar defects produced by Au irradiation at the fluence of $5\times10^{10}\,cm^{-2}$ are relatively stable against thermal annealing. Therefore, the recovery of defects due to thermal annealing is relatively small. On the other hand, in the case of Kr irradiation which makes the columnar defects of a smaller diameter, J_c gradually decreased by thermal annealing for the specimen irradiated with Kr ions to the fluence of $5\times10^{10}\,cm^{-2}$. This means the columnar defects are easily recovered due to thermal annealing. For the specimen irradiated with Kr ions to the fluence of $5\times10^{11}\,cm^{-2}$, on the other hand, J_c once decreased in 1h annealing, and slightly increased due to thermal annealing above 3h. This suggests that complex columnar defects, which are as stable as the columnar defects produced by Au irradiation, are produced of overlapped or adjacent columnar defects due to thermal annealing.

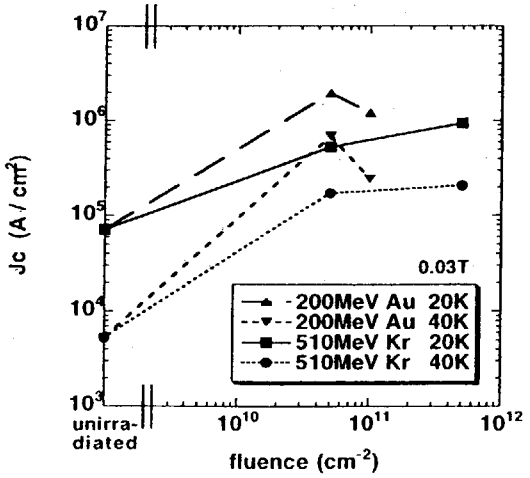

Fig.1. Fluence dependence of J_c

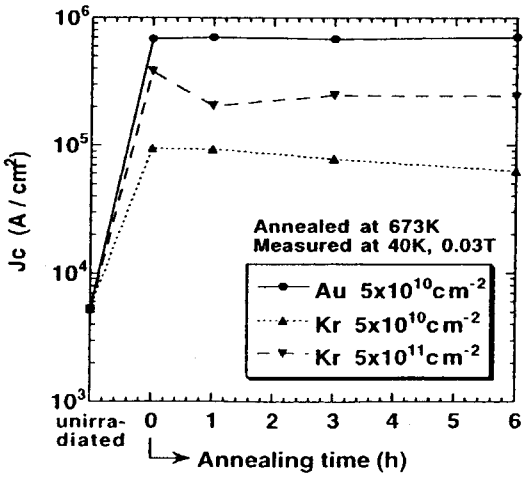

Fig.2. Annealing time dependence of J_c

References

[1] T. Terai et al., Physica C **282-287** (1997) 2285.
[2] E.M. Gyorgy et al., Appl. Phys. Lett. **55** (1989) 283.
[3] Y. Zhu et al., Phys. Rev. B **48** (1993) 6436.

5.11 LOSS OF INTERLAYER COHERENCE PROBED BY ASYMMETRIC FIELD PROFILE OF IRRADIATED $YBa_2Cu_3O_{7-\delta}$

K. ITAKA[1], M. YASUGAKI[1], T. SHIBAUCHI[1], T. TAMEGAI[1], and S. OKAYASU

One of the effective ways for increasing the critical current density (J_c) in high temperature superconductors (HTSC's) is the introduction of the correlated disorder. Heavy-ion irradiation makes columnar defects (CD's), which act as the correlated pinning centers [1]. In the vortex liquid phase of $Bi_2Sr_2CaCu_2O_{8+y}$ (BSCCO), Josephson plasma resonance (JPR) studies demonstrated that the presence of drastic enhancement of c-axis correlation at around $1/5 \sim 1/3B_\Phi$, where B_Φ is dose-equivalent matching field [2,3]. Theoretically, a Monte Carlo simulation [4] suggested that there is a field-driven boundary with enhancement of vortex trapping rate by CD's at $B_\Phi/3$ and the interlayer coherence increases there in the vortex liquid phase whereas the interlayer coherence decreases there in the phase below the irreversibility line, so-called Bose Glass phase [5]. In Bose glass phase, however, no experiments for the interlayer coherence have been performed, because the plasma frequency in Bose glass phase is much higher than in liquid phase. Recently, we reported that the asymmetric field profile was observed in YBCO under tilted CD's [6]. We demonstrated

[1]Department of Applied Physics, The University of Tokyo

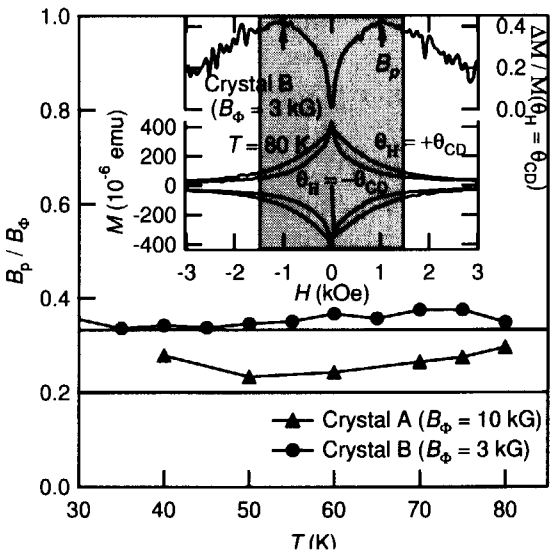

Fig. 1 Characteristic peak field B_p normalized by the matching field B_Φ as a function of temperature in crystal A (B_Φ = 10 kG) and crystal B (B_Φ = 3 kG). Inset lower panel:Magnetization hysteresis loop at T = 80 K in the case of $\theta_H = +\theta_{CD}, -\theta_{CD}$ in crystal B. The shaded area shows the field region where we performed MO imaging. Upper panel show $\Delta M/M$ as a function of the field, where ΔM is $M(\theta_H = +\theta_{CD}) - M(\theta_H = -\theta_{CD})$. B_p is defined as the peak field of M (crystal A) and $\Delta M/M$ (crystal B), because the enhancement of the magnetization by CD's is small in crystal B.

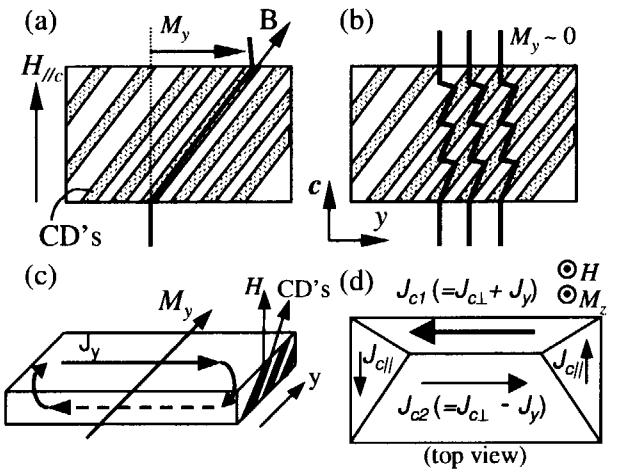

Fig. 2 Schematic figures which explain the mechanism of generating the in-plane magnetization, (a) when the vortex is completely trapped at a lower field, and (b) when the vortex is partially trapped at a higher field. Zigzag lines on the figure show vortex lines. In the case (a), in-plane magnetization M_y is generated. In-plane (c) and out-of-plane (d) components of magnetization and their accompanying shielding current in the field decreasing branch at a positive field. Arrows on the sample show the direction and magnitude of shielding current density. J_{c1} and J_{c2} are determined by the constraint that the sum of currents in (c) and (d) cannot exceed the in-plane critical current density $J_{c\perp}$.

that the asymmetry (the shift of the central current discontinuity line (d-line)) is originated from the in-plane magnetization, which is caused by trapped vortices onto CD's. In this paper, we examined the interlayer coherence in Bose Glass phase probed by the asymmetric field profile.

Experimental details are described in Ref. 6. The critical temperature of the pristine sample is around 91 K. Crystals were irradiated along the direction $\theta_{CD} = 10°$ from the c axis with 600 MeV iodine ions at doses corresponding to $B_\Phi = 10$ kG (crystal A) and $B_\Phi = 3$ kG (crystal B) using the tandem Van de Graaff accelerator with superconducting booster at JAERI. We defined θ_{CD} as the angle of CD's from the c axis, θ_H as the angle of the applied field from the c axis.

The inset of Fig. 1 shows magnetization M and $\Delta M/M$ as a function of the applied field H at $T =$ 80 K in crystal B with $\theta_H = \theta_{CD}$. The enhancement of the irreversible magnetization shows a maximum at around $B_\Phi/3$ and we define B_p as the peak field of M and $\Delta M/M$ (see caption). Main panel of Fig. 1 shows B_p normalized by the matching field B_Φ as a function of temperature in both crystals. B_p/B_Φ is almost independent of temperature and its value is around $1/3 \sim 1/5$, which is similar to that reported in BSCCO [7]. Figure 2 schematically shows our proposed model which explains the asymmetric field profile (see caption). The detail of our model is described in Ref. 6. When the vortex line becomes zigzag-like as shown in Fig. 2 (b), the in-plane magnetization M_y will disappear. So M_y yields important information on the interlayer coherence. In Fig. 2, the ratio $(1 + \Delta y)/(1 - \Delta y)$ gives J_{c1}/J_{c2}, and Δy is therefore equal to the ratio of the current densities $J_y/J_{c\perp}$ [8,9]. Our model concludes that the asymmetry of the field profile (the shift of d-line) corresponds to the existence of the in-plane magnetization M_y. Therefore, the asymmetry of the field profile in the critical state is a powerful probe for the interlayer coherence.

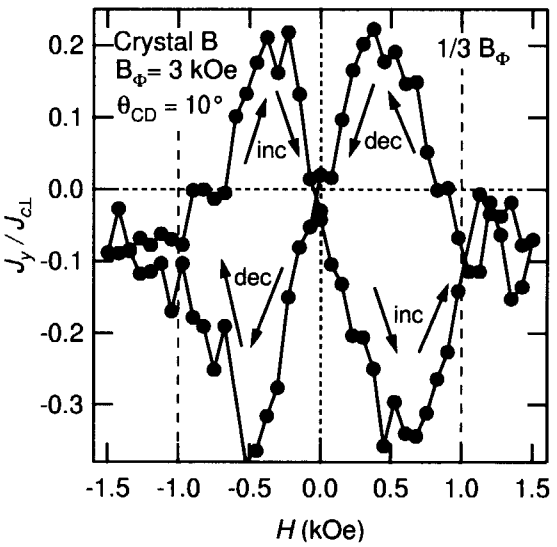

Fig. 3 $J_y/J_{c\perp}$ as a function of the applied field H at $T = 55K$ in crystal B. Arrows with "inc" and "dec" indicate the field sweep directions.

Next let us discuss what happens on the asymmetry when we cross B_p in crystal B. Figure 3 shows $J_y/J_{c\perp}$ as a function of the applied field H at $T = 55$ K and $\theta_H = 0°$. Surprisingly, the absolute value of $J_y/J_{c\perp}$ has a maximum at around $B_\Phi/5$ and becomes almost zero (with no hysteresis) above $B_\Phi/3$. This behavior indicates that vortices are aligned along CD's below $B_\Phi/3$, and the interlayer coherence is suppressed above $B_\Phi/3$. This field range of the interlayer coherence anomaly is quite similar to that of field-induced recoupling in the vortex liquid phase of irradiated BSCCO observed by JPR studies [2,3,10]. Moreover, our results that the interlayer coherence shows a drastic decrease instead of the increase in the liquid state are consistent with the prediction of the simulation result [4] in the Bose glass phase. The anomalous interlayer coherence around $(1/5 \sim 1/3)B_\Phi$ may also explain the peak observed at the similar field range in M-H curves (Fig. 1).

In conclusion, we observed an asymmetric critical-state field profile in YBCO with CD's when the field is tilted away from CD's. The asymmetry in terms of the in-plane magnetization is considered to be originated from the alignment of vortices along CD's. We proposed that the asymmetry of the critical state can be used as a powerful probe of the interlayer coherence. We observed for the first time the coherence of vortices along CD's has a maximum at around $B_\Phi/5$ and becomes small

at around $B_\Phi/3$ in Bose glass phase. This result in YBCO is analogous to the results of Josephson plasma resonance in BSCCO.

References

[1] L. Civale *et al.*, Phys. Rev. Lett. **67** (1991) 648.
[2] M. Sato *et al.*, Phys. Rev. Lett. **79** (1997) 3759.
[3] M. Kosugi *et al.*, Phys. Rev. Lett. **79** (1997) 3763.
[4] R. Sugano, T. Onogi, K. Hirata, and M. Tachiki, Phys. Rev. Lett. **80** (1998) 2925.
[5] D. R. Nelson and V. M. Vinokur, Phys. Rev. B **48** (1993) 13060.
[6] K. Itaka *et al.*, J. Low Temperat. Phys. **117** (1999) 1369.
[7] N. Chikumoto *et al.*, Phys. Rev. B **57** (1998) 14507.
[8] T. Schuster, H. Kuhn, E. H. Brandt, and S. Klaumunzer, Phys. Rev. B **56** (1997) 3413.
[9] T. Haage *et al.*, Phys. Rev. B **56** (1997) 8404.
[10] Y. Tsuchiya *et al.*, Phys. Rev. B **59** (1999) 11568.

5.12 ELECTRONIC EXCITATION EFFECTS ON PEROVSKITE OXIDES BY HIGH ENERGY HEAVY ION IRRADIATION

N. MATSUNAMI[1], M. SATAKA and A. IWASE

The number of atomic displacements is one of the key quantities of ion irradiation effects and there is a considerable interest of electronic excitation effects on atomic displacement. To investigate the electronic excitation effects on ion-induced atomic displacement in some perovskite oxides, we have measured the sputtering yields of $YBa_2Cu_3O_{7-\delta}$ (YBCO) and $SrCe_{0.95}Yb_{0.05}O_{3-\delta}$ (SCO) by using 200 MeV I^{12+} ions. It should be noticed that the sputtering yield measurement is a "direct" method for the observation of atomic displacements. YBCO and SCO samples are prepared on MgO by sputter-deposition and pulsed-laser deposition methods, respectively. The thickness of both samples is about 100 nm. During ion irradiation up to a dose of 10^{14} /cm^2 in vacuum of ~10^{-5} Pa, sputtered atoms are collected on carbon(C-) foil (4 mm in diameter and about 100 nm in thickness) which is placed in front of the samples. Since the calculated energy loss and Bohr straggling in the C-foil for 200 MeV I are only 1.6 MeV and 0.07 MeV, respectively, the C-foil does not disturb the experiments. The amount of sputtered atoms collected in the C-foils is analyzed by the MeV He Rutherford backscattering spectroscopy (RBS).

Collection efficiency of the C-foils, fc, is calibrated by 120 keV Ne^+ ions using the same assembly as for high energy heavy ion irradiation. The calculated energy loss and Bohr straggling in the C-foil for 120 keV Ne^+ ions are 60 keV and 13 keV, respectively. Experimentally, sputtering of YBCO and SCO by 100 keV Ar is found to be nearly stoichiometric and hence stoichiometric sputtering is assumed in evaluation of fc. Preliminary results are given in Table 1.

Using the values in Table 1, the sputtering yields of YBCO and SCO by 198 MeV I are summarized in Table 2. It appears that the sputtering of both samples is not stoichiometric in contrast to that by low energy ions such as 100 keV Ar and Ne. The total sputtering yields of YBCO and SCO are ~600 and ~1700 atoms per ion, respectively, excluding oxygen contribution. These values are larger by a factor of ~1000 than the calculated sputtering yield by TRIM code and by utilizing linear relationship between the sputtering yield and the nuclear stopping power, indicating a contribution of the electronic excitation to the sputtering phenomena. Investigations are under way for different energies and ions to vary the electronic energy deposition density. Considerable mixing is also observed by the MeV He RBS between YBCO or SCO film and MgO substrate.

We thank Prof. M. Ishigame and Dr. N. Sata for supplying us SCO samples.

[1] Dept. Energy Engineering and Science, School of Engineering, Nagoya University

Table 1 Collection efficiency of carbon foil, fc = atoms on C-foil/(dose・sputtering yield・composition ratio), calibrated by using 120 keV Ne. The energy loss in C-foil (~100 nm) for 120 keV Ne is approximately 60 keV. The sputtering yield Ys by 120 keV Ne after transmission through the C-foil was experimentally obtained as 1.1 and 0.61 for YBCO and SCO, respectively. An estimated error of fc is 20%.

YBCO	Y	Ba	Cu	Dose investigated
(Ys=1.1)	0.048	0.076	0.061	15~23x10^{15}/cm^2
composition ratio	1/13	2/13	3/13	

SCO(5%Yb)	Sr	Yb	Ce	Dose investigated
(Ys=0.61)	0.031	0.025	0.013	4~23x10^{15}/cm^2
composition ratio	1/5	0.05/5	0.95/5	

Table 2 Sputtering yield of YBCO/MgO and SCO/MgO by 198 MeV I^{12+} ion impact. Values in the parentheses are the composition ratios of the collected atoms. Oxygen contribution is not included in the total sputtering yield. The calculated sputtering yield (TRIM92) are 0.1 for both YBCO and SCO, assuming that the surface binding energies are 3 and 4.5 eV for YBCO and SCO, respectively. Ys-values in the square bracket are the sputtering yield derived from the experimental sputtering yields by 100 keV Ar and Ne, assuming that the sputtering yield is proportional to the nuclear stopping power.

YBCO	Dose(10^{14}/cm^2)	Y	Ba	Cu	Total
[Ys= 0.42]	1.1	18.9 (0.23	161 2	328 4.1)	508
	0.5	67.5 (0.42	321 2	274 1.7)	663
	0.17	70 (0.23	602 2	287 0.95)	959

SCO	Dose(10^{14}/cm^2)	Sr	Ce	Yb	Total
[Ys= 0.25]	1.1	560 (1	903 1.6	18 0.032)	1481
	0.5	934 (1	1021 1.1	32.5 0.035)	1988

5.13 RADIATION DEFECTS IN NANOCRYSTALLINE MATERIALS

H.OHTSUKA, H.SUGAI, K.HOJO, H.MAETA[1]

The aim of this study is to see the size or structural effects of the nanocrystalline against radiation damage. When the size of the structural crystal is comparable to or less than the defect free zone, the defects by the irradiation would easily escape from the crystal leaving no damage in it. If we were able to show a positive result, this would lead to a proposal of a new material for irradiation circumstances. We report here progresses during this period (FY 1999) of both apparatus and a preliminary experimental result. In this study Au nanocrystalline that is made by the gas deposition method is used as the sample because of its chemical stability. Using a transmission electron microscope (TEM) we discuss defect cluster formation.

Because the basic process of that phenomenon is diffusion of the simple defects, we consider that the temperature of the sample is an important parameter. We have made an experimental chamber, which is capable of heating samples, on a beam line of the tandem accelerator. By a rotation mechanism each sample holder can be faced the beam without vacuum break. A problem is to avoid an influence of the heat from the neighboring sample holder. By thermal insulation and cooling mechanism a temperature rise of the neighboring sample is limited within a tolerable level, 20 ℃ for example, when a sample is heated up to 300 ℃.

We have already observed defect cluster formation, mostly stacking-fault tetrahedra (SFT), in Au nano-particles after a heavy ion irradiation at the room temperature. In the present experiment temperature dependence of the defect formation is investigated. In the 200 ℃ case the SFT formation still appeared as shown in Figure 1. This figure is not so different from that so far observed at room temperature. At 300 ℃, however, such defect cluster is scarcely observed. That indicates that the critical temperature of the defect annihilation lies between 200 and 300 ℃. Analysis of diffusion of defects in nano-particles using those data is now under study .

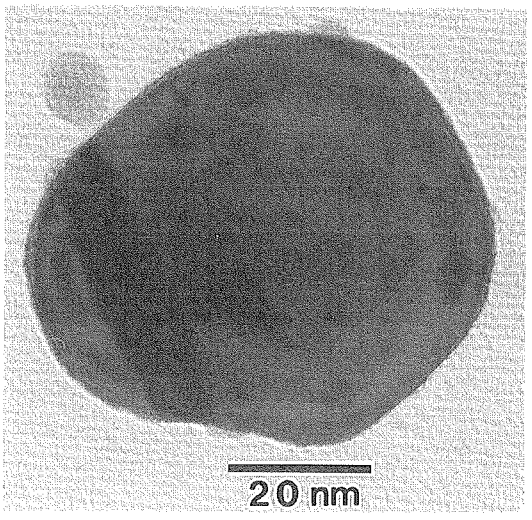

Fig.1 TEM observation of a nano-particle irradiated with iodine ions at 200 ℃. Black spots in the particle are defect clusters

[1] Faculty of Engineering, Hiroshima Kokusai Gakuin University

5.14 DISORDERING OF HYDROGEN ATOMS INDUCED BY HIGH ENERGY ION IRRADIATION IN Pd- H SYSTEM

K. ADACHI[1], Y. CHIMI, A. IWASE, N. ISHIKAWA and K. YAMAKAWA[1]

It is well known that in Pd- H(D) system hydrogen atoms are ordered on their interstitial sublattice below 50K[1]. The ordering of hydrogen atoms leads to the increase in electrical resistivity of Pd- H [2]. We have studied the effects of high energy ion irradiation on the ordered state of hydrogen in Pd-H system at low temperatures by using the electrical resistivity measurements.

Palladium foil 1.5 μm thick was doped with hydrogen to the atomic ratio, H/Pd, of about 0.5. The Pd- $H_{0.5}$ specimen was gradually cooled to 10K in order to realize the ordered state of hydrogen. Then, it was irradiated with 60 MeV carbon ions, and the electrical resistivity of the specimen was measured as a function of ion- fluence. The irradiation and the resistivity measurement were performed at 10K.

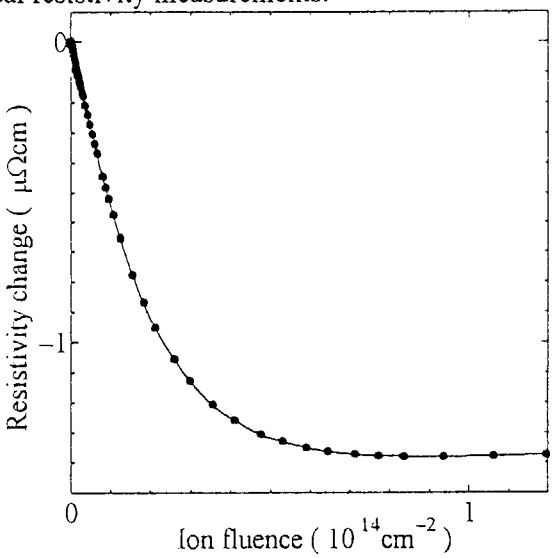

Fig. 1. Resistivity change of PdH as a function of ion fluence

In Fig. 1, the change in resistivity is plotted against the ion- fluence. The resistivity decreases with increasing the ion- fluence. This result means that the ion- irradiation induces the disordered state of hydrogen. The resistivity decrease rate (the decrease per unit ion-fluence) for 60MeV carbon ion irradiation is 10^5 times as large as for 0.5MeV electron irradiation[3]. The extremely high rate of the hydrogen disordering by carbon ions may be due to the large cross section for the elastic collisions between incident ions and hydrogen atoms, and/or the ion induced high density electronic excitation.

References

[1] O. Blaschko, P. Fratzl and R. Klemencic, Phys. Rev. **B24**(1981) 277.

[2] T. Skoskiewics and B. Baranowski, Phys. Stat. Sol. **30**(1968) K33.

[3] K. Adachi, Y. Chimi, N. Ishikawa, A. Iwase and K. Yamakawa, JAERI- Research(2000) to be published.

---

[1]Faculty of Engineering, Ehime University

5.15 RADIATION ANNEALING INDUCED BY HIGH-DENSITY ELECTRONIC EXCITATION IN IRON

Y. CHIMI, A. IWASE, N. ISHIKAWA, N. KURODA and T. KAMBARA[1]

Effects of high-density electronic excitation on radiation annealing, i.e., annihilation of defects during irradiation have been studied by high-energy heavy ion irradiation in iron [1]. Specimens were polycrystalline iron thin films (~200nm thick) which were deposited on α-Al_2O_3 single crystal substrates. Several heavy ion irradiations were performed at a low temperature (~77K). Irradiating ions were as follows; 84-200MeV ^{12}C-^{197}Au ions from a 20MV tandem accelerator at JAERI-Tokai (Japan Atomic Energy Research Institute, Tokai Research Establishment) and 3.1-3.8GeV ^{136}Xe-^{209}Bi ions from a ring cyclotron at RIKEN (The Institute of Physical and Chemical Research). In order to extract the electronic excitation effects, irradiations with 0.5-2.0MeV ^{1}H-^{40}Ar ions from a 2MV Van de Graaff accelerator at JAERI-Tokai were also performed. The increment in electrical resistivity of the specimen was measured as a function of ion fluence during each irradiation, and the cross-sections for defect production and defect annihilation were derived from the irradiation behavior.

The defect annihilation cross-sections, σ_r's, for ~100MeV and GeV heavy-ion irradiations were much larger than those for ~1MeV ion irradiations at the same nuclear stopping power. This means that for high-energy heavy ion irradiation the defect annihilation is enhanced by the electronic excitation. In Fig.1, therefore, the values of σ_r are plotted against the electronic stopping power, S_e, for each high-energy ion irradiation. Except for a few kinds of ions (Br, I, Au), σ_r is nearly proportional to S_e^2. In the case of Br, I and Au ions, the values of σ_r are larger than that for the other ions even at the same S_e. This difference is caused by the difference in ion velocity (what is called the velocity effect). The lower velocity ions cause the more defect annihilation. A similar velocity effect has been seen on damage creation in bismuth [2]. Thus, it appears that S_e is not appropriate for describing this irradiation behavior. As a candidate for the scaling parameter, we suggest the primary ionization rate (dJ/dx), which is the number of atoms primarily ionized by an incident ion per unit length along the ion path. The dependence of σ_r on dJ/dx is shown in Fig. 2. For all the high-energy ion irradiations, σ_r is proportional to $(dJ/dx)^2$. This result implies that the defect annihilation may be triggered by the ion explosion mechanism [3]. Detailed interpretation of the radiation annealing process during high-energy ion irradiation is under consideration.

References

[1] Y.Chimi, A.Iwase, N.Ishikawa, N.Kuroda and T.Kambara, Nucl. Instrum. Methods **B164-165**(2000)408.

[2] Z.G.Wang, Ch.Dufour, B.Cabeau, J.Dural, G.Fuchs, E.Paumier, F.Pawlak and M.Toulemonde, Nucl. Instrum. Methods **B107**(1996)175.

[3] R.L.Fleischer, P.B.Price, R.M.Walker and E.L.Hubbard, Phys. Rev. **156**(1967)353.

[1]Atomic Physics Laboratory, The Institute of Physical and Chemical Research (RIKEN)

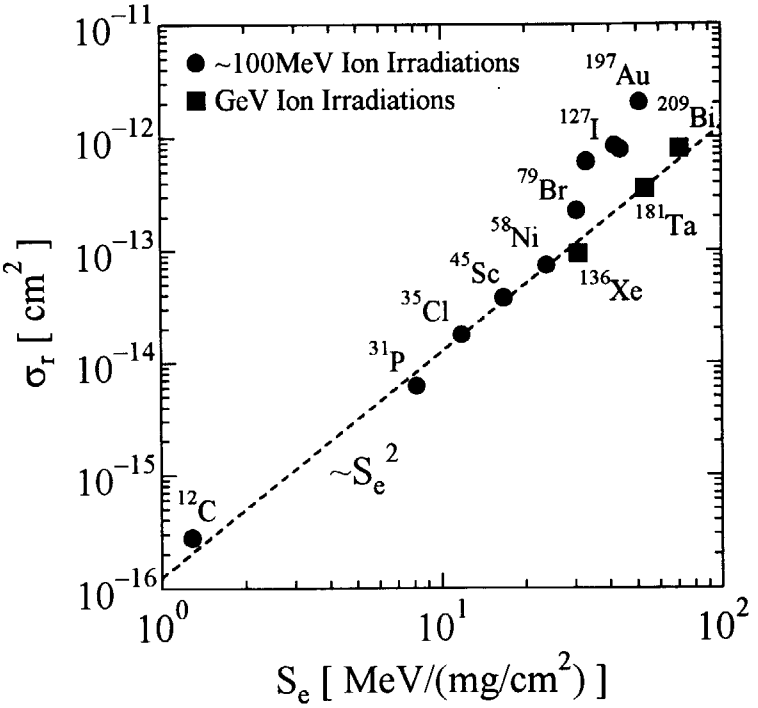

Fig. 1. Defect annihilation cross-section, σ_r, plotted against electronic stopping power, S_e, for each high-energy ion irradiation.

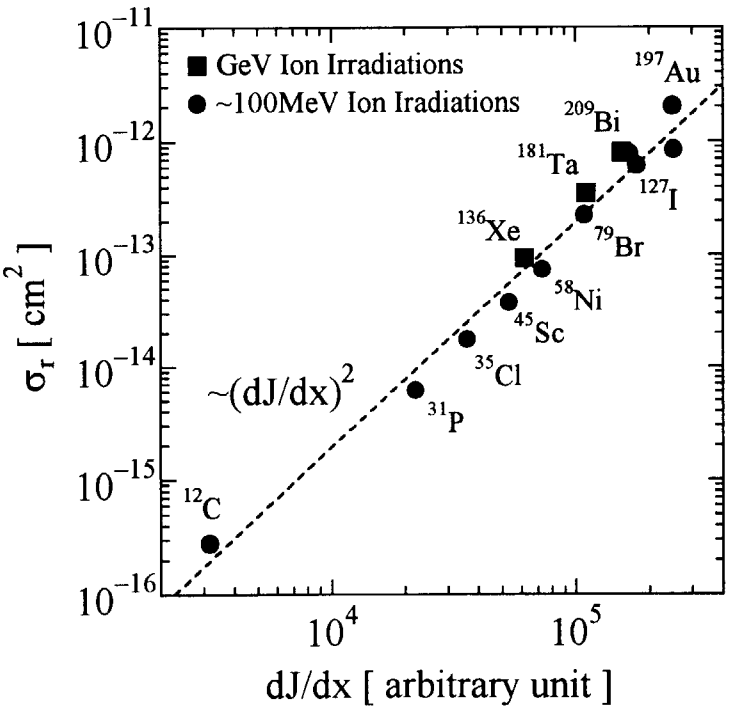

Fig. 2. Defect annihilation cross-section, σ_r, plotted against primary ionization rate, dJ/dx, for each high-energy ion irradiation.

5.16 STUDY OF IRRADIATION EMBRITTLEMENT MECHANISM ON PRESSURE VESSEL STEELS BY HIGH ENERGY HEAVY ION IRRADIATION

T.HASEGAWA[1], S.ISHINO[2], T.TOBITA, Y.CHIMI, N.ISHIKAWA AND A.IWASE

To elucidate the mechanism of radiation embrittlement in pressure vessel steels, it is very important to clarify the effect of each parameter which might be involved in the embrittlement phenomena and then to make a model by integrating the effects of these parameters. A lot of experiments on irradiation embrittlement in pressure vessel steels have been carried out so far mainly by using energetic neutrons from materials testing reactors. However, it is difficult to control the parameters contributing to irradiation embrittlement independently in neutron irradiation experiments. On the other hand, irradiation experiments by using energetic ions are able to overcome such problems to some extent.

Four model Fe-Cu alloys which have largely different Cu concentration (Cu: 0.02, 0.1, 0.6 and 1.2wt%) were chosen as specimens. Four specimens were arranged on the specimen holder to irradiate simultaneously under an identical irradiation condition. Irradiations were performed with 200MeV Au and Ni ions using the JAERI-Tokai tandem accelerator. By covering a part of the specimen surface with a stainless sheet, we could get irradiated and unirradiated areas in the same specimen. In this study, hardness measurements were performed to derive information concerning the embrittlement. Hardness of irradiated and unirradiated areas in the specimen was measured with a Vickers type diamond pyramid indenter. The difference in hardness between the irradiated and unirradiated areas, ΔHV, was used as a measure of embrittlement. Indentation load was varied from 3 to 10kgf.

Fig 1 shows the dose rate dependence of ΔHV for several Fe-Cu specimens irradiated up to 0.44mdpa with Ni ions at 250℃. It appears that the irradiation of lower dose rate is more effective for the hardness increase than that of higher dose rate, and the increase in hardness is proportional to the dose rate to the power between -1/5 and -1/3.
Fig 2 shows the dose dependence of ΔHV for Fe-0.6wt%Cu alloys in comparison with another experiment[1]. The experimental curve of the relation between dose and ΔHV for the ion irradiations has a similar trend to that of electron irradiations. However, this trend may shift to lower dose side because the dose rate of ion irradiations is about two orders of magnitude higher than that of electron irradiations.

[1] Course of Applied Science, Graduate School of Engineering, Tokai University
[2] Department of Nuclear Engineering, School of Engineering, Tokai University

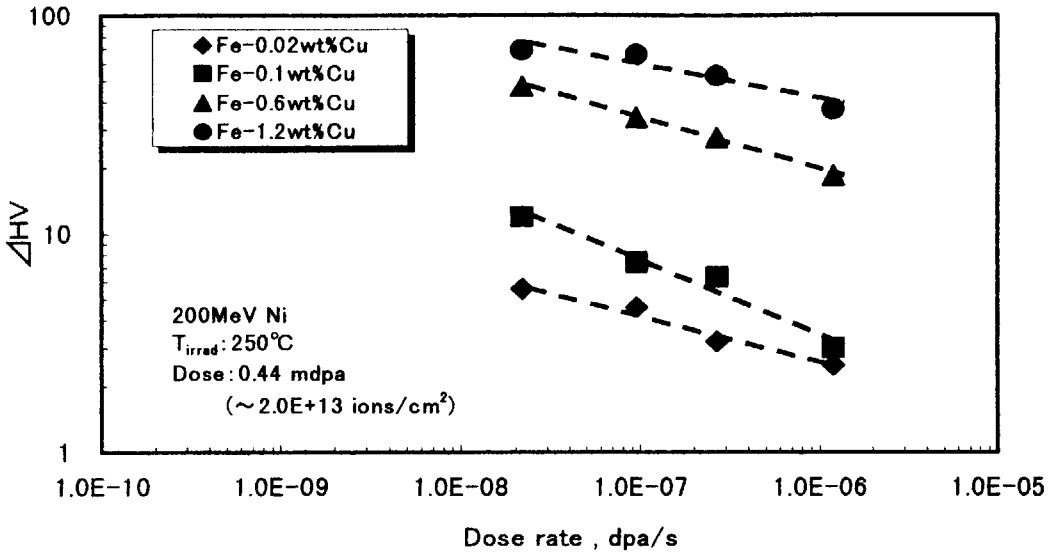

Fig.1. Dose rate dependence of ⊿HV irradiated with 200MeV Ni ions up to 0.44mdpa at 250℃.

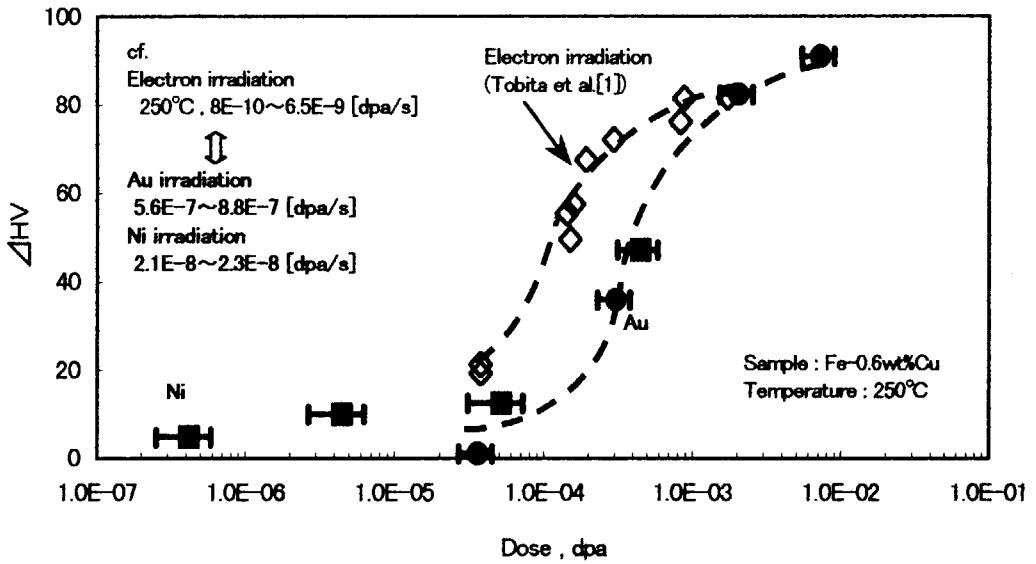

Fig.2. Dose dependence of ⊿HV for Fe-0.6wt%Cu alloys with 200MeV Au and Ni ions at 250℃. For comparison, the data of electron irradiations[1] are plotted.

[1] T.Tobita, M.Suzuki, Y.Idei, A.Iwase and K.Aizawa, Proc. Transaction of the 15th International Conference on Structural Mechanics in Reactor Technology, Seoul, Korea (1999)

5.17 STUDY OF RADIATION DAMAGE IN Li_2TiO_3 CERAMICS IRRADIATED BY HIGH ENERGY OXYGEN IONS

V.GRISMANOVS, T.NAKAZAWA, D.YAMAKI, Y.KATANO and A.IWAMOTO

Lithium metatitanate ceramics (Li_2TiO_3) is regarded as one of the most suitable candidate for the solid tritium breeder material of D-T fusion reactors. It is common knowledge that in an operating fusion reactor, the radiation damage in Li_2TiO_3 will be produced by fast neutrons, energetic tritons (2.7 MeV) and helium ions (2.1 MeV) generated by the $^6Li(n,\alpha)^3H$ reaction. The damage caused by ionizing radiation may result in the microstructure changes and hence may have an impact on the tritium release behaviour, thermal and mechanical properties of Li_2TiO_3. Thus, the study of irradiation defects and damage microstructure in Li_2TiO_3 is essential in order to evaluate its irradiation performance.

The Li_2TiO_3 ceramic specimens (78% of theoretical density) were irradiated at ambient temperature by high energy oxygen ions (30, 80 and 120 MeV) with a tandem accelerator of JAERI. The accumulated ion fluence was in the range from $2.0x10^{18}$ to $2.0x10^{20}$ ion/m^2. Then, the irradiated samples have been examined by Raman spectroscopy, Fourier transform infrared photo-acoustic spectroscopy (FT-IR PAS), electron-spin resonance (ESR) spectroscopy, scanning electron microscopy (SEM) and X-ray diffraction (XRD) technique.

The examinations of Li_2TiO_3 ceramics exposed to high energy oxygen ions by FT-IR PAS deduced no evidence of the destruction of Li_2TiO_3 structure. Some small changes of the Raman spectra and XRD patters of irradiated specimens were found but those gave no way for analytical analysis. Furthermore, the ESR measurement showed that there are no paramagnetic radiation defects in Li_2TiO_3 irradiated by oxygen ions.

The SEM observations disclosed beyond a doubt that the surface layer of Li_2TiO_3 ceramics was melted due to the radiation induced heating (Figure 1). In such a manner one can suggest that the changes in the Raman spectra and XRD patters are associated with an evaporation of Li from the surface layers of Li_2TiO_3 ceramics causing a formation of other Li_2O–TiO_2 compounds in a very small quantity. The thickness of the melted region is estimated at about 15–20 μm and it almost independent on the energy of incident ions. The small pores of the size less then 1 μm can be seen in the melted region of Li_2TiO_3 specimen (Figure 2).

In summary, the radiation damage of the Li_2TiO_3 structure was unfeasible to discover after the irradiation by MeV oxygen ions since the radiation induced heating results in the melting of irradiated surface. It seems plausible and necessary to conduct such investigations if the single crystals of Li_2TiO_3 will be available in the future. Hopefully that, in the case of single crystals possessing a better thermal conductivity, the heat will be efficiently removed from the irradiated surface and the melting process will be prevented.

[1]OECD Halden Reactor Project, P.O. Box 173, N-1751, Halden, NORWAY

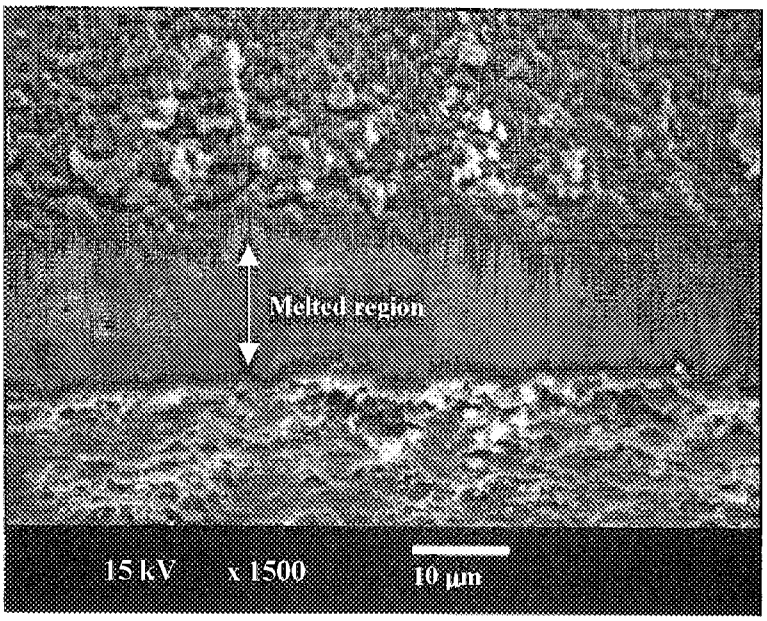

Figure 1: Bulk micrographs of Li_2TiO_3 ceramics irradiated by 120 MeV O^{7+} ions to the fluence up to $2.4x10^{18}$ ion/m^2.

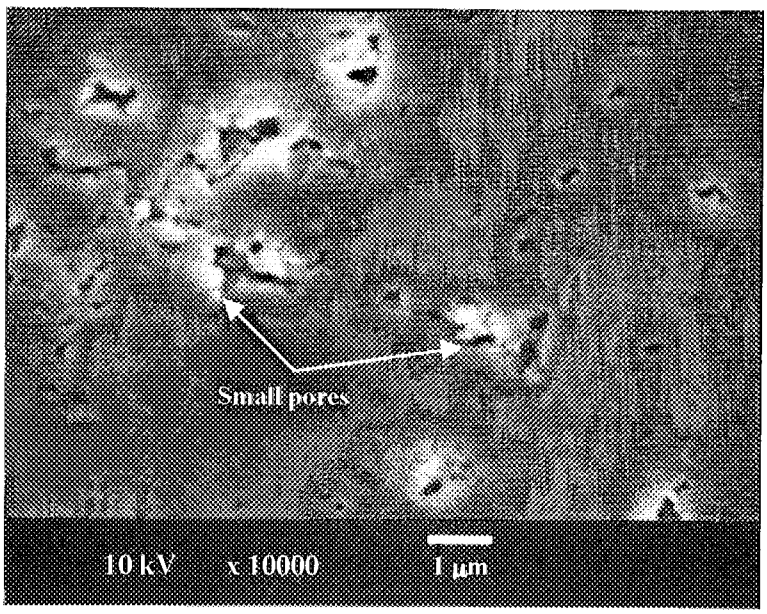

Figire 2: Bulk micrographs of the melted region of Li_2TiO_3 ceramics irradiated by 120 MeV O^{7+} ions to the fluence up to $2.4x10^{18}$ ion/m^2.

5.18 ION IRRADIATION EFFECT ON MECHANICAL PROPERTIES OF CARBON FIBERS

T. OKU[1], A. KURUMADA[1], M. ISHIHARA, K. HAYASHI, S. BABA and J. AIHARA

Carbon/carbon composite materials are candidates for plasma facing components of fusion reactors in the future. There are several research subjects to be investigated furthermore in future; deterioration of thermal and mechanical properties due to radiation damage effects, surface erosion of carbon materials due to high heat flux from plasma, and so on. It is well known that the radiation damage in less crystalline materials is larger than that in higher crystalline ones. Carbon fibers in C/C composites are generally less crystalline than the matrix part. Consequently, it is important to investigate the radiation damage on the thermal and mechanical properties of carbon fibers for C/C composite materials.

Four kinds of carbon fibers with different microstructures in the cross section were selected, and carbon ion irradiation experiment was carried out using the TANDEM accelerator. They were a PAN based fiber (M55JB by Toray Co.), a pitch based fiber (K13C2U by Mitsubishi Chemical Co.) and two mesophase pitch based fibers (YS-15-60S and YS-70-60S by Nippon Graphite Fiber Corp.). The fibers were irradiated with 100 MeV carbon ions up to a particle fluence of 8.5×10^{13}particles/cm^2. The estimated projected range and the total fluence calculated by the TRIM code were about 160 μm and 1×10^{-5} dpa, respectively.

Tensile test and SEM observation were conducted separately before and after ion irradiation. Cross-sectional area was measured using SEM, and Young's modulus was evaluated by the tensile stress-strain curve of the carbon fiber.

Table 1 shows changing ratios in cross-sectional area, Young's modulus and tensile strength of carbon fibers due to carbon ion irradiation. In this table, the effect of 175 MeV argon ion irradiation using TIARA up to an ion fluence of 1.9×10^{14}ions/cm^2 was also listed. The estimated projected range and the total fluence were about 40 μm and 1×10^{-3} dpa, respectively. From this table, it was found clearly that the cross-sectional area increased after ion irradiation, and the specimens irradiated with argon ions showed higher increasing rate. One of the reasons would be understood from the irradiation effects of the crystal growth of graphite in c-axis direction by the neutron irradiation, since the c-axis direction of graphite crystal was coincident with radial direction in the cross section of the fiber. As an example, figure 1 shows SEM images of the cross section of the YS-70-60S fiber before and after carbon ion irradiation by TANDEM.

It seemed that the Young's modulus of the mesophase pitch based fibers were comparatively stable to radiation damage effects, because the changing ratio of the YS-15-60S fiber due to ion irradiation was close to 1.00.

Changes in tensile strength of carbon fibers due to ion irradiation showed a similar tendency to that of the Young's modulus. It might be concluded, therefore, that the mesophase pitch based fibers were stable to radiation damage effects.

---

[1] Faculty of Engineering, Ibaraki University

Table 1 Changing ratios in mechanical properties of carbon fibers due to carbon ion irradiation by TANDEM.

	Changing ratio in cross-sectional area	Changing ratio in Young's modulus	Changing ratio in tensile strength
M55JB (PAN based fiber)	1.36 (1.53)	1.44 (0.93)	1.00 (0.69)
K13C2U (Pitch based fiber)	1.26 (1.26)	0.72 (1.10)	0.56 (0.77)
YS-15-60S (Mesophase pitch based fiber)	- (1.38)	- (1.05)	- (1.03)
YS-70-60S (Mesophase pitch based fiber)	1.62 (1.79)	0.78 (0.78)	0.74 (0.78)

Values in parentheses indicate the effects of argon ion irradiation using TIARA.

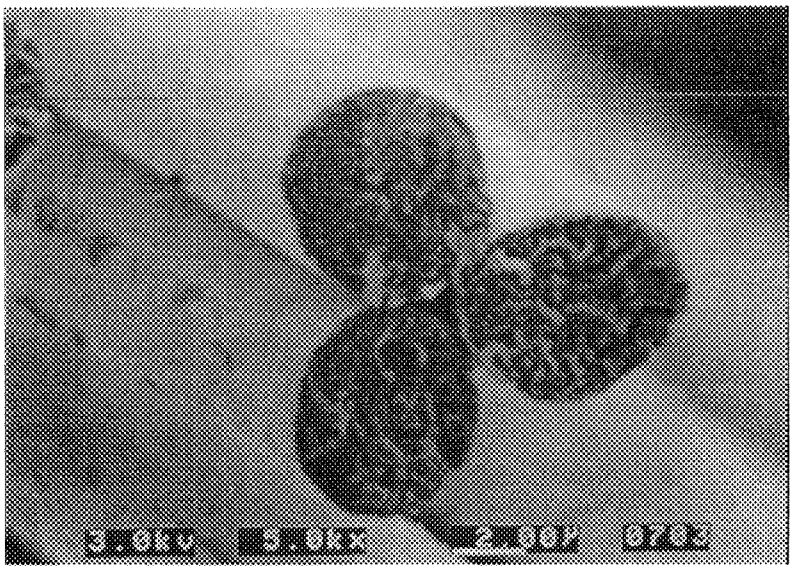

(a) Before irradiation

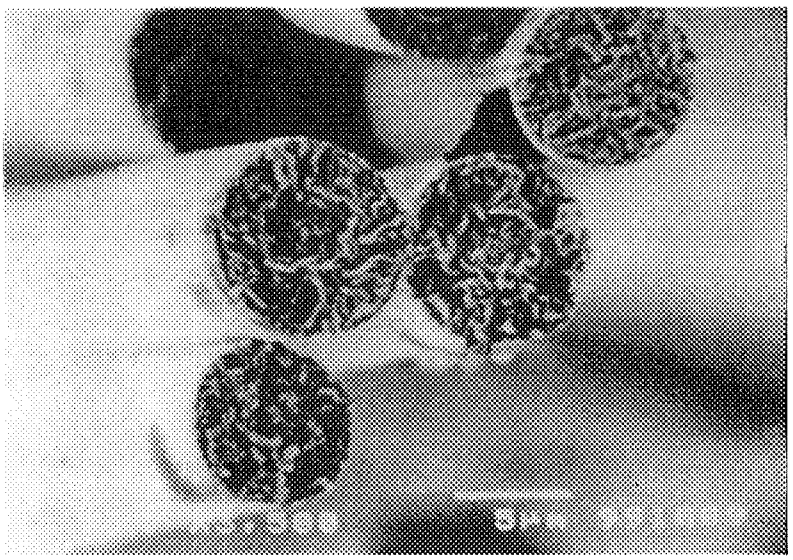

(b) After irradiation

Fig.1. SEM images of the cross section of the YS-70-60S carbon fiber before and after carbon ion irradiation.

5.19 EVALUATION OF SINGLE EVENT BURNOUT IN POWER MOSFETS CAUSED BY HIGH-ENERGY HEAVY IONS

S. KUBOYAMA [1], T. HIRAO, H. SHINDO [1]
H. ITO, T. HIROSE [2], T. ABURAYA [1]
H. OHIRA [2], Y. NAGAI [2] and S. MATSUDA [1]

Single-event effects (SEE) is the most serious problem in applying highly sophisticated modern electronic devices in space environments. Single Event Burnout (SEB) was identified as a possible catastrophic failure mode for Power MOSFETs. In order to develop SEB tolerance devices, it is indispensable to understand the transportation mechanisms of electric charge induced in a MOSFET subjected to energetic ion irradiation. SEB is triggered when a heavy ion passed through a power MOSFET biased in the OFF state. Transient currents generated by the heavy ion turn on a parasitic bipolar transistor (BJT) inherent to the device structure, create a short-circuit between the source and drain which destroys the device [1].

To determine the design parameters of Power MOSFET, we aim at the width of P^{++}-type diffusion region in Power MOSFET as one of the protection structure of SEB. It is known that the voltage drop generated by the current along the body layer cause the activation of the parasitic BJT as trigger of SEB [2]. So it can be expected to increase SEB tolerance as decreasing the resistance of the body layer. The expansion of the width of P^{++} region decreases the resistance of the body layer. We started to experimental study about the relationship between the width of P^{++} region and the tolerance of SEB in Power MOSFET. Test samples were performed by using Energetic Particle Induced Charge Spectroscopy (EPICS) system [2]. Using EPICS system, SEB of PowerMOSFET was observed non-destructively.

Fig. 1 shows the block diagram of EPICS used in this experiment. We used the Ni ion 250MeV from the TANDEM accelerator in JAERI. Beam current was controlled about 1.0 uA. Its ion beam was scattered by Au foil to obtain uniform intensity over the surface of the samples. Scatter angle was about 25 degree. In this experiment, LET was about 28MeV/(mg/cm2). The detail conditions are shown in table 1. Energy Spectrum and flux are monitored by SSD before the irradiation test.

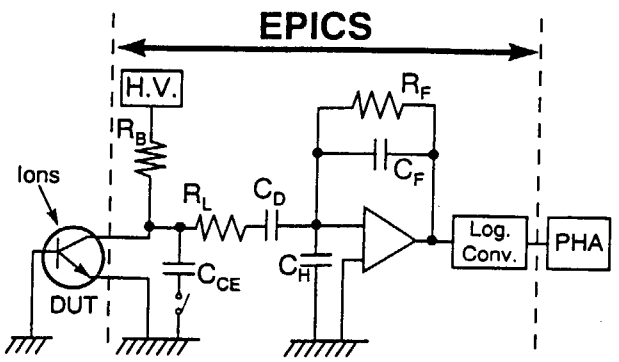

Fig. 1. Block diagram of EPICS

Six samples were prepared and tested. These samples were based on 2SK3041 (Power MOSFET, rated V_{DSS}=250V, (V_{DSS}: Drain-Source Breakdown Voltage)) which NASDA had developed previously. The characteristics of samples and heavy ion irradiation test conditions are shown in Table 1. In this table, Sample #1 is a reference sample based on 2SK3041.

[1]Electronic and Information Technology Laboratory, Office of Research and Development, National Space Development Agency of Japan.
[2]Components Engineering Section, Engineering Dept., RYOEI TECHNICA Corporation.

P^{++} region width of sample #2～#5 are different from that of reference sample #1. Δ Wp++ means the expansion width of P^{++} region from the reference. Irradiation test result is shown in Table 1 and Fig. 2.

Table 1. Experimental result of test samples

S/N	Δ Wp++ [μ m]	LET [MeV/(mg/cm^2)]	Range [μ m]	SEB threshold V_{DS} [V]
#1 (Reference)	0	28.0	37.3	76
#2	2.2	28.0	37.3	107
#3	2.2	27.5	40.1	95
#4	2.8	28.0	37.3	120
#5	2.8	28.1	36.9	130
#6	4.0	28.0	37.3	210

S/N : sample number

Δ Wp++ : Expansion width of the P^{++} region from the reference (#1)

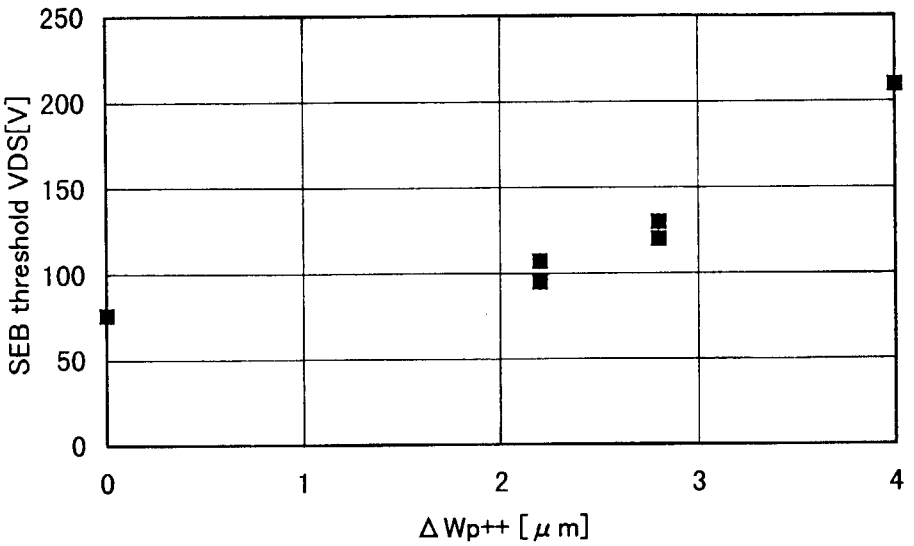

Fig. 2. V_{DS}- Δ Wp++ characteristic

It is said, from the Table 1. that the increase of Δ Wp++ increase the threshold V_{DS} from 76V to 210V. The experimental result suggests that the expansion of P^{++} region width reduce the resistance of the body layer, and increase the tolerance of SEB. But we don't have enough data to explain the mechanism clearly, because only one type of Power MOSFET (2SK3014) is tested now. We need to test many type of samples to make sure the mechanism. For farther study, we also need to start simulation study, and to compare with the experimental result. We expect that such test results are very helpful to develop Power MOSFET which have high SEB tolerance.

REFERENCES

[1] M.Allenspach, et al, IEEE. Trans.Nucl.Sci., Vol.NS-**43**,No.6 (1996) 2927
[2] S.Kuboyama, et al, IEEE. Trans.Nucl.Sci. Vol.NS-**39**,No.6(1992) 1698

6. Publication in Journal and Proceedings, and Contribution to Scientific Meetings

This is a blank page.

ACCELERATOR OPERATION AND DEVELOPMENT

Journal/Proceedings

(Eds.) Iwamoto, A., Yoshida, T. and Takeuchi, S.
Materials Science Symposium" Heavy ion science in Tandem energy region"
Mito, JAERI-Conf. 99-013 (1999)

Takeuchi, S.
ECR plasma cleaning for superconducting cavities
Proc. of the 2nd Superconducting Linear Accelerator Meeting in Japan,
Tsukuba (1999) pp.122-125.

Yoshida, T., Kanda, S., Takeuchi, S., Hanashima, S., Ohuchi, I., Horie, K.,
Tsukihashi, Y., Abe, S., Ishizaki, N., Tayama, H., and Matsuda. M.,
The status of the JAERI Tandem accelerator
Proc. of the 12th Workshop of the Tandem Accelerator and their Associated
Technology, Kyoto (1999)pp.51-54.

Yoshida,T.
JAERI Tandem accelerator and resent utilization
Proc. of the Materials Science Symposium"Heavy Ion Science in Tandem Energy Region", JAERI-Conf. 99-013 (1999)pp.3-5.

Meetings

Takeuchi, S.
ECR plasma cleaning for superconducting cavities
The 2nd Superconducting Linear Accelerator Meeting in Japan,
Tsukuba (May 27-28, 1999)

Yoshida, T., Kanda, S., Takeuchi, S., Hanashima, S., Ohuchi, I., Horie, K.,
Tsukihashi, Y., Abe, S., Ishizaki, N., Tayama, H., and Matsuda. M.,

The status of the JAERI Tandem accelerator

12th Workshop of the Tandem Accelerator and their Associated Technology, Kyoto(Jul. 7-8, 1999)

NUCLEAR STRUCTURE

Journal/Proceedings

Asai, M., Ichikawa, S., Tsukada, K., Nishinaka, I., Nagame, Y., Sakama, M., Osa, A., Kojima, Y., Shibata, M. and Kawade, K.
Decay spectroscopy for neutron-rich A=160-170 nuclei using the JAERI-ISOL
JAERI- Conf. 99-013 (1999) 136.

Haba, H., Tsukada. K., Nishinaka, I., Asai, M., Hirata, M., Sakama, M., Goto, S., Ichikawa, S.and Nagame, Y.
Chemistry of heaviest elements
-Plans for systheses of transactinide elements and their chemistries in JAERI
KURRI-KR-42 (1999) 21.

Hatsukawa, Y., Hayakawa, T., Toh, Y., Shinohara, N. and Oshima, M
Application of multidimensional spectrum for alalytical chemistry
Proc. of Int. Conf. On Experimental Nuclear Physics in Europe, Spain, Sevilia, 1999 (AIP, New York, 1999)p. 429.

Hayakawa, T., Oshima, M., Hatsukawa, Y., Katakura, J., Iimura, H., Matsuda, M., Mitarai, S., Shimizu, Y.R., Ohtsubo, S.-I., Shizuma, T., Sugawara, M. and Kusakari, H.
Rotational bands of ^{155}Gd
Nucl. Phys. A **657** (1999) 3.

Hayakawa, T., Oshima, M., Hatsukawa, Y., Katakura, J., Iimura, H., Matsuda, M., Mitarai, S., Shimizu, Y.R., Ohtsubo, S.-I., Shizuma, T., Sugawara, M. and Kusakari, H.
Rotaional bands of ^{155}Gd
Proc. of Int. Conf. on Experimental Nuclear Physics in Europe, Spain, Sevilla, 1999 (AIP, New York, 1999) pp. 235-236.

Hirata, M.
Electronic structure of transactinide compounds
KURRI-KR-42 (1999) 43.

Hirata, M.
Electronic structure of transactinide compounds -theory – theoretical approach to the experimental chemistry of Rf -
JAERI-Conf. 2000-002(2000)67

Ichikawa, S., Asai, M., Tsukada, K., Osa, A., Sakama, M., Kojima, Y.,
Shibata, M., Nishinaka, I., Nagame, Y., Oura, Y. and Kawade, K.
β-decay half-lives of new neutron-rich isotopes of elements from Pm to Tb
Proc. of Int. Conf. on Experimental Nuclear Physics in Europe,
Sevilla, Spain, 1999 (AIP, New York, 1999) pp. 103-106.

Ichikawa, S., Asai, M., Tsukada, K., Nishinaka, I., Nagame, Y.,
Osa, A., Kojima, Y., Shibata, M., Kawade, K., Sakama, M. and Oura, Y.
Decay studies of neutron-rich isotopes produced in proton-induced fission of actinides
Proc. of the 2nd Int. Conf. on Fission and Properties of Neutron-rich Nuclei,
St. Andrews, Scotland, 1999 (World Scientific, Singapore, 2000) pp. 203-205.

Ishii, T., Asai, M., Makishima, A., Hossain, I., Ogawa, M., Hasegawa, J.,
Matsuda, M. and Ichikawa, S.
Core-excited states in the doubly magic ^{68}Ni and its neighbor ^{69}Cu
Phys. Rev. Lett. **84** (2000) 39.

Ichikawa, S., Asai, M., Tsukada, K., Nishinaka, I., Nagame, Y., Osa, A.,
Shibata, M., Kawade, K., Kojima, Y., Sakama, M. and Oura, Y.
Identification of new neutron-rich lanthanoide isotopes
JAERI-Conf. 99-010 (1999) 4.

Ishii, T., Asai, M., Makishima, A., Hossain, I., Ogawa, M., Hasegawa, J.,
Matsuda, M. and Ichikawa, S.
Core-excited states in the doubly magic ^{68}Ni and its neighbor ^{69}Cu

Proc. of the Int. Conf. on Experimental Nuclear Physics in Europe,
Sevilla, Spain, 1999 (AIP, New York, 1999) pp. 67-70.

Kleinheinz, P., Ishii, T., Ogawa, M., Gadea, A. and Blomqvist, J.
Shell model analyses of aligned j^2j' three-particle isomers
Proc. of the Int. Conf. on Experimental Nuclear Physics in Europe,
Sevilla, Spain, 1999 (AIP, New York, 1999) pp. 71-73.

Makishima, A., Asai, M., Ishii, T., Hossain, I., Ogawa, M., Ichikawa, S. and Ishii, M.
$(\nu g_{9/2}^{-2})_{8^+}$ isomers in $^{82}Se_{48}$ and $^{80}Ge_{48}$ populated by deep-inelastic collisions
Phys. Rev. C **59** (1999) R2331.

Nagame, Y.
Chemistry and physics of the heaviest elements
KURRI-KR-42(1999)1.

Nagame, Y., Ichikawa S., Tsukada, K., Nishinaka, I., Asai, M.,
Sakama, M. and Ishida, Y.
Heavy element nuclear chemistry at JAERI
JAERI-Conf. 99-013 (1999) 59.

Nagame, Y.
Research plans of heavy element nuclear chemistry in JAERI
JAERI-Conf. 2000-002 (2000) 90.

Nishio, K., Ikezoe, H., Mitsuoka, S. and Lu, J.
α-decay of ^{217}Th populating excited states in ^{213}Ra
Phys. Rev. C **61** (2000) 034309.

Ogawa, M., Hossain, I., Ishii, T., Asai, M., Makishima, A., Ichikawa, S.,
Itoh, M., Kleinheinz, P. and Ishii, M.
Yields of neutron rich isomers produced via deep inelastic collisions
Proc. of the Int. Conf. on Experimental Nuclear Physics in Europe,

Sevilla, Spain, 1999 (AIP, New York, 1999) pp. 317-318.

Oura, Y., Sakama, M., Ohyama, T., Sueki, K., Nakahara, H., Shinata, M.,
Kawade, K., Ichikawa, S., Tsukada, K., Asai, M., Nishinaka, I.
and Nagame, Y.
Identification of new Neutron-rich actinide isotopes
JAERI-Conf. 99-010 (1999) 12.

Sakama, M., Tsukada, K., Asai, M., Ichikawa, S., Oura, Y., Haba, H., Nishinaka, I.,
Nagame, Y., Goto, S., Kojima, Y., Shibata, M., Kawade, K.,
Ebihara, M. and Nakahara, H.
Decay properties of neutron-deficient actinides
JAERI-conf. 2000-005 (2000) 313.

Tsukada, K., Asai, M., Nishinaka, I., Nagame, Y. and Sakama, M.
Chemistry of heaviest elements
KURRI-KR-42 (1999) 16.

Tsukada, K.
Chemistry and heavt- and trans-actinide elements
-Experiments-
JAERI-Conf. 2000-002(2000)71.

Zhao, Y.L., Nishinaka, I., Nagame, Y., Tanikawa, M., Tsukada, K.,
Ichikawa, S., Sueki, K., Oura, Y., Ikezoe, H., Mitsuoka, S., Kudo, H.,
Ohtsuki, T. and Nakahara, H.
Symmetric and asymmetric scission properties: Identical shape elongations
of fissioning nuclei
Phys. Rev. Lett. **82** (1999) 3408.

Zhao, Y.L., Nakahara, H., Sueki, K., Nagame, Y. and Nishinaka, I.,
Invariance of shape elongations of scissioning suclei
KURRI-KR-42 (1999) 84.

Zhao, Y.L., Nakahara, H., Sueki, K., Nagame, Y. and Nishinaka, I.
New formulas for TKE release in nuclear fission
JAERI-Conf. 2000-005 (2000) 376.

Meetings

Asai, M., Ishii, T., Makishima, A., Hossain, I., Ogawa, M., Hasegawa, J., Matsuda, M. and Ichikawa, S.
The ($\nu g^2_{9/2}\, \nu p^{-2}_{1/2}$) $_{8+}$ isomer in doubly-closed shell nucleus ^{68}Ni
Fall Meeting of the Physical Society of Japan, Shimane (Sep. 25, 1999)

Asai, M., Sakama, M., Tsukada, K., Ichikawa, S., Haba, H., Nishinaka, I., Nagame, Y., Goto, S., Kojima, Y., Oura, Y., Nakahara, H., Shibata, M. and Kawade, K.
Nuclear structure of ^{236}Pu and ^{236}Am
Spring Meeting of the Physical Society of Japan, Osaka (Apr.1, 2000)

Hatsukawa, Y., Hayakawa, T., Toh, Y., Shinohara, N. and Oshima, M.,
Application of multidimensional spectrum for alalytical chemistry
Int. Conf. on Experimental Nuclear Physics in Europe in Sevilia, Spain (Jun. 21, 1999)

Hatsukawa, Y., Hayakawa, T., Toh, Y., Shinohara, N. and Oshima, M.
Microanalysis by using γ-ray detector array, GEMEIN
1999 The Physical Society of Japan Autumn meeting Fall Meeting in Matsue (Sep. 24, 1999)

Hatsukawa,Y. Oshima, M., Hayakawa,T., Toh, Y. and Shinohara, N.
Application of array of germanium detectors for analytical chemistry
The 43th Symposium on Radiochemistry in Tsukuba (Oct. 13, 1999)

Hatsukawa,Y. Oshima, M., Hayakawa,T., Toh, Y. and Shinohara, N.

Application of multidimensional spectrum analysis for neutron activation method
2000 The Chemical Society of Japan Spring meeting in Chiba (Mar. 29, 2000)

Hayakawa, T., Oshima, M., Hatsukawa, Y., Katakura, J., Iimura, H.,
Matsuda, M., Mitarai, S., Shimizu, Y. R., Ohtsubo, S.-I., Shizuma, T.,
Sugawara, M. and Kusakari, H.
Rotaional bands of ^{155}Gd
Int. Conf. on Experimental Nuclear Physics in Europe, Spain (Jul. 21, 1999)

Hayakawa, T., Oshima, M., Hatsukawa, Y., Katakura, J., Iimura, H., Mitarai,
S., Shimizu, Y., Outsubo, S., Shizuma, T., Sugawara, M. and Kusakari., H.
Identical band of N=91 isotone
Fall Meeting of the Physical Society of Japan, Shimane (Sep. 25, 1999)

Hayakawa, T., Toh, Y., Oshima, M., Hatsukawa, Y., Matsuda, J., Shinohara, N.,
Zhang, Y.H. and Kusakari., H.
Observation of interband E1 transitions in ^{157}Gd
Spring Meeting of the Physical Society of Japan, Osaka (Aug. 1, 2000)

Ichikawa, S., Asai, M., Tsukada, K., Osa, A., Haba, H., Nishinaka, I.,
Nagame, Y., Kojima, Y., Shibata, M., Oura, Y., Sakama, M. and Kawade, K.
Decay spectroscopy of neutron-rich lanthanide isotopes
The 43rd Symposium on Radiochemistry, Tsukuba (Oct. 13, 1999)

Iimura, H., Ishida, Y., Ichikawa, S. and Horiguchi, T.
Collinear laser spectroscopy on radioactive isotopes
The First Symposium on Advanced Photon Research, Kyoto (Nov. 9, 1999)

Iimura, H., Ishida, Y., Ichikawa, S., Koizumi, M., Shibata, T., Shinohara, N., Horiguchi,
T. and Schuessler, H.A.
Hyperfine structure and isotope shift measurements of light rare-earth elements
by collinear laser spectroscopy
Research Meeting on the Science with Low-Energy Short-Lived Nuclear Beam,

Tanashi (Mar. 12, 2000)

Ishii, T., Asai, M., Makishima, A., Hossain, I., Ogawa, M., Hasegawa, J., Matsuda, M. and Ichikawa, S.
Excited states in neutron-rich ^{69}Cu and its shell model calculation
Fall Meeting of the Physical Society of Japan, Shimane (Sep. 25, 1999)

Ishii, T., Asai, M., Makishima, A., Hossain, I., Liu, Z., Ogawa, M., Ichikawa, S., Matsuda, M., Oshima, M., Hayakawa, T. and Toh, Y.
L-forbidden M1 transitions in ^{67}Cu and ^{64}Co
Spring Meeting of the Physical Society of Japan, Osaka (Apr. 1, 2000)

Nishio, K., Ikezoe, H., Mitsuoka, S. and Lu, J.
α-decay of ^{217}Th populating excited states in ^{213}Ra
Spring meeting of the Physical Socierty of Japan, Osaka (Apr. 1, 2000)

Nishio, K., Ikezoe, H., Mitsuoka, S. and Lu, J.
α-decay of ^{217}Th populating excited states in ^{213}Ra
Spring meeting of the Atomic Energy Socierty of Japan, Ehime (Mar. 28, 2000)

Raman, S., Yonezawa, C., Matsue, H., Iimura, H. and Shinohara, N.
Efficiency calibration of a Ge detector in the 0.1-11.0 MeV region
Spring Meeting of the Physical Society of Japan, Osaka (Mar. 31, 2000)

Sakama, M., Tsukada, K., Asai, M., Ichikawa, S., Oura, Y., Haba, H., Nishinaka, I., Nagame, Y., Goto, S., Kojima, Y., Shibata, M., Kawade, K., Ebihara, M. and Nakahara, H.
Decay properties of neutron-deficient americium isotopes
1999 Symposium on Radiochemistry in Tsukuba (Oct. 13, 1999)

Sakama, M., Tsukada, K., Asai, M., Ichikawa, S., Oura, Y., Haba, H., Nishinaka, I., Nagame, Y., Goto, S., Kojima, Y., Shibata, M., Kawade, K., Ebihara, M. and Nakahara, H.

Decay properties of neutron-deficient actinides
1999 Symposium on Nuclear Data (Nov. 18, 1999)

Sakama, M., Tsukada, K., Asai, M., Ichikawa, S., Oura, Y., Haba, H., Nishinaka, I., Nagame, Y., Goto, S., Kojima, Y., Shibata, M., Kawade, K., Ebihara, M. and Nakahara, H.
Alpha-decay of new isotope, ^{233}Am
Spring Meeting of the Physical Society of Japan, Osaka (Mar. 30, 2000)

Sugawara, M., Kusakari, H., Mitarai, S., Oshima, M., Hayakawa, T., Hatsukawa,,Y., Katakura, J. and Iimura, H.
Nuclear structure of $^{79,80}Kr$
1999 Fall Meeting of Physical Society of Japan, Simane (Sep. 25, 1999)

Sugawara, M., Mitarai, S., Kusakari, H., Sugie, M., Sato, Y., Oshima, M., Hayakawa, T., Toh. Y., Katakura, J., Hatsukawa, Y., Iimura, H. and Zhang, Y.
Nuclear structure of ^{156}Gd
1999 Workshop on the Frontier of Gamma-ray Spectroscopy and Short-lived nuclei, Tokai (Dec. 9, 1999)

Sugawara, M., Mitarai, S., Kusakari, H., Sugie, M., Sato, Y., Oshima, M., Hayakawa, T., Toh, Y., Katakura, J., Hatsukawa, Y., Iimura, H.and Zhang,,Y.
Band structure of ^{156}Gd
2000 Spring Meeting of Physical Society of Japan, Osaka (Apr. 1, 2000)

Toh, Y., Czosnyka, T., Oshima, M., Hayakawa, T., Hatsukawa, Y., Katakura, J., Matsuda, M., Shinohara, N., Kusakari, H., Nishimiya, D., Sugawara, M. and Zhang, Y.
Development of position-sensitive particle detector for Coulomb excitation experiment
Japan Physical Society, Shimane (Sept. 26, 1999)

Toh, Y., Oshima, M., Hayakawa, T., Hatsukawa, Y., Kusakari, H.,

Sugawara, M. and Czosnyka, T.,
The multiple Coulomb excitation of ^{74}Ge beam
Japan Physical Society, Osaka (Mar. 31, 2000)

Tsukada, K., Sakama, M., Asai, M., Ichikawa, S., Nishinaka, I., Haba, H.,
Goto, S., Nagame, Y., Oura, Y., Nakahara, H., Shibata, M.,
Kawade, K. and Kojima, Y.
Identification of new isotope ^{233}Am using JAERI-ISOL
The 78th CSJ National Meeting, Funabashi (Mar. 29, 2000)

Zhao, Y., Nishinaka, I., Nagame, Y., Tanikawa, M., Sueki, K., Tsukada, K.,
Ichikawa, S., Goto, S., Oura, Y. and Nakahara, H.
Category of the deformation degree of the fissioning nucleus
The 43th Symposium on Radiochemistry, Tsukuba, Japan(Oct.13,1999)

NUCLEAR REACTIONS

Journal/Proceedings

Haba, H., Tsukada, H., Nishinaka, I., Asai, M., Hirata, M., Sakama, M., Goto, S., Ichikawa, S. and Nagame, Y.
Chemistry of the heaviest elements - plans for syntheses of transactinide elements and their chemistries
JAERI -KUR Report KURRI-KR 42 (1999) 21.

Ikezoe, H.
Heavy-ion fusion reaction for synthesis of super heavy elements
Proc. of the symposium on frontier nuclear physics (FRONP99)
JAERI-Conf. 99-015 (1999) 80.

Ikezoe, H., Mitsuoka, S., Nishio, K., Lu,J. and Sato, K.
Fusion of heavy deformed nuclei
Proc. of the Workshop on the Nuclear Sciences of the Heaviest Elements, JAERI-Conf. 2000-002 (1999) 43.

Ikezoe, H., Mitsuoka, S.,Nishio, K.,Lu, J. and Sato, K.
Synthesis of superheavy nuclei using heavy-ion fusion reactions
Proc. of the 1999 Symposium on Nuclear Data,
JAERI-Conf. 2000-005 (1999) 87.

Nagame, Y.
Systematic features of mass yield curves in low-energy fission of actinides
JAERI-Conf. 99-007 (1999) 110.

Nishinaka, I., Zhao, Y. L., Nagame, Y., Tsukada, K., Ichikawa, S., Ikezoe, H., Tanikawa, M. and Nakahara, H.
Correlation between mass division modes and deformation of fission fragments in proton induced fission af actinides

JAERI- Conf 99-013 (1999) 139.

Nishio, K., Ikezoe, H., Mitsuoka, S. and Lu, J.
Fusion of $^{28}Si+^{198}Pt$ and $^{76}Ge+^{150}Nd$ at the Coulomb energy region
Proc. of the Specialist's Meeting of the Nuclear Chemistry of Heavy Elements at KURRI, KURRI-KR-42 (1999) p.73.

Nishio, K., Ikezoe, H., Mitsuoka, S. and Lu, J.
Fusion of deformed nuclei in the reactions of $^{76}Ge+^{150}Nd$ and $^{28}Si+^{198}Pt$ at the Coulomb barrier region
Phys. Rev. C**62** (2000) 014602.

Ohtsuki, T., Nagame, Y. and Nakahara, H.
Bimodal Nature of Actinide Fission
"Heavy elements and related new phenomena",
vol.1, edited by W. Greiner and R.K. Gupta, World Scientific, (1999) 507.

Qin, Z., Tsukada, K., Shinohara, N., Zhao, Y. L., Hatsukawa, Y., Nishinaka, I., Ichikawa, S., Hata, K. and Nagame, Y.
Mass yield distributions in proton-induced fission of ^{248}Cm
Radiochim. Acta **84** (1999) 115.

Sugiyama, Y., Hamada, S. and Yamazaki, A.
Nuclear Josephson effect in the heavy-ion collision
JAERI-Conf. 99-013 (2000) 64.

Takamiya, K., Nakanishi, K., Yokoyama, A., Saito, T., Baba, H., Nishinaka, I., Nagame, Y., Zhao, Y. and Tanikawa, M.
Excitation energies of fragments in the proton-induced fission of uranium-238
JAERI- Conf. 99-013 (1999) 130.

Tsukada, K., Nishinaka, I., Ichikawa, S., Nagame, Y., Shinohara, N., Tanikawa, M., Ohtsuki, T., Sueki, K. and Nakahara, H.
Highly asymmetric mass division in proton-induced fission of actinides
JAERI- Conf. 99-013 (1999) 142.

Yamazaki, A.,Sugiyama, Y.,Hamada, S. et al.
Nuclear structure in light nuclei via three-nucleon transfer reactions
JAERI-Conf. 99-013 (2000) 99.

Zhao, Y. L., Tanikawa, M., Sueki, K., Nishinaka, I., Tsukada, K., Oura, Y., Nagame, Y. and Nakahara, H.
Angular momentum effects on mass division in actinide eission
Radiochim. Acta **86** (1999) 79.

Meetings

Hirata, M., Bastug, T. and Nagame Y.
Electronic structure of tetravalent Zr, Hf and Rf nitrates
The 1st International Conference on the Chemistry and Physics of theTransactinide Elements, Seeheim, Germany, (Sept.26-30,1999)

Hirata, M., Bastug, T. and Nagame Y.
Electronic structure of rutherfordium nitrate
The 43th Symposium on Radiochemistry, Tsukuba, Japan(Oct.15,1999)

Ikezoe., H.
Fusion of deformed nuclei in sub-barrier energy region
Workshop on Nuclear Structure and Reaction, RIKEN (Feb. 4-6, 2000)

Ikezoe, H., Mitsuoka, S., Nishio, K. and Sato, K.
Fusion reaction of ^{64}Ni on deformed target ^{154}Sm
Spring Meeting of the Physical Society of Japan, Osaka(Mar. 30-Apr. 2, 2000)

Nagame, Y., Zhao, Y. L., Ohtsuki, T., Nishinaka, I., Tsukada, K.,
Ichikawa, S. and Nakahara, H.
Variation of fission characteristics over the nuclear chart
The 2nd International Conference on Fission and Properties of Neutro-rich Nuclei, St. Andrews, Scotland, (Jun.28-Jul.3, 1999)

Nagame, Y., Zhao, Y.L., Nishinaka, I., Ohtsuki, T., Tanikawa, M., Tsukada, K.,
Sueki, K., Ichikawa, S. and Nakahara, H.
Fission characteristics of very heavy nuclides
The 1st International Conference on the Chemistry and Physics of the Transactinide Elements, Seeheim, Germany, (Sept.26-30, 1999)

Nagame, Y., Zhao Y., Nishinaka, I., Ohtsuki, T., Tsukada, K., Ichikawa, S.,
and Nakahara, H.
Fission characteristics of heavy nuclei
The 43th Symposium on Radiochemistry, Tsukuba, Japan(Oct.13,1999)

Nishinaka, I., Nagame, Y., Tsukada, K., Ichikawa, S., Ikezoe, H.,
Tanikawa, M., Zhao, Y.L., Sueki, K. and Nakahara, H.
Deformation of fragments with A=130 in two mode fission
The 2nd International Conference on Fission and Properties of Neutro-rich Nuclei, St. Andrews, Scotland, (Jun. 28-Jul.3, 1999)

Nishinaka, I., Goto, S., Tanikawa, M., Zhao Y., Nagame, Y., Tsukada, K.,
Asai, M., Ichikawa, S., and Nakahara, H.
Properties of proton-induced fission of actinides
Fall Meeting of the Physical Society of Japan, Matsue(Sept.26,1999)

Nishinaka, I., Goto, S., Tanikawa, M., Zhao Y., Nagame, Y., Tsukada, K.,
Asai, M., Ichikawa, S. and Nakahara, H.
Anomalous excitation energy depemdence of mass
and kinetic energy distributions
The 43th Symposium on Radiochemistry, Tsukuba, Japan(Oct.15,1999)

Nishio, K., Ikezoe, H., Mitsuoka, S. and Lu, J.
Measurement of evaporation residue cross sections for $^{28}Si+^{198}Pt$ and $^{76}Ge+^{150}Nd$
Fall meeting of the Physical Socierty of Japan, Shimane (Sept. 26, 1999)

Nishio, K., Ikezoe, H., Mitsuoka, S. and Lu, J.
Measurement of evaporation residue and fission cross sections for $^{28}Si+^{198}Pt$
Fall meeting of the Atomic Energy Socierty of Japan, Niigata (Sept. 12, 1999)

Yamazaki, A.,Sugiyama, Y.,Hamada, S. et al.
Nuclear structure in A=15,19 mirror nuclei through ($^{6}Li,^{3}He$) and ($^{6}Li,t$) reactions
Annual Meeting of the Physical Society, Japan, Matsue (Sep. 26, 1999)

Zhao, Y. L., Nakahara, H., Nishinaka, I., Nagame, Y. and Sueki, K.
Understanding of the fission process from the deformation properties of fissioning nuclei
The 2nd International Conference on Fission and Properties of Neutro-rich Nuclei, St. Andrews, Scotland, (Jun.28-Jul.3, 1999)

NUCLEAR THEORY

Journal/Proceedings

Chikazumi, S., Maruyama, T., Koji Niita, K. and Iwamoto, A
QMD simulation of expanding nuclear matter
Physics Letters (Section) B **476** (Mar. 2000) 273.

Iwamoto, A., Bonasera, A. and Kondratyev, V. N.
Effect of nucleon exchange in sub-and above-barrier fusion
Heavy Ion Physics **10**(1999)265.

Kido, T., Maruyama, T., Niita, K. and Chiba, S.
MD simulation study for nuclear mater
Nucl. Phys. A **663** & **664**(2000)877c.

Kondratyev, V. N., Maruyama, T. and Chiba, S.
Magnetic field effect on nuclear shell structure and implications to physics of neutron Stars
JAERI-Research 99-065(1999)

Kondratyev, V. N., Maruyama, T. and Chiba, S.
Shell structure of nuclei in strong magnetic fields in neutron star crust
Phys. Rev. Lett. **84**(2000) 1086.

Kondratyev, V. N., Bonasera, A. and Iwamoto, A.
Kinetics in subbarrier fusion of spherical nuclei
Phys. Rev. C **61**(2000) 044608.

Lee, Y. O., Chang, J., Fukahori, T. and Chiba, S.
Evaluation of neutron- and proton-induced nuclear data on ^{27}Al up to 2 GeV
J. Nucl. Sci. Technol. **36**(1999) 1125.

Mao, G., Chiba, S., Greiner, W. and Oyamatsu, K.
Vacuum discharge as a possible source of Gamma-ray bursts
JAERI-Research 99-072(1999)

Maruyama, Toshiki, Niita, K., Oyamatsu, K., Maruyama, Tomoyuki, Chiba, S. and Iwamoto, A.
Nuclear matter structure studied with quantum molecular dynamics
Nucl. Phys. A **654**(1999) 908c.

Maruyama, Tomoyuki and Chiba, S.
Equation of state of neutron-star matter and the isovector nucleon optical model potential
J. Phys. G.: Nucl. Part. Phys. **25**(1999) 2361.

Maruyama, T. and Chiba, S.
Isoscalar giant quadrupole resonance state in the relativistic approach with the momentum-dependent self-energies
Phys. Rev. C **61**(2000) 037301.

Nakagawa, T., Chiba, S., Ohsaki, T. and Igashira, M.
Maxwellian-averaged cross sections calculated from JENDL-3.2
JAERI-Research 2000-002(2000)

Nara, Y., Otuka, N., Ohnishi, A., Niita, K. and Chiba, S.
Relativistic nuclear collisions at 10AGeV energies from p+Be to Au+Au with the hadronic cascade model
Phys. Rev. C **61**(1999) 024901.

Sukhovitskij, E. S., Iwamoto, O., Chiba, S. and Shibata, K.
New options of coupled channels optical model code OPTMAN Ver. 6 (1999)
JAERI-Data/Code99-028(1999)

Sukhovitskij, E. S., Chiba, S., Iwamoto, O. and Fukahori, T.
^{238}U optical potential up to 100 MeV incident nucleon energies
JAERI-Research 99-040(1999)

Sukhovitskij, E. S., Iwamoto, O., Chiba, S. and Fukahori, T.
Nucleon optical potential of ^{238}U up to 150 MeV
J. Nucl. Sci. Technol. **37**(2000) 120.

Meetings

Chikazumi, S., Maruyama, T., Niita, K. and Iwamoto, A
QMD simulation of expanding nuclear matter
YTTP Symposium on Frontiers of Nuclear Collision Dynamics,
Kyoto (Nov. 21,1999)

ATOMIC PHYSICS, SOLID STATE PHYSICS AND RADIATION EFFECTS IN MATERIALS

Journal/Proceedings

Chimi, Y., Iwase, A., Ishikawa, N., Kuroda, N. and Kambara, T.
Radiation annealing induced by electronic bxcitation in iron
Nucl. Instrum. Methods in Phys. Res. B**164-165** (2000) 408.

Chimi, Y., Iwase, A., Ishikawa, N., Kuroda, N. and Kambara, T.
Radiation annealing induced by electronic excitation in iron
RIKEN Accel. Prog. Rep. 33 (2000) 89.

Fujiyoshi, T., Sueyoshi, T., Ishikawa, N., Iwase, A., Chimi, Y.,
Kiss, T. and Miyahara, K.
Optical response and transport properties of epitaxial $YBa_2Cu_3O_{7-\delta}$thin films with columnar defects
Advances in Superconductivity **XI** (1998) 597.

Fujiyoshi, T., Ohashi, K., Yamafuji, K., Kiss, T. and Inoue, M.
The ac loss near the glass-liquid transition temperature in high-Tc superconductors-an extended Bean model
Superconductor Science and Technology **12** (1999) 1063.

Gevorgyan, S., Movsesyan, A., Kiss, T., Hanayama, Y., Matsushita, T.,
Takeo, M. and Vysotsky, V.
Study on the magnetization of HTSC films by the new method based on tunnel diode oscillator with open-flat coil
Advances in Superconductivity **XI** (1999) 601.

Grismanovs, V., Kumada, T., Tanifuji , T.and Nakazawa, T.
ESR spectroscopy of γ-irradiated Li_2TiO_3 ceramics
Radiat. Phys. Chem., **58** (2000) 113.

Inoue, M., Hasegawa, K., Kiss, T., Takeo, M., Irie, F., Awaji, S. and Watanabe, K.
Transport E(J) characteristics of high-Tc superconductors in a wide B-T plane up to 27 T
Advances in Superconductivity **XI** (1999) 605.

Ishikawa, N. , Chimi, Y., Iwase, A., Wakana, H. and Michikami, O.
Irradiation temperature dependence of swift heavy ion iInduced defects in oxide superconductor $EuBa_2Cu_3Oy$
Nucl. Instr. Meth. B **164-165** (2000) 384.

Ishikawa, N., Chimi, Y., Kuroda, N., Iwase, A. and Kambara, T.
Ion-velocity effects on defect production in high-Tc superconductors and metals irradiated with swift heavy ions
Physica Scripta T**80** (1999) 559.

Ishikawa, N., Chimi, Y., Iwase,A., Kuroda, N., Michikami, O.,
Wakana, H. and Kambara, T.
Defect production via electronic excitation in oxide superconductors irradiated with high energy heavy ions
RIKEN Accel. Prog. Rep. **33** (2000) 87.

Itaka, K., Yasugaki, Y., Shibauchi, T., Tamegai, T. and Okayasu, S.
Novel asymmetric critical state in $YBa_2Cu_3O_{7-\delta}$ with columnar defects
J. Low Temp. Phys. **117** (1999) 1369.

Iwase, A. and Ishino, S.
Comparison between radiation effects in some FCC and BCC metals irradiated with energetic heavy ions - A review
J. Nucl. Mater. **276** (2000) 178.

Kakeya, I., Nakamura, R., Kadowaki, K. and Okayasu, S.
It systematic study of Josephson plasma resonance in

$Bi_2Sr_2CaCu_2O_{8+\delta}$ with Columnar defects
Physica B **284-288** (2000) 881.

Kimura, K., Koshida, R., Okayasu, S., Sataka, S., Kazumata, Y.,
Kwok, W. K., Crabtree, G. W. and Kadowaki, K.
Systematic magnetization measurements on $Bi_2Sr_2CaCu_2O_{8+\delta}$ with Columnar defects
J. Low Temp. Phys. **117**(1999)1471.

Kimura, K., Koshida, R., Okayasu, S., Sataka, S., Kazumata, Y.,
Kwok, W. K., Crabtree, G. W. and Kadowaki, K.
Anomalous magnetization behavior in the vortex liquid State in $Bi_2Sr_2CaCu_2O_{8+\delta}$
Advances in Superconductivity XII edited by T. Yamashita and K. Tanabe,
Springer Verlag, Proceeding of the 12th
International Symposium on Superconductivity (ISS'99), (1999) 413.

Kiss, T., Vysotsky, V., Ilyin, Y., Inoue, M., Hasegawa, K., Takeo, M.,
Okamoto, H. and Irie, F.
Quench characteristics in HTSC devices
IEEE Trans. Appl. Supercon. **9** (1999) 1073.

Kiss, T., Hasegawa, K. Inoue, M., Takeo, M., Okamoto, H. and Irie, F.
Critical current properties in HTS
Teionkougaku **34** (1999) 322.

Kiss, T. and Inoue, M., Hasegawa, K., Kiuchi, M., Takeo, M.,
Matsushita, T. and Irie, F.
Anisotropic properties of flux pinning in YBCO thin films
Proc. The 9th International Workshop on Critical Currents
in Superconductors (1999) 130.

Kiss, T., Inoue, M., Hasegawa, K., Takeo, M., Okamoto, H. and Irie, F.
Critical current distribution and its thermodynamic properties in YBCO thin films: Comparison to the power E(J) model

Proc. the 9th International Workshop on Critical Currents
in Superconductors (1999) 33.

Kiss, T., Inoue, M., Hasegawa, K., Ogata, K., Takeo, M. and Irie, F.
Quench characteristics of YBCO thin film
Advances in Superconductivity **XI** (1999) 457.

Kiss, T., Matsushita, T. and Irie, F.
Relationship among flux depinning, irreversibility and phase transition in a disordered HTS material
Superconductor Science and Technology **12** (1999) 1079.

Matsushita, T. and Kiss, T.
Thermal depinning of flux lines in superconductors
Phys. C **315** (1999) 12.

Matsushita, T. and Kiss, T.
Theoretical study on vortex glass-liquid transition in pinned superconductors
IEEE Trans. Appl. Supercon., **9** (1999) 2629.

Nakamura, T., Hoshino, T., Muta, I., Kiss, T., Matsushita, T. and Takeo, M.
Transport characteristics in YBaCuO thin films under applying DC and AC transport currents
Advances in Superconductivity **XI** (1999) 637.

Ogikubo,K., Terai,T., Yamaguchi,K. and Yamawaki,M.
Change in pinning properties of $Bi_2Sr_2CaCu_2O_{8+x}$ single crystals due to particle-beam irradiation followed by thermal annealing
Advances in Superconductivity **XII** (Springer-Verlag, Tokyo, 2000) 260.

Okamoto, H., Irie, F., Kiss, T., Hasaegawa, K. and M. Kanazawa
Scaling law of distributed local critical currents in a Bi-2223/Ag wires estimated by V-I characteristics

Advances in Superconductivity **XI** (1999) 481.

Okamoto, H., Irie, F., Kiss, T., Inoue, M. and Kanazawa, M.
Pinning characteristics of Bi-2223 and Bi-2212 wires with consideration of Jc distribution
Superconductor Science and Technology **12** (1999) 1102.

Sasaki, Y,. Huang, D. X. and Ikuhara, Y.
Ion-irradiation defects on high temperature super conductor.
電子顕微鏡、**34**、No.3 (1999) 173.

Sasase, M., Okayasu, S., Kurata, H. and Hojou, K.
Effect of Au^{24+} ion iradiation on the superconductive properties and microstrucuture of $EuBa_2Cu_3O_x$ thin films.
Surface and Coating Technology **103-104**(1998)pp. 360-364.

Sasase, M., Satou, T.,Okayasu, S., Kurata, H. and Hojou, K.
Defect structure of high-Tc superconductor by high-energy heavy ion irradiation.
Advances in Superconductivity **XII** (ISS'99) (1999)pp. 314-316.

Sueyoshi, T., Ishikawa, N., Iwase, A., Chimi, Y., Kiss, T.,
Fujiyoshi, T. and Miyahara, K.
Critical scaling analysis of transport characteristics before and after heavy-ion irradiation in a $YBa_2Cu_3O_{7-\delta}$ thin film
Advances in Superconductivity **XI** (1999) 593.

Yamafuji, K. and Fujiyoshi, T. and Kiss, T.
Effect of flux pinning on the Nernst and Ettingshausen effects in T_c superconductors
Phys. C **311** (1999) 253.

Yamafuji, K., Fujiyoshi, T., Kiss, T., Inoue, M., Sasaki, T. and Kobayashi, N.
The Nernst effect in high-Tc cuprate superconductors
Phys. C **328** (1999) 230.

Meetings

Adachi, K., Chimi, Y., Iwase, A. and Yamakawa, K.
Effects of ion irradiation in Pd-H system
Fall Meeting of the Physical Society of Japan, Morioka (Sept. 24, 1999)

Chimi, Y., Iwase, A., Ishikawa, N., Kuroda, N. and Kambara, T.
Radiation annealing induced by electronic excitation in iron
18th International Conference on Atomic Collisions in Solids, Odense,
Denmark (Aug. 6, 1999)

Chimi, Y., Iwase, A., Ishikawa, N., Kuroda, N. and Kambara, T.
Electronic excitation and atomic displacements induced by high-energy heavy ion irradiation in Fe(II)
Fall Meeting of the Physical Society of Japan, Morioka (Sep. 27, 1999)

Gevorgyan, S., Kiss, T. , Movsisyan, A., Shirinyan, H., Ohyama, K.,
Takeo, M., Matsushita, T. and Funaki, K.
Advantages of measurement in flat geometry high-Tc cuprates by an open-flat coil magnetometer demon-strating its wide possibilities for detection
The 8th International Workshop on Low Temperature Detectors, Dalfsen,
The Netherlands (Aug. 1999)

Gevorgyan, S., Kiss, T. , Shirinyan, S., Katsube, H., Ohyama, T.,
Matsushita, T., Takeo, M. and Funaki, K.
The possibility of determination of the material parameters in HTS by means of the improved "LC resonator" method
International Symposium on Superconductivity, Morioka (Oct. 17-19, 1999)

Hasegawa, T., Morita, K., Ishino, S., Tobita, T., Suzuki, M., Chimi, Y.,
Ishikawa, N. and Iwase, A.
Irradiation effect with high energy heavy ions on Fe-Cu alloys
Fall Meeting of Atomic Energy Society of Japan, Niigata(Sept. 10-12, 1999)

Hasegawa, T., Ishino, S., Tobita, T., Suzuki, M., Chimi, Y.,
Ishikawa, N. and Iwase, A.
Irradiation effect with high energy heavy ions on Fe-Cu alloys(Ⅱ)
Spring Meeting of Atomic Energy Society of Japan, Ehime(Mar. 28-30, 2000)

Imai M., Kawatsura, K. Sataka, M, Kitazawa, S., Komaki, K., Yamazaki, Y.,
Tawara, H., Shibata, H., Azama, T. and Kanai, Y.
Electron spectra from highly excited sulfur ion studied by zero-degree electron spectroscopy
XXIst Int. Conf. on the Physics of Electronic and Atomic Collisions (ICPEAC-XXI), Sendai (Jul. 1999)

Inoue, M., Kiuchi, M., Kiss, T., Takeo, M., Matsushita, T.,
Awaji, S. and Watanabe, K.
Anisotropy of E-J characteristics in YBCO superconductors
International Symposium on Superconductivity, Morioka (Oct. 17-19, 1999)

Ishikawa, N., Sueyoshi , T., Iwase, A., Chimi, Y., Fujiyoshi ,T.,
Miyahara, K. and Kiss, T.
In-situ measurements of transport characteristics in heavy-ion irradiated $YBa_2Cu_3O_y$ under magnetic field
22nd International Conference on Low Temperature Physics, Helsinki, Finland (Aug. 9, 1999)

Ishikawa, N. , Chimi, Y., Iwase, A., Wakana, H. and Michikami, O.
Irradiation temperature dependence of swift Heavy Ion Induced defects in oxide superconductor $EuBa_2Cu_3O_y$
18th International Conference on Atomic Collisions in Solids, Odense, Denmark (Aug. 5, 1999)

Ishikawa, N., Sueyoshi , T., Iwase, A., Chimi, Y., Fujiyoshi , T.,
Miyahara, K. and Kiss, T.
Effects of splayed columnar defects in Y-based high-Tc superconductors

irradiated with heavy ions
Fall Meeting of the Physical Society of Japan, Morioka (Sep. 24, 1999)

Itaka, K., Yasugaki, Y., Shibauchi, T., Tamegai, T. and Okayasu. S.
Novel asymmetric critical state in $YBa_2Cu_3O_{7-\delta}$ with columnar defects
Physics and Chemistry of Molecular and Oxide Superconductors (MOS99) at KTH in Stockholm, Sweden, (Jul. 28, 1999)

Itaka, K., Yasugaki, Y., Shibauchi, T., Tamegai, T. and Okayasu, S.
Magnetization anomaly near zero field in heavily-ion irradiated $YBa_2Cu_3O_{7-\delta}$
54th Annulal Meeting of the Physical Society of Japan,
Hiroshima (Mar. 28, 1999)

Iwase, A., Chimi, Y., Ishikawa, N. and Kambara, T.
Atomic displacements induced by high density electronic excitation in iron
XXI International Conference on the Physics of Electronic and Atomic Collisions, Sendai (Jul. 27, 1999)

Iwase, A.
Interaction between high-energy particles and solids (High-density energy transfer process)
Special Lecture for Advanced Nuclear Science at Tohoku University, Sendai (Aug. 25, 1999)

Iwase, A.
Swift heavy ion irradiation effects and high density electronic excitation in metals
Symposium of Research Center for Nuclear Science and Technology at University of Tokyo, Tokyo (Dec. 2, 1999)

Iwase, A.
Outlook on utilization of swift heavy ion beam for inorganic materials
Branch Meeting on Development for Utilization of Ion Beam by Super

Conductive AVF Cyclotron, Takasaki (Feb. 23, 2000)

Iwase, A.
High density energy deposition and atomic displacements by swift particle irradiation
Symposium in Spring Meeting of the Physical Society of Japan,
Suita (Mar. 23, 2000)

Kabashima, K., Kiss, T., Matsushita, T. and Takeo, M.
Study on the flux pinning characteristics around G-L transition by the Monte-Carlo simulation
International Symposium on Superconductivity, Morioka (Oct. 17-19, 1999)

Kakeya, I., Nakamura, R. and Kadowaki, K.
It systematic study of Josephson plasma resonance in $Bi_2Sr_2CaCu_2O_{8+\delta}$ *with Columnar defects*
22nd International Conference on Low Temperature Physics (LT22),
Espoo, Finland (Aug. 10, 1999)

Kimura, K., Koshida, R., Okayasu, S., Sataka, S., Kazumata, Y.,
Kwok, W. K., Crabtree, G. W. and Kadowaki, K.
Systematic magnetization measurements on $Bi_2Sr_2CaCu_2O_{8+\delta}$ *with Columnar defects*
Internatinal Conference on Physics and Chemistry of Molecular
and Oxide Superconductors (MOS'99), Stockholm, Sweden (Jul. 29, 1999)

Kimura, K., Koshida, R., Okayasu, S., Sataka, S., Kazumata, Y.,
Kwok, W. K., Crabtree, G. W. and Kadowaki, K.
Magnetization anomalies above the vortex lattice melting transition
22nd Internatinal Conference on Low Temperature Physics (LT22),
Espoo and Helsinki, Finland (Aug. 5, 1999)

Kimura, K., Koshida, R., Okayasu, S., Sataka, S., Kazumata, Y.,
Kwok, W. K., Crabtree, G. W. and Kadowaki, K.
Correlation between the vortex phase transition and disorders in $Bi_2Sr_2CaCu_2O_{8+\delta}$
Fall Meeting of the Physical Society of Japan, Morioka (Sept. 24, 1999)

Kimura, K., Koshida, R., Okayasu, S., Sataka, S., Kazumata, Y.,
Kwok, W. K., Crabtree, G. W. and Kadowaki, K.
Anomalous magnetization behavior in the vortex liquid state in $Bi_2Sr_2CaCu_2O_{8+\delta}$
12th International Symposium on Superconductivity(ISS'99), Morioka (Oct. 18, 1999)

Kimura, K., Koshida, R., Okayasu, S., Sataka, S., Kazumata, Y.,
Kwok, W. K., Crabtree, G. W. and Kadowaki, K.
Weak pinning phenomena in liquid state in $Bi_2Sr_2CaCu_2O_{8+\delta}$with Columnar defects
6th Internatinal Conf. Materials and Mechanisms of Superconductivity
and High Temperature Superconductors (M2S-HTSC-VI), Houston,
Texas (Feb. 21, 2000)

Kimura, K., Koshida, R., Okayasu, S., Sataka, S., Kazumata, Y.,
Kwok, W. K., Crabtree, G. W. and Kadowaki, K.
Pinning and vortex state in $Bi_2Sr_2CaCu_2O_{8+\delta}$with Columnar defects
Spring Meeting of the Physical Society of Japan, Osaka (Mar. 23, 2000)

Kiss, T., Inoue, M., Kiuchi, M., M.Takeo, Matsushita, T., Awaji, S. and Watanabe, K.
Anisotropic current transport property and its scaling in a YBCO film
under the magnetic fields up to 27T
Europian Conf. on Appl. Supercon., Barcelona, Spain (Sept. 14-17, 1999)

Kitazawa, S., Sataka, M., Tawara, H., Imai M., Shibata, H., Komaki, K.,
Kawatsura, K., Kanai, Y. and Azama, T.
Ejected electron spectra from high energy highly charged oxygen ions
in the collisions with atoms
XXIst Int. Conf. on the Physics of Electronic and Atomic Collisions (ICPEAC-XXI),
Sendai (Jul. 1999)

Kitazawa, S., Sataka, M., Tawara, H., Imai M., Shibata, H., Komaki, K.,
Kawatsura, K., Kanai, Y. and Azama, T.,
Coster-Kronig transition from high and low energy highly charged oxygen ions and atom collision
XVIth Int. Seminar on Ion-Atom Collisions (ISIAC-16), Kyoto (Jul, 1999)

Nishimura, S., Kiss, T., Takeo, M. and Matsushita, T.
Error analysis in the study of transport characteristics in HTS using a statistic model
International Symposium on Superconductivity, Morioka (Oct. 17-19, 1999).

Ogikubo, K., Terai, T., Yamaguchi, K. and Yamawaki, M.
Pinning poperty change of high-energy heavy-ion irradiated
Bi-2212 single crystals due to thermal annealing after irradiation
6th International Conference; Materials and Mechanisms of Superconductivity
and High Temperature Superconductors, Houston, USA (Feb. 20-25, 2000)

Ogikubo, K., Terai, T., Yamaguchi, K., Yamawaki, M.,
Okayasu, S. and Hojou, K.
Change in critical current density of $Bi_2Sr_2CaCu_2O_{8+x}$ single crystal
by high-energy heavy-ion irradiation followed by thermal annealing
47th Spring Meeting; The Japan Society of Applied Physics
and Related Societies, Aoyama Gakuin University, Tokyo (Mar.28-31, 2000)

Ohtsuka H., Sugai H., Hojo K. and Maeta, H.
Radiation defects in Au nano-particles
Spring Meeting of the Physical Society of Japan, Suita (Mar. 25, 2000)
Sasase, M., Satou, T., Okayasu, S., Kurata, H. and Hojou, K.
Defect structure of high-Tc superconductor by high-energy heavy ion irradiation
Fall Meeting of the Japan Society of Applied Physics, Kobe (Sep. 1, 1999)

Sasase, M., Satou, T.,Okayasu, S., Kurata, H. and Hojou, K.
Defect structure of high-Tc superconductor by high-energy heavy ion irradiation
International Symposium on superconductivity (ISS'99), Morioka (Oct. 19, 1999)

Sekioka, T., Terasawa, M., Sataka, M., Kitazawa, S. and Niibe, M.

Emission of secondary ions from conductive materials bombarded with high energy ions

XXI Int. Conf. on the Physics of Electronic and Atomic Collisions,

Sendai (Jul. 24, 1999)

This is a blank page.

7. Personnel and Committees

This is a blank page.

(1) Personnel (FY 1999)

Department of Materials Science

Hiroshi	Katsuta	Director
Akira	Iwamoto	Deputy Director
Satoshi	Takemori	Administrative Manager

Tandem Accelerator Group

Scientific Staff

Tadashi	Yoshida*
Suehiro	Takeuchi
Susumu	Hanashima
Makoto	Matsuda

Technical Staff

Susumu	Kanda
Isao	Ohuchi
Katsuzo	Horie
Yoshihiro	Tsukihashi
Shinichi	Abe
Nobuhiro	Ishizaki
Hidekazu	Tayama

Research Group for Innovative Nuclear Science

Masumi	Oshima*	
Akihiro	Iwase	
Nobuo	Shinohara	
Hideki	Iimura	
Youichi	Hatsukawa	
Norito	Ishikawa	
Yasuhiro	Chimi	
Yosuke	Toh	
Tadayuki	Hasegawa	(Student)

Research Group for Solid State Phyics under Extreme Conditions

Kiichi	Hojou*
Masao	Sataka
Hideo	Ohtsuka
Satoru	Okayasu
Sin-iti	Kitazawa

Masato Sasase

Research Group for Radiation Effects and Analyses

Shiro Jitsukawa*
Tetsuya Nakazawa
Daijyu Yamaki
Viktor Grismanvs (Research fellow)

Advanced Science Research Center

Research Group for Inverse Compton

Masumi Oshima*
Takehito Hayakawa

Research Group for fusion of Heavy Deformed Nuclei

Hiroshi Ikezoe*
Tetsuro Ishii
Yasuharu Sugiyama
Shin-ichi Mitsuoka
Katsuhisa Nishio

Research Group for Hadron Science

Satoshi Chiba*
Toshiki Maruyama
Hiroki Takemoto
V. N. Kondratyev (Research Fellow)
Shinpei Chikazumi (Student)

Research Group for Nuclear Chemistry of Heavy Elements

Yuichiro Nagame*
Shin-ichi Ichikawa
Kazuaki Tsukada
Ichiro Nishinaka
Hiromitsu Haba
Masato Asai
Shin-ichi Goto (Student)

Department of Health Physics

Radiation Control Division II

Yukihiro Miyamoto
Yuuichi Takaba
Kouichi Sato

Takasaki Radiation Chemistry Research Establishment

Radiation Engineering Division

Toshio Hirao

Oarai Research Establishment

High Temerature Irradiation Laboratory

Kimio Hayashi*

Masahiro Ishihara

Shinchi Baba

Jun Aihara

* : Head

(2)Tandem Consultative Committee

(Chairman)	Toru	Nomura	(Professor, Prime Scientist, High Energy Accelerator Research Organization (KEK))
(Vice Chairman)	Hiroshi	Katsuta	(Director, Department of Materials Science)
	Hiroyasu	Ejiri	(Professor Emeritus of Osaka University)
	Kohei	Furuno	(Professor, Tsukuba University)
	Jun	Imasato	(Professor, High Energy Accelerator Research Organization (KEK))
	Kenji	Katori	(Professor Emeritus of Osaka University)
	Kenichiro	Komaki	(Professor, The University of Tokyo)
	Shigeru	Kubono	(Associate professor, The University of Tokyo)
	Hisaaki	Kudo	(Associate professor, Niigata University)
	Hiroshi	Kudo	(Professor, Tsukuba university)
	Shunpei	Morinobu	(Professor, Kyushu University)
	Kenji	Morita	(Professor, Nagoya University)
	Hiroshi	Nakahara	(Professor, Tokyo Metropolitan University)
	Naoto	Sekimura	(Professor, The University of Tokyo)
(Secretary)	Akira	Iwamoto	(Deputy Director, Department of Materials Science)
(Secretary)	Masao	Sataka	(Research Group for Solid State Physics under Extreme Conditions)
(Secretary)	Satoshi	Takemori	(Administrative Manager, Department of Materials Science)
(Secretary)	Suehiro	Takeuchi	(Tandem Accelerator Group)
(Secretary)	Tadashi	Yoshida	(Head, Tandem Accelerator Group)

(3)Research Planning and Assessment Committee

(a) Sub-committee for Nuclear Physics and Nuclear Chemistry

Akira	Iwamoto	(Deputy Director, Department of Materials Science)
Shigeru	Kubono	(Associate professor, The University of Tokyo)

	Hiromichi	Nakahara	(Professor, Tokyo Metropolitan University)
	Shunpei	Morinobu	(Professor, Kyushu University)
	Kouhei	Furuno	(Professor, Tsukuba University)
	Hiroshi	Ikezoe	(Head, Research Group for Fusion of Heavy Deformed Nuclei)
	Toshiaki	Sekine	(Research Group for Innovative Nuclear Science)
(Secretary)	Suehiro	Takeuchi	(Tandem Accelerator Group)
(Secretary)	Tadashi	Yoshida	(Head, Tandem Accelerator Group)

(b) Sub-committee for Materials and Radiation Damage

	Akira	Iwamoto	(Deputy Director, Department of Materials Science)
	Naoto	Sekimura	(Professor, The University of Tokyo)
	Kenichiro	Komaki	(Professor, The University of Tokyo)
	Kenji	Morita	(Professor, Nagoya University)
	Hiroshi	Kudo	(Professor, Tsukuba University)
	Kiichi	Hojou	(Head, Research Group Solid State Physics under Extreme Condition)
	Akihiro	Iwase	(Research Group for Innovative Nuclear Science)
(Secretary)	Suehiro	Takeuchi	(Tandem Accelerator Group)
(Secretary)	Tadashi	Yoshida	(Head, Tandem Accelerator Group)

This is a blank page.

8. Cooperative Researches

This is a blank page.

	Title	Contact person Organization
1.	Systematic Investigation on Magnetic Rotation in Atomic Nucleus	Masahiko SUGAWARA Department of Natural Science, Chiba Institute of Technology
2.	Study of Electromagnetic Properties of Nuclear High-spin State through Crystal Ball (Ⅱ)	Tetsuro KOMATSUBARA Tandem Accelerator Center, Tsukuba University
3.	Investigation on Anomalous Phenomena of Electromagnetic transitions between Multipole Deformed State	Hideshige KUSAKARI Faculty of Education, Chiba University
4.	Nuclear Structure of Neutron-rich Nuclides using Deep Inelastic Scattering	Masao OGAWA Department of Energy Science, Tokyo Institute of Technology
5.	Correlation between Fission Modes and Mass-number of Fission Products	Hiromichi NAKAHARA Faculty of Science, Tokyo Metropolitan University
6.	Precise measurement of Gamma-ray Emission Probability for Proton-rich nuclides	Hiroshi MIYAHARA Department of Radiological Technology, School of Health Science, Nagoya University
7.	Laser Spectroscopy of Light La-isotopes	Takayoshi HORIGUCHI Hiroshima Kokusai Gakuen University
8.	Study of Nucear Science by Coulomb Exitation	Hideshige KUSAKARI Faculty of Education, Chiba University

9. Study of Nuclear Josephson Effects in Heavy Ion Collision	Shigeru KUBONO Institute of Nuclear Study, The University of Tokyo
10. Electronic Excitation Effects in Oxides by High Energy Heavy Ion	Noriaki MATSUNAMI School of Engineering, Nagoya University
11. Study of Single-events Induced by High Energy Ions	Sumio MATSUDA NASDA, Tsukuba
12. High-energy Ion Beam Irradiation of Functional Electronic Materials	Takayuki TERAI Engineering Research Institute, School of Engineering, The University of Tokyo
13. Electron Excitation Effect on Sputtering Induced by Heavy Ion Bombardment	Mititaka TERASAWA Faculty of Engineering, Himeji Institute of Technology
14. Electron Spectra Induced by the Collision of Highly Charged Ions with Matter	Ken-ichiro KOMAKI Graduate School of Arts and Science, The University of Tokyo
15. Study of Property and Microstructure on the Oxide Superconductors Irradiated with High Energy Ions	Yukichi SASAKI Japan Fine Ceramics Center, Nagoya
16. Vortex Motion of High Tc Superconductors Irradiated by Heavy ions	Tsuyoshi TAMEGAI The University of Tokyo
17. Study of Vortex State for High Tc Superconductors with Columnar Defects	Kazuo KADOWAKI Tsukuba University

18. Electron Wave Interference Effects in the Ballistic conductive Region due to Defects induced by Heavy Ion Irradiation	Yuuichi OCHIAI Chiba University
19. Observation of Dynamical Interaction between Vortices and Columnar Defects by Lorentz Microscpopy	Akira TONOMURA Advanced Research Laboratory, Hitachi Ltd.
20. Study on Damage Production Mechanism in Steel Materials Irradiated with High Energy Ions	Shiori ISHINO Faculty of Engineering, Tokai University
21. Effect of Ion Irradiation for New Carbon Composite Materials and Fibers with High Thermal Conductivity	Tatsuo OKU Faculty of Engineering, Ibaraki University
22. Electron Transfer in Collisions of Multicharged Ions and Atoms	Ken-ichiro KOMAKI Graduate School of Arts and Science, The University of Tokyo
23. Study on Transport Property Change in High-Tc Superconductors by Introducing Columnar Defects	Takanobu KISS Department of Electrical and Electronic Systems Engineering, Kyushu University

This is a blank page.

国際単位系 (SI) と換算表

表 1　SI基本単位および補助単位

量	名称	記号
長さ	メートル	m
質量	キログラム	kg
時間	秒	s
電流	アンペア	A
熱力学温度	ケルビン	K
物質量	モル	mol
光度	カンデラ	cd
平面角	ラジアン	rad
立体角	ステラジアン	sr

表 2　SIと併用される単位

名称	記号
分，時，日	min，h，d
度，分，秒	°，′，″
リットル	l，L
トン	t
電子ボルト	eV
原子質量単位	u

1 eV = 1.60218 × 10^{-19} J

1 u = 1.66054 × 10^{-27} kg

表 5　SI接頭語

倍数	接頭語	記号
10^{18}	エクサ	E
10^{15}	ペタ	P
10^{12}	テラ	T
10^{9}	ギガ	G
10^{6}	メガ	M
10^{3}	キロ	k
10^{2}	ヘクト	h
10^{1}	デカ	da
10^{-1}	デシ	d
10^{-2}	センチ	c
10^{-3}	ミリ	m
10^{-6}	マイクロ	μ
10^{-9}	ナノ	n
10^{-12}	ピコ	p
10^{-15}	フェムト	f
10^{-18}	アト	a

表 3　固有の名称をもつSI組立単位

量	名称	記号	他のSI単位による表現
周波数	ヘルツ	Hz	s^{-1}
力	ニュートン	N	m·kg/s^2
圧力，応力	パスカル	Pa	N/m^2
エネルギー，仕事，熱量	ジュール	J	N·m
工率，放射束	ワット	W	J/s
電気量，電荷	クーロン	C	A·s
電位，電圧，起電力	ボルト	V	W/A
静電容量	ファラド	F	C/V
電気抵抗	オーム	Ω	V/A
コンダクタンス	ジーメンス	S	A/V
磁束	ウェーバ	Wb	V·s
磁束密度	テスラ	T	Wb/m^2
インダクタンス	ヘンリー	H	Wb/A
セルシウス温度	セルシウス度	℃	
光束	ルーメン	lm	cd·sr
照度	ルクス	lx	lm/m^2
放射能	ベクレル	Bq	s^{-1}
吸収線量	グレイ	Gy	J/kg
線量当量	シーベルト	Sv	J/kg

表 4　SIと共に暫定的に維持される単位

名称	記号
オングストローム	Å
バーン	b
バール	bar
ガル	Gal
キュリー	Ci
レントゲン	R
ラド	rad
レム	rem

1 Å = 0.1 nm = 10^{-10} m

1 b = 100 fm^2 = 10^{-28} m^2

1 bar = 0.1 MPa = 10^5 Pa

1 Gal = 1 cm/s^2 = 10^{-2} m/s^2

1 Ci = 3.7 × 10^{10} Bq

1 R = 2.58 × 10^{-4} C/kg

1 rad = 1 cGy = 10^{-2} Gy

1 rem = 1 cSv = 10^{-2} Sv

（注）

1. 表1　5は「国際単位系」第5版，国際度量衡局 1985年刊行による。ただし，1 eVおよび1 uの値はCODATAの1986年推奨値によった。
2. 表4には海里，ノット，アール，ヘクタールも含まれているが日常の単位なのでここでは省略した。
3. barは，JISでは流体の圧力を表わす場合に限り表2のカテゴリーに分類されている。
4. EC閣僚理事会指令ではbar，barnおよび「血圧の単位」mmHgを表2のカテゴリーに入れている。

換　算　表

力	N(=10^5 dyn)	kgf	lbf
	1	0.101972	0.224809
	9.80665	1	2.20462
	4.44822	0.453592	1

粘度　1 Pa·s(N·s/m^2) = 10 P(ポアズ)(g/(cm·s))

動粘度　1 m^2/s = 10^4 St(ストークス)(cm^2/s)

圧力	MPa(=10 bar)	kgf/cm^2	atm	mmHg(Torr)	lbf/in^2(psi)
	1	10.1972	9.86923	7.50062 × 10^3	145.038
	0.0980665	1	0.967841	735.559	14.2233
	0.101325	1.03323	1	760	14.6959
	1.33322 × 10^{-4}	1.35951 × 10^{-3}	1.31579 × 10^{-3}	1	1.93368 × 10^{-2}
	6.89476 × 10^{-3}	7.03070 × 10^{-2}	6.80460 × 10^{-2}	51.7149	1

エネルギー・仕事・熱量	J(=10^7 erg)	kgf·m	kW·h	cal(計量法)	Btu	ft·lbf	eV
	1	0.101972	2.77778 × 10^{-7}	0.238889	9.47813 × 10^{-4}	0.737562	6.24150 × 10^{18}
	9.80665	1	2.72407 × 10^{-6}	2.34270	9.29487 × 10^{-3}	7.23301	6.12082 × 10^{19}
	3.6 × 10^6	3.67098 × 10^5	1	8.59999 × 10^5	3412.13	2.65522 × 10^6	2.24694 × 10^{25}
	4.18605	0.426858	1.16279 × 10^{-6}	1	3.96759 × 10^{-3}	3.08747	2.61272 × 10^{19}
	1055.06	107.586	2.93072 × 10^{-4}	252.042	1	778.172	6.58515 × 10^{21}
	1.35582	0.138255	3.76616 × 10^{-7}	0.323890	1.28506 × 10^{-3}	1	8.46233 × 10^{18}
	1.60218 × 10^{-19}	1.63377 × 10^{-20}	4.45050 × 10^{-26}	3.82743 × 10^{-20}	1.51857 × 10^{-22}	1.18171 × 10^{-19}	1

1 cal = 4.18605 J(計量法)
= 4.184 J　(熱化学)
= 4.1855 J　(15 °C)
= 4.1868 J(国際蒸気表)

仕事率　1 PS(仏馬力)
= 75 kgf·m/s
= 735.499 W

放射能	Bq	Ci
	1	2.70270 × 10^{-11}
	3.7 × 10^{10}	1

吸収線量	Gy	rad
	1	100
	0.01	1

照射線量	C/kg	R
	1	3876
	2.58 × 10^{-4}	1

線量当量	Sv	rem
	1	100
	0.01	1

（86年12月26日現在）